OULU 2016
C 594

ACTA

UNIVERSITATIS OULUENSIS

Bouchra Darif

SYNTHESIS AND CHARACTERIZATION OF CATALYSTS USED FOR THE CATALYTIC OXIDATION OF SULFUR-CONTAINING VOLATILE ORGANIC COMPOUNDS

FOCUS ON SULFUR-INDUCED DEACTIVATION

UNIVERSITY OF OULU GRADUATE SCHOOL;
UNIVERSITY OF OULU,
FACULTY OF TECHNOLOGY

ACTA UNIVERSITATIS OULUENSIS
C Technica 594

BOUCHRA DARIF

SYNTHESIS AND CHARACTERIZATION OF CATALYSTS USED FOR THE CATALYTIC OXIDATION OF SULFUR-CONTAINING VOLATILE ORGANIC COMPOUNDS

Focus on sulfur-induced deactivation

Academic dissertation to be presented with the assent of the Doctoral Training Committee of Technology and Natural Sciences of the University of Oulu for public defence in the Arina auditorium (TA105), Linnanmaa, on 12 December 2016, at 12 noon

UNIVERSITY OF OULU, OULU 2016

Acta Univ. Oul. C 594, 2016

Supervised by
Professor Riitta Keiski
Docent Satu Ojala
Professor Rachid Brahmi
Professor Mohammed Bensitel

Reviewed by
Professor Leonid Kustov
Professor Sergio Botelho de Oliveira

Opponent
Professor Tapio Salmi

ISBN 978-952-62-1421-4 (Paperback)
ISBN 978-952-62-1422-1 (PDF)

ISSN 0355-3213 (Printed)
ISSN 1796-2226 (Online)

Cover Design
Raimo Ahonen

JUVENES PRINT
TAMPERE 2016

Darif, Bouchra, Synthesis and characterization of catalysts used for the catalytic oxidation of sulfur-containing volatile organic compounds. Focus on sulfur-induced deactivation

University of Oulu Graduate School; University of Oulu, Faculty of Technology
Acta Univ. Oul. C 594, 2016
University of Oulu, P.O. Box 8000, FI-90014 University of Oulu, Finland

Abstract

The work in this thesis concentrates on finding more active and durable catalysts for the demanding environmental application of the oxidation of sulfur-containing volatile organic compounds (S-VOCs). This application is challenging due to the high purification levels required and the catalyst deactivating nature of sulfur. In this thesis, dimethyldisulfide (DMDS) was used as the model molecule to represent S-VOCs since it is often present in odorous emissions and it is more difficult to treat than most of the other S-VOCs.

It was found that the addition of a very small amount of Pt (0.3%) especially improves the selectivity of copper oxide based catalysts towards complete oxidation products ((carbon dioxide (CO_2), water (H_2O) and sulfur dioxide (SO_2)) in DMDS oxidation. Catalyst characterization by transmission electron microscopy, temperature programmed reduction and X-ray photoelectron spectroscopy analyses suggests that this promoting effect is most likely due to the close interaction between Cu and Pt species on the bimetallic PtCu/γ-Al_2O_3 catalyst.

The drawback of using the Al_2O_3 support is that it is not resistant towards sulfur poisoning. The deactivation of the self-made catalysts was studied with the help of an accelerated ageing procedure that was developed based on the information from the industrially aged volatile organic compound (VOC) catalysts. Industrial deactivation was caused by the sintering of the support and active metals and by the formation of metal sulfates with the support. After accelerated ageing, the silica doped alumina $(Al_2O_3)_{0.8}(SiO_2)_{0.2}$ supported catalyst, showed remarkably promising results in terms of stability towards sulfur poisoning and the activity in DMDS oxidation was very close to that of the most active PtCu/Al_2O_3. The addition of less than 20% of SiO_2 on the Al_2O_3 support led to a catalyst that is more selective and resistant to sulfur poisoning.

Keywords: deactivation by sulfur, dimethyldisulfide, Pt-Cu catalyst, stability, sulfur containing volatile organic compound

Darif, Bouchra, Rikkipitoisten orgaanisten yhdisteiden hapetukseen käytettyjen katalyyttimateriaalien synteesi ja karakterisointi. Katalyyttien rikkideaktivoituminen
Oulun yliopiston tutkijakoulu; Oulun yliopisto, Teknillinen tiedekunta
Acta Univ. Oul. C 594, 2016
Oulun yliopisto, PL 8000, 90014 Oulun yliopisto

Tiivistelmä

Väitöskirjassa tuotetaan uutta tietoa rikkipitoisten orgaanisten yhdisteiden (S-VOC) hapetukseen soveltuvien uusien katalyyttisten materiaalien synteesistä ja karakterisoinnista. S-VOC-yhdisteiden käsittely on vaativa katalyyttisen polton sovellus, koska näiden päästöjen käsittely edellyttää korkeaa puhdistustehoa, ja lisäksi yhdisteiden sisältämä rikki on katalyyttimyrkky. Tässä väitöskirjassa valittiin S-VOC-yhdisteitä edustavaksi malliaineeksi dimetyylisulfidi (DMDS), koska se on usein mukana käsiteltävissä S-VOC-päästöissä ja sen käsittely on vaativampaa kuin useiden muiden S-VOC-yhdisteiden käsittely.

Tutkimustulosten mukaan hyvin pieni Pt-lisäys (0.3 %) parantaa erityisesti kuparioksidikatalyyttien selektiivisyyttä DMDS:n kokonaishapetustuotteiksi (CO_2, H_2O, SO_2). Katalyyttien karakterisoinnin (läpäisyelektronimikroskopia, lämpötilaohjattu pelkistysreaktio, röntgensädefotoelektronispektroskopia) perusteella voidaan esittää parannuksen syyksi kuparin ja platinan läheinen kontakti bimetallisen PtCu/γ-Al_2O_3-katalyytin pinnalla.

Al_2O_3-tukiaineen heikkoutena on sen deaktivoitumisherkkyys rikkiyhdisteiden läsnä ollessa. Väitöskirjatyössä valmistettujen katalyyttien deaktivitumista tutkittiin laboratoriomittakaavassa nopeutettujen ikäytyskokeiden avulla, jotka kehitettiin teollisessa käytössä deaktivoituneen katalyytin karakterisointien avulla saadun tiedon perusteella. Teollisessa käytössä olleen katalyytin deaktivoitumisen syyksi havaittiin tukiaineen ja aktiivisten metallien sintrautuminen sekä metallisulfidien muodostuminen tukiaineen kanssa. Nopeutettujen ikäytyskokeiden tulosten perusteella havaittiin, että piidioksidin lisäys alumiinioksiditukiaineeseen paransi tukiaineen rikin kestoa merkittävästi. Tutkimuksissa havaittiin myös, että piidioksidilla muokatun katalyytin aktiivisuus oli hyvin lähellä vastaavaa PtCu/γ-Al_2O_3-katalyytin aktiivisuutta. DMDS:n hapetuksessa selektiivisempi ja stabiilimpi katalyytti voidaan aikaansaada alle 20 %:n SiO_2-lisäyksellä Al_2O_3-tukiaineeseen.

Asiasanat: dimetyylidisulfidi, Pt-Cu-katalyytti, rikkideaktivoituminen, rikkiä sisältävä haihtuva orgaaninen yhdiste, stabiilisuus

To my parents

Acknowledgements

This research has been undertaken at the University of Oulu in the Environmental and Chemical Engineering research unit during the years 2011 to 2016. I would like to express my gratitude to my supervisors, Professor Riitta Keiski and Professor Rachid Brahmi, and to my co-supervisors, Dr. Satu Ojala and Professor Mohammed Bensitel, for the inspirational ideas for my research and support during this thesis. I give special thanks to Professor Riitta Keiski for her positive encouragement and for organising funding for this work. The official reviewers of this thesis, Professors Leonid Kustov and Sérgio Botelho de Oliveira, are greatly appreciated for their efforts and valuable comments on this thesis. I gratefully acknowledge the financial support of the Council of Oulu Region from the European Regional Development Fund via the Sulka project (A32164, 524/2012) and the Advanced Materials Doctoral Programme at the University of Oulu Graduate School (ADMA-DP/UniOGS). I would also like to thank the UniOGS for awarding me a conference travel grant. My thanks go to Dr. Mika Huuhtanen for acting as the chair in my follow-up group as well as to all the members of the follow-up group: Prof. Päivi Mäki-Arvela, Dr. Katariina-Rahkamaa-Tolonen and Dr. Celine Fontaine.

Also many thanks go to my colleagues and friends within the research group of Environmental and Chemical Engineering at the University of Oulu (Dr. Satu Pitkäaho, Mrs. Sanna Antikainen, Dr. Kati Orasvisjärvi, Dr. Minna Pirilä, Mrs. Marja Kärkkäinen, Ms. Anna Valtanen, Mrs. Linda Omodara, Ms. Piia Häyrynen, Mrs. Ritva Isomäki, Mrs. Liisa Myllykoski, Mrs. Hanna Valkama, Mrs. Niina Koivikko, Mrs. Auli Turkki, Mr. Esa Muurinen, Mrs. Tiina Laitinen and all the others), the University of Poitiers, France (especially Professor Laurence Pirault-Roy for her supervision during my research visit to the IC2MP laboratory) and the University of Chouaib Doukkali, Morocco (Dr. Zouhair El Assal and Mr. Anass Mouammine) for all their help and inspirational discussions during these years. Mr. Jorma Penttinen, Ms. Kirsi Ahtinen, Mrs. Kaisu Ainassaari and Mr. Markus Riihimäki are especially acknowledged for their assistance with analyses. I also want to express my warmest thanks to Dr. Teuvo Maunula from Dinex-Ecocat Ltd for the valuable discussions and advice given during the thesis work.

Special thanks go to my friends near and far for just being there and giving me other things to think about. I would like to thank my parents for everything that they have given me. I thank also my sisters Karima and Khaoula and my brother Omar; you bring a lot of happiness into my life. Finally, I would like to

express my deepest gratitude to my husband Zakari, who was always by my sides and believes that nothing is impossible for me.

I am not sure if I have acknowledged everyone I wanted to. Actually I think I was very lucky, firstly because I got the golden opportunity to do my research at the University of Oulu under the supervision of Professor Riitta Keiski, and secondly because I believe that many people have contributed to my work by showing me their points of view, helping with experimental work or just giving me possibilities to think about other things than research from time to time. All your contributions have been very important and will not be forgotten!

Oulu, September 2016 Bouchra Darif

Abbreviations

BET	Brunauer-Emmet-Teller
BJH	Barrett-Joyner-Halenda
C_0	The outlet concentration of DMDS [ppm]
C_i	The initial feed concentration of dimethyldisulfide DMDS [ppm]
CVOCs	Chlorinated volatile organic compounds
DMDS	Dimethyl disulfide
DMS	Dimethyl sulfide
EDS	Energy dispersive X-ray spectroscopy
EU	European Union
FESEM	Field emission scanning electron microscopy
FTIR	Fourier transform infrared spectroscopy
GHSV	Gas hourly space velocity
HPy	Hydrogen bounded pyridine
ICDD	International centre for diffraction data
ICP-OES	Inductively coupled plasma-optical electron spectroscopy
In situ IR	In situ infrared
IR	Infra red
IUPAC	International Union of Pure and Applied Chemistry
LPy	Lewis pyridine
MM	Methylmercaptan
n	Mole [mole]
NEC	National emissions ceilings
NMVOC	Non-methane volatile organic compound
p/p_0	Relative pressure
PGM	Platinum group metal
Py	Pyridine
RCO	Regenerative catalytic oxidizers
Rt	Room temperature
RTO	Regenerative thermal oxidizers
S-VOC	Sulfur-containing volatile organic compound.
TCD	Thermal conductivity detector
TEM	Transmission electron microscopy
TPR	Temperature programmed reduction
TRS	Total reduced sulfur compounds
UV	Ultraviolet

VOC	Volatile organic compound
V_p	Pore volume
X	Conversion [%]
XPS	X-ray photoelectron spectroscopy
XRD	X-ray diffraction
XRF	X-ray fluorescence
Y	Yield [%]

Contents

1 Introduction and aims

Volatile organic compounds, or VOCs, belong to the group of major air pollutants together with O_3, CO, NO_x, PM, NH_3 and SO_2 (Colls 2000). VOCs comprise a large variety of organic air pollutants, from pure hydrocarbons to partially oxidized hydrocarbons and organic compounds containing chlorine, sulfur or nitrogen (EPA 2014, EW 2008). The numbers of studies on VOCs' degradation vary greatly from one VOC to another – some VOCs are well-studied, and others are not.

VOC emissions originate from both anthropogenic (human-made) and natural sources, but it is the anthropogenic sources of VOCs in populated and industrialized areas that are the main contributors to air quality problems (EPA 2014). The major source of VOC emissions in Europe is the use of solvents and solvent-containing products (EEA 2013). VOC emissions from commercial products are a significant factor contributing to the creation of air pollution in urban areas.

This thesis concentrates on a specific class of VOCs, namely sulfur-containing VOCs (S-VOCs). Very often S-VOCs cause an obnoxious and unbearable odour, even at very low concentrations. It is therefore essential to study the abatement possibilities and the nature of these substances as well as assess their impacts. Dimethyldisulfide (DMDS) is used in this study as a model molecule to represent S-VOCs since it is regularly present in industrial effluents and it is more difficult to oxidize than the other sulfur-containing compounds that are typically present in waste gas streams. In our research, relatively high concentrations of DMDS are studied since, in the case of pulp mill emission abatement, S-VOCs can be present in much higher concentrations (10–10000 ppm of DMDS and 100–45000 ppm of dimethyl sulfide (DMS)), based on the data from Andersson *et al.* (1973) and the EPA (1973) than those used in the earlier studies (70–400 ppm) (Cellier *et al.* 2004, Wang 1997, Lin 2014). This thesis work concentrates on the catalytic abatement of S-VOC emissions, since it has proven to be an efficient and environmentally sound technology for VOC treatment. Ojala *et al.* (2015) have shown how to utilize VOC emissions as an economically and environmentally important idea that supports the sustainability of the processes. However, the rather high sulfur content in the emissions sets an important challenge to catalyst development.

1.1 VOC's definition and legislation

Various states in the world have implemented directives, laws and regulations whose objective is to reduce the emission of VOCs in order to diminish their impact on health and the environment. First, we need to define what exactly VOCs are.

Indeed, there are many definitions of a VOC, which vary from country to country and from one piece of legislation to another. According to the EC Directive 1999/13/EC (Solvent Emissions Directive 1999), "Volatile Organic Compounds (VOCs) are functionally defined as organic compounds having at 293.15 K (i.e., 20 °C) a vapour pressure of 0.01 kPa or more, or having a corresponding volatility under particular conditions of use". An organic compound is defined as "any compound containing at least the element carbon and one or more of hydrogen, halogens (e.g., chlorine, fluorine or bromine), oxygen, sulfur, phosphorus, silicon, or nitrogen, with the exception of carbon oxides and inorganic carbonates and bicarbonates." Methane, ethane, CO, CO_2, organometallic compounds and organic acids are excluded from this definition. For hydrocarbon solvents, a vapour pressure of 0.01 kPa at 20 ºC grossly corresponds to a boiling point or initial boiling point in the range of 215–220 ºC. (Directive 1999/13/EC). The definition of a VOC in the Solvent Emissions Directive is the most used VOC definition in Europe.

The European legislation standardizes VOC emissions from industrial activities under the Industrial Emissions Directive. This includes dry cleaning, shoe making, advertisement and magazine printing, surface cleaning, vehicle coating and certain pharmaceutical production. Above a specified amount of solvent use, such activities have to comply with the emission limits (Directive 2010/75/EU).

The EU also lists VOC emissions from products such as paints and varnishes in order to limit their negative effects on human health and the environment. The EU's Paints Directive 2004/42/EC obliges producers to gradually reduce the amount of solvents in certain paints and varnishes (Directive 2004/42/CE). Other products – such as coatings for corrosion protection, road markings, hairsprays and deodorants – are not covered by EU legislation despite their contribution to VOC emissions.

The overall VOC emissions of each EU member state are also limited via the National Emissions Ceilings (NEC) Directive 2001/81/EC (2001). The NEC Directive is a critical instrument in reducing overall levels of air pollution –

including VOCs – and limiting the effects of transboundary air pollution (EEA 2013). The NEC Directive requires member states to draw up programmes for the progressive reduction of the four pollutants. The directive covers emissions from all sources of the pollutants which arise as a result of human activities (Directive 2001/81/EC).

S-VOCs, such as organic sulfides and disulfides, as part of the VOCs, are subject to the order of March 1st, 1993, under the guidelines established within the EU. Their concentration in the exhaust gas that has high flow rates (e.g. 5000 m^3h^{-1}) must be less than 20 mgm^{-3} (De Guardia 1996).

Because of the harmful effects of VOCs, some other countries, e.g. the United States and Canada, set VOC limits several years ago on diverse VOC-containing products, such as solvents. Hong Kong has also started to set policies on the emissions of VOCs to help ease their ozone and smog pollution problems and thus preserve the health of the inhabitants of Hong Kong. These regulations set restrictions on the VOC content of architectural, vehicle refinishing and vessel paints and coatings, adhesives, sealants, printing inks and selected consumer products in order to reduce the emissions of VOCs that enter the atmosphere. Importantly, the requirement of an annual reporting of sales, product information display, and labelling and/or prior notification for these regulated products was set (EPD 2010).

Under the Environment Act 1995, the government of the UK and the devolved administration are required to make a national air quality strategy. This act was last reviewed and published in 2007. The air quality strategy fixes the air quality objectives in the UK and recognises that actions at national, regional and local levels may be needed, depending on the scale and nature of the air quality problem (DEFRA 2011).

After an analysis of the regulations controlling VOC emissions, based on selected examples, the appropriate techniques for their control should be discussed. The next section will present details about the different sources, impacts and abatement technologies of VOCs.

1.2 The sources, impacts and treatment of VOC emissions

In order to be able to treat the emissions that contain VOCs, it is necessary to determine the sources and the quality of these emissions. Once in the atmosphere, VOCs participate in many atmospheric reactions that cause harm to the environment and human health.

1.2.1 The sources of VOC emissions

VOC emission sources are numerous, as already briefly mentioned. The emissions are caused by certain industrial processes that both involve solvent implementation (e.g. basic and fine chemicals, metal degreasing, paint application, printing, adhesives and glues, rubber, cleaning products, perfumes and cosmetics), or do not involve solvents (e.g. oil refining, the production of alcoholic beverages and bread). The use of fuels in combustion plants in the industry slightly contributes to these emissions but not as much as it contributes to SO_2 and NO_x. However, the VOC emissions from small individual wood combustion plants are a significant source of VOCs (EPA 2014).

Biogenic VOC emissions (or those related to nature) are emissions from forests and crops, including grassland. The VOCs emitted by vegetation comprise a wide range of compounds containing mainly hydrocarbons, including isoprene and monoterpenes, and are considered to be both the most abundant and more photo-reactive than others. These exhaust emissions are directly dependent on the ambient temperature and the amount of sunshine. Biogenic NMVOC (non-methane volatile organic compound) emissions will therefore vary greatly from month to month, reaching the maximum emission load during the summer season (EPA 2014).

According to a study made in Finland, emissions were calculated for the years 1995–1997. The estimated annual anthropogenic VOC emission was 193 kilotonnes (Lindfors *et al.* 2000). At a global level, according to Müller (1992), the total anthropogenic NMVOC emissions are about 150 Tg yr^{-1}.

Concerning the EU-27, the major sectors concerned in NMVOC emissions are solvent and product use (41%), road and non-road transportation (18%), and commercial, institutional and household associated emissions (14%) (EEA 2010). Concerning the industrial sources of VOCs, Figure 1 illustrates the contributions from various industrial sectors to EU-27 NMVOC industrial emissions in 2008 (European Pollutant Release and Transfer Register 2008). The three most important industrial sources are the energy sector (41%), the chemical industry (22%), and coating and surface treatment activities (18%).

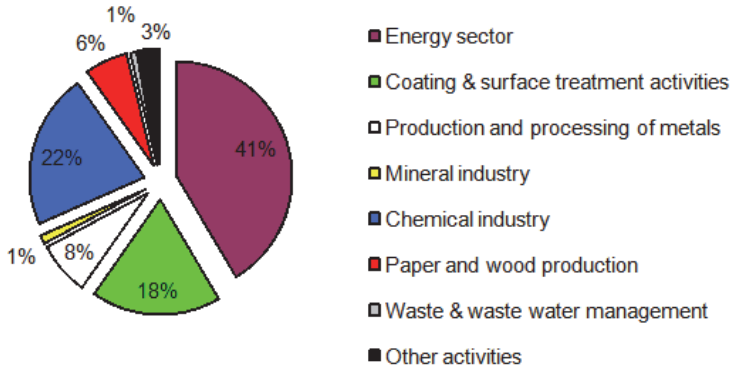

Fig. 1. The distribution of NMVOC industrial emissions in the EU-27 in 2008 (EEA 2010).

Since 2010, all EU member states are obliged to meet their emission ceilings set for the main air pollutants in Directive 2001/81/EC (Directive 2001/81/EC). However, according to the NEC directive (Directive 2001/81/EC) it was reported that from the year of 2010 four member states have persistently exceeded their respective emission ceilings for NMVOCs (Denmark, Germany, Ireland and Luxembourg). The highest exceedance in 2014, in percentage terms, was reported for Ireland (58%). The largest emitters of NMVOCs were Germany, Italy and the UK (EEA 2015). The possible reason for the four countries not meeting their emission ceilings limits was road transport, which contributes largely to the EU-28 emissions in total. This is one of the main reasons for the large number of VOC exceedances since 2010. The lowering in VOC reductions can partly be due to the unexpectedly high growth of transport that cannot be controlled (EEA 2015).

Even though (with the help of current legislation) the total VOC emission levels have decreased from the year when the first VOC directive was launched (1999), the current information indicates the need for further efforts. The next section will shed the light on the different impacts of VOC emissions either on human well-being or on the environment and it will further highlight the importance of VOC emission reduction.

1.2.2 The impacts of VOC emissions

VOC emissions have a dual impact: the impact on health and on the environment (ADEME 2016). The impacts in general are very varied due to the heterogeneous group of compounds fitting in the VOC definition. In the following, certain rather general examples are given.

The impact on health

VOCs have an indirect effect on human health by influencing the ozone formation in the stratosphere as precursors of this gas in the air: the consequences of ozone overproduction on health vary according to the exposure level, the volume of air inhaled and the duration of the exposure. Several health impacts can be generated, such as a cough, chest discomfort and painful discomfort when taking a deep breath, shortness of breath and nasal, eye and throat irritations. These effects, however, differ depending on the individual and the general state of their health (ADEME 2016).

An example of the direct effect is that certain VOCs are considered toxic substances to extreme levels of severity that warrants a strict classification. There are some harmful VOCs that are classified as carcinogenic, mutagenic and toxic to reproduction. It is therefore imperative to take the greatest precautions before handling or being exposed to these compounds and imperative to consult all available information on the compound that is being considered for use (ADEME 2016).

The impact on the environment

In the atmosphere, VOCs degrade and contribute to disrupt chemical equilibrium, which results in the formation or accumulation of ozone. This overproduction of ozone has an adverse effect on vegetation (it alters plant resistance) and accelerates the degradation of some materials like plastic (ADEME 2016). VOCs contribute to the greenhouse effect by capturing the infrared radiation reflected from the surface of the Earth in the troposphere. VOCs are also direct pollutants for human beings and plants, and contribute to odour pollution (ADEME 2016).

Concerning the S-VOCs, they are known as prominent air pollutants, especially volatile sulfur compounds such as DMS and DMDS. Even at very low concentrations these pollutants can produce unbearable odours (Wang *et al.* 2002).

Besides this, these pollutants are able to prevent infrared (IR) radiation from escaping into space. This leads to a rise in the temperature on our planet, causing the greenhouse effect (ADEME 2013).

Regarding the present work, DMDS has been chosen as the model molecule for S-VOCs. DMDS is an organo-sulfur compound with high toxicity and volatility, and strong corrosiveness. DMDS can be oxidized to sulfuric acid in the atmosphere (as a major component of acid rain) (Bentley *et al.* 2004). It is released through natural processes such as anaerobic or human activities (Guillard *et al.* 2007) and it can also be generated during poultry production (Krügera *et al.* 2009). It is commonly found in various industrial processes, waste streams and facilities for effluent treatment (Nevanperä *et al.* 2016).

1.2.3 The abatement of VOCs

There are two principle treatment possibilities for effluents containing VOCs: the recovery and the destruction methods. Recovery may be done by absorption, adsorption and condensation, or by membrane separation. For destruction, one can distinguish between radiation (UV, plasma, photo-oxidation radiation), biological processes (biofilters, bioscrubbers, biotrickling), thermal oxidation and catalytic oxidation. The applicability of these techniques depends on several parameters including gas flow, final temperature, the nature and concentration of VOCs, security, human skills and price. The selection of the processing method that best suits the VOC containing stream therefore requires a detailed analysis of each case (William and Lead 1997).

Recovery processes

The main idea of using recovery systems is to be able to recover the evaporated organic solvent. The recovery from an emission stream or air can be done using several techniques (Khan *et al.* 2000).

The *absorption* of a compound from the gaseous phase to the liquid phase is a mass transfer process. The efficiency of this technique is generally greater than 90%. This process is used primarily in the chemical, petrochemical and pharmaceutical industries and is the most adopted method to recover heavy products, e.g. ketones or tetrahydrofuran. The absorbing liquids should not be highly volatile or highly viscous and they should be non-toxic, non-flammable, and cheap and have a high wetting level. All these criteria are valid for water. The

cleaning of charged liquid can in principle be carried out by distillation, by liquid-liquid or solid-liquid extraction (Khan *et al.* 2000).

Adsorption is based on the property that a solid surface has in order to fix certain molecules reversibly by weak bonds of the Van der Waals type. In the process (Ruthven 1984), the treated gas flow passes through a column containing a solid adsorbent. At a certain point the adsorbent is saturated with the treated VOCs and at that moment the adsorbent needs to be replaced or regenerated. Adsorption phenomenon is exothermic by nature (Khan *et al.* 2000) and it is mostly used in the case of odours and Chlorinated Volatile Organic Compounds (CVOCs). The proper adsorbent choice depends upon the application, but activated carbon and styrene/divinylbenzene macroporous resins are the preferred adsorbents for VOC recovery (Khan *et al.* 2000). The efficiency of adsorption is dependent on the adsorbent material, it is typically 80–90% for activated carbons and 90–95% for zeolites (Khan *et al.* 2000).

The principle of *membrane techniques* is based on contacting the polluted effluent with a selective membrane. This technique allows separating and recovering, for example, simple gases (H_2, O_2, N_2 ...). The choice of a membrane depends on the physical state of the substances to be separated. Gas permeation and reverse osmosis are the techniques used in the application of solvent recovery (the recovery of VOCs) from air. These techniques are in the research stage and have yet to be commercialised, though a few pilot plant studies have been done with continuous monitoring of the performance (Khan *et al.* 2000). The efficiencies achieved so far are in the level of 90–99% (Deng *et al.* 1996). Table 1 shows the different processes of this technique, and the modes of transport and separation.

Table 1. The types of membrane processes used in industrial applications (Khan *et al.* 2000).

Process	Driving force	Mechanism
Pre-evaporation	Concentration	Selective physico-chemical transport of the solvent
Electro-dialysis	Electrochemical potential	Selective ion transport
Dialysis	Concentration gradient	Diffusive solute transport
Reverse osmosis	Pressure differential	Diffusive solvent transport
Gas permeation	Concentration gradient	Diffusion transport

Since 1986 many different kinds of membranes have been used in this technique as porous supports to the silicon rubber-coating layer – such as polymeric films,

composite silicon rubber membranes, polysulfone, polyhydantoine and polyimide – and, according to Deng *et al.* (1996), it was shown that controlling the conditions of the membrane preparation properly could produce membranes that have both high selectivity and reasonably high permeability.

Regarding the *condensation* treatment, the method comprises transforming the gaseous VOCs into a liquid or solid form by lowering the temperature to recover the condensed matter. The condensed matter is then treated for reuse or destruction (Barakat 2012, Khan *et al.* 2000). Condensation is most efficient for VOCs that have boiling points above 38 °C at relatively high concentrations (i.e. above 5000 ppm).

In the presence of a single substance, the temperature required to achieve condensation is determined by the recovery efficiency or emission limits objective. In the presence of a VOC mixture, the temperature to be reached is determined by the characteristics of the most volatile compound (Barakat 2012, Khan *et al.* 2000).

The condensation process is generally carried out in several stages, first is the cooling stage of the effluent and disposal of water, the second stage is recovering the less volatile compounds and the third is recovering the most volatile compounds. These recovered VOCs can be reused within the process, used as washing solvents during the equipment clean up, burned as an alternative boiler fuel, shipped off-site for disposal or resold for reuse by others. Concerning the recovered water, it should be sent to a wastewater treatment plant before final release. The cleaning efficiency of the condensation technique is around 70–85% (Khan *et al.* 2000).

Destructive processes

Destructive techniques are often employed when the VOC waste stream is odorous, toxic or carcinogenic. The treatment results in either the alteration or the destruction of VOCs. The oxidisers, while totally destroying the VOCs, emit CO_2, NO_x, CO and other oxidation products as by-products of the combustion process (Muzenda *et al.* 2013).

Oxidation (also called incineration) is the most used technique for the treatment of VOCs. All VOCs can be incinerated; however, some of them can generate secondary products during their oxidation that may be more aggressive or toxic than the original VOCs. In these cases, the use of additional emission treatment units for the secondary products may be required. Furthermore, the

chemical compatibility of the treatment equipment with the secondary products needs to be assessed. The oxidation reaction involves decomposing VOC into CO_2, H_2O and various oxides or oxidation products (Muzenda *et al.* 2013).

Oxidation processes are exothermic and a certain input of energy is needed to start the oxidation reactions. In addition to different heating possibilities for improving the energy efficiency of the process, two principles exist for heat recovery purposes, namely the recuperative and regenerative techniques. Recuperative oxidizers operate at temperatures from 760 °C to 815 °C, using for example a tube-in-shell stainless steel heat exchanger as an air pre-heater. Recuperative oxidizers are usually more economic than straight thermal incinerators. As for regenerative oxidizers, which use a high-density media such as a ceramic packed bed, are still hot from the previous cycle in order to preheat the incoming VOC-laden waste gas stream before entering the combustion chamber and this partially oxidises the gas stream. The regenerative thermal oxidizers are designed to destroy the air pollutants emitted from process exhaust streams at temperatures ranging from 815 °C to 980 °C (Muzenda *et al.* 2013).

The oxidation process can be thermal or catalytic, and choosing the type of oxidation is always based on technical and economic criteria. Thermal oxidation is thermal destruction that occurs in very specific conditions that involve the following factors (ADEL 2013):

- *Temperature*: the medium temperature must be above the auto-ignition temperature of the pollutant, often in the order of 900 °C.
- *Turbulence*: the mixture should be homogeneous.
- *Residence time*: the typical residence time is between 0.5 and 1.5 seconds. It must be long enough that the heat exchange can occur and that the kinetics have time to develop.

The catalytic oxidation technique is based on the same principle as thermal incineration, but the addition of a catalytic bed in the combustion chamber lowers the required oxidation temperature to the level of 200–450 °C by lowering the activation energy needed for combustion. Due to higher reaction rates, the residence time required is rather low. This results in a lower need for energy (lower consumption of fuel) for oxidizing the same effluent with respect to thermal oxidation. The catalytic treatment process consists of a preheating burner, a mixing chamber, a catalytic bed and a recovery system (a regenerative or recuperative system). The regenerative and recuperative heat recovery systems are identical to those detailed before (ADEL 2013, Muzenda et al. 2013). The

catalyst itself must present (as far as possible) the following qualities (ADEL 2013):

- High activity
- High selectivity
- A low pressure drop
- Satisfactory mechanical and thermal properties
- Long life
- Low cost.

Thus, as mentioned previously, catalysts allow the oxidizing reaction to occur at a lower temperature compared to thermal incinerators. This is also why similar purification efficiencies for waste gas flows at large thermal units can be achieved using smaller catalytic incinerators. Lower operating temperatures also reduce fuel requirements (Muzenda *et al.* 2013). For these reasons, catalytic oxidation has been adopted in this work: catalytic oxidation will be discussed in more detail later.

Next, three slightly different biological treatments are presented. In *biofilters*, microorganisms are fixed on a material (e.g. peat, fibres, compost, bark, wood shavings, ceramic beads) in a reactor in which a flow charged with VOC passes through the system, either from top to bottom, bottom to higher levels or horizontally. On this material, which is drained periodically, a biofilm is formed. During the treatment, VOCs are degraded by microorganisms (mainly bacteria). Bacteria use organic compounds as an indispensable source of energy for the degradation of a substrate (catabolism) and as a carbon source for their biosynthesis (metabolism) (ADEL 2013). In principle, a biofilter regenerates itself by the removal of the biological mass in excess. VOCs such as aldehydes, ketones, alcohols, ethers, esters and organic acids can degrade rapidly in bio-filters. Nevertheless, halogenated hydrocarbons and poly-aromatic hydrocarbons are not easily degradable (Muzenda *et al.* 2013).

In *bioscrubbers*, two steps are carried out separately: absorption is carried out in a spray scrubber (bioscrubbers are in principle only applied to water-soluble VOCs) and biodegradation occurs in an activation basin containing biomass in suspension. After washing, the water containing VOC is treated in an activated sludge reactor. The water circulates in a closed circuit: it first passes through the bioscrubber and then to the reactor and again back to the bioscrubber. The objective of designing the bioscrubber technology was to overcome two problems experienced with biotrickling filters, namely to improve the absorption of

pollutants into the liquid and to prolong the contact time of the microbes with the pollutants (Muzenda *et al.* 2013).

Biotrickling filters are a combination of bioscrubbers and biofilters. In trickling filters, the biofilm grows on the surface of the fixed support of an inert material (the filter) that has a structure ensuring the maximum contact area between the exhaust air and water. The microorganisms produce enzymes that are able to destroy VOCs: they are transformed into carbon dioxide, water vapour and organic mass (minerals). This filter is watered continuously. VOCs and oxygen are absorbed first by the irrigation water and then transported in an aqueous form to the support material. The biofilm around thus creates a liquid phase through which the VOC and oxygen are absorbed and transferred to the biofilm. The irrigation water may optionally contain a nutritional supplement and NaOH (neutralization). By this system, a large number of VOCs, both water-soluble and hardly hydrosoluble (toluene, xylene, benzene, methylene chloride), may be treated. However, VOCs with high chlorine concentrations are less easy to remove with this method (Muzenda et al. 2013).

The ultraviolet (UV) irradiation technique consists of the oxidation of VOC and some inorganic contaminants (like NH_4 and H_2S) in the presence of an oxidizing agent (e.g. ozone, peroxide) under UV irradiation of a wavelength between 150 and 250 nm at room temperature (Rt). The use of this technique requires secondary treatment to complete the purification, generally carried out by absorption or adsorption on activated carbon (Barakat 2012, ADEL 2013). The use of photocatalysts with UV irradiation requires temperatures < 40 °C and a relative humidity < 85% and, concerning the VOC concentration, it must be < 500 mgm^{-3}. If the temperature is lower than 40 °C but the relative humidity is higher than 85%, a heating element before the lamps has to be added in order to reduce the humidity (ADEL 2013). The number of UV lamps increases with either the VOC concentration or the requested abatement yield or both. Above 500 mgm^{-3} of VOC and at 95% abatement efficiency, the working costs for the UV-C lamps become high (ADEL 2013).

Plasma technology – better known for its use in surface treatment – eliminates VOCs by using non-thermal plasma ('cold oxidation'), which destroys VOCs by exposing them to the action of microwaves. These microwaves ionize oxygen in the air, thereby producing plasma of electrons and hydroxyl radicals which disassociate VOCs into carbon dioxide and water (Chang 2009). This technique is used in air pollution control and waste treatment, but it primarily applies to low concentration effluents. The investment and operating costs are low

compared to other techniques; it should by this fact perfectly fit small companies presenting low volume flow solvents (e.g. spray-paint booths). However, the plasma treatment often results in the formation of NO_x and ozone (Chang 2006).

Table 2 summarizes all the above-mentioned techniques and their efficiencies.

Table 2. A summary of efficiencies of different VOC treatment techniques (ADEL 2013).

Technique	Efficiency [%]	Flows [m^3h^{-1}]	Concentrations [gm^{-3}]
Regenerative thermal oxidation	95–99.9	100–300 000	1–8
Recuperative thermal oxidation	95–99.9	100–30 000	6–30
Regenerative catalytic oxidation	95–99.9	70 000	0–6
Recuperative catalytic oxidation	95–99.9	100–300 000	1–12
Adsorption	95	100–1 000 000	1–50
Absorption	90–98	100–1 000 000	2–50
Biofiltration	90	5000–1 000 000	0.2–3
Condensation	80–90	2000	10vol-%
Membrane	50–90	600–6000	2–50

According to all that was described before and among the destruction methods, thermal destruction methods are the most commonly used methods. The coming section will concentrate specifically on the details of the catalytic oxidation of VOCs.

1.3 Catalytic treatment of VOCs

Catalytic oxidation is a rather mature technology that has been used since the 1940s. Over the years, through improvements in the field of catalysis and reactor technology, catalytic incineration has become less expensive and more energy efficient (Jennings *et al.* 1985).

All the VOCs can be converted into inorganic compounds by total oxidation. According to the elemental composition of the VOCs that are to be destroyed, the compounds formed are either only CO_2 and H_2O, or a mixture containing CO_2, H_2O and the oxidation products of other atoms (e.g. nitrogen (NO, NO_2); chlorine (HCl), sulfur (SO_2)). These are secondary pollutants that need to be taken into

account. Several parameters are important to consider in order optimizing thermal or catalytic oxidation to improve the purification efficiency (Jennings *et al.* 1985).

The oxidation of VOCs needs certain activation energy before the reaction can start. The utilization of catalysts makes the activation energy barrier lower for oxidizing VOCs and thus reduces the required reaction temperatures. By using a catalyst, only one third of the energy is needed compared to thermal oxidation. The activation energy level depends on how strong the chemical bonds are between hydrogen (H_2), carbon (C) and other possible atoms. This means that the required reaction temperatures vary quite a lot case by case (Kamal *et al.* 2016).

The activation energy needed to start up the oxidation reactions is optimized by the presence of a catalyst (Clark 2013b). As a consequence, the reactions can already start at 150 °C and accelerate rapidly up to 300 °C. Initially, when the reactions start, their rate is controlled by chemical kinetics, which means that the slowest step in the heterogeneous reaction is the reaction on the catalyst surface, but over 300 °C, the situation changes. The reaction rate on the catalyst surface accelerates exponentially and then the slowest step in the reaction chain is the diffusion of the reactants into the catalyst pores, the so-called internal mass transfer. The internal diffusion rate depends on the shape of the flow channels and the temperature (Lylykangas 2010).

The most important advantage of catalytic oxidation over thermal oxidation is its an approximately 500 °C lower reaction temperature, which is the reason why it needs less energy to heat the gas stream up to operational temperature. In the case of a relatively small VOC application with a capacity of 10000 Nm^3h^{-1}, it will need nearly 28 MW of power to heat it to thermal oxidation temperature and slightly less than 1 MW to heat it to catalytic oxidation temperature. If heat exchangers have 90% efficiency, the heat loss is respectively 280 kW and 100 kW. This is the motive for why some existing regenerative thermal oxidizers (RTOs) are changed to regenerative catalytic oxidizers (RCOs) by installing catalysts in the burning chambers (Lylykangas 2010). Other advantages of catalytic oxidation over thermal oxidation are a very high (99.9%) conversion rate, negligible NO_x and CO emissions, and small equipment sizes because of the short residence time (Lylykangas 2010).

In this study, heterogeneous catalysis (where the catalyst is in a different phase from the reactants [Clark 2013a]) with two different phases, which involves a solid catalyst and the reactants as gases, is applied. In general, the catalyst can consist of both of the following (Bartholomew and Farrauto 2006):

- *Active species* that are distinguished by two major types of catalyst – the catalysts based on precious metals (e.g. platinum, palladium, rhodium) and those based on metal oxides (Cr-based oxides, Fe, Mo, W, Mn, Co, Cu, Ni)
- *An inorganic high surface area support,* such as γ-Al_2O_3, on which the active phase is deposited.

Catalyst particle size and shape distribution provide useful information for optimizing the catalytic reactions with a high yield (Akhtar *et al.* 2014). The size and shape of the catalyst granules can play an important role in attaining the goals of both minimizing pore diffusion effects in the catalyst particles (which requires small sizes) and achieving the pressure drop across the reactor (which requires large particle sizes). For these reasons, many structures of catalysts exist. Microporous materials – such as activated carbons, metal organic frameworks, zeolites and aluminum phosphates – are suitable for catalysis and separation applications (Akhtar *et al.* 2014). Usually these high surface area materials are produced in particulate forms but need to be transformed into larger structures for real applications (Akhtar *et al.* 2014). The structuring of powder form catalysts facilitates mass transfer, reduces pressure drop and improves heat management as well as mechanical and chemical stability (Akhtar *et al.* 2014). In the gas treatment, structures such as extrudes, the coatings of scaffolds and honeycombs are used in order to ensure enough free volume in the reactor to reach a high throughput, a good ratio of catalyst surface and reactant volume, because it is crucial for controlling the reaction kinetics and high permeability within the reactor in order to have a stable and high flow of reactants (HORIBA 2016).

The important characteristics of catalysts for an industrial process depend mainly on the following three properties: activity, selectivity and stability (deactivation behaviour). Which of these functions is the most important? It is generally difficult to decide because the demands made on the catalyst are different for each process. First, let us define the above-mentioned terms (Hagen 2006).

Activity is a measure of how fast one or more reactions proceed in the presence of a catalyst. Activity can be defined in terms of kinetics or from a more practically oriented viewpoint. In a formal kinetic treatment, it is appropriate to measure reaction rates in the temperature and concentration ranges that will be present in the industrial reactor.

The *selectivity* of a reaction is the fraction of the starting material that is converted to the desired product. It is expressed by the ratio of the amount of

desired product to the reacted quantity of a reaction and therefore gives information about the course of the reaction. In addition to the desired reaction, parallel and intermediate reactions can also occur.

Stability is related to the lifetime of a catalyst in industrial reactors. It is determined by chemical, thermal and mechanical stability. The stability of the catalyst can be affected by several factors, including decomposition, coking and poisoning. Catalyst deactivation can be followed by measuring activity or selectivity as a function of time.

To summarize, it is very important to develop novel catalysts with high activities for energetically challenging reactions, with high selectivity to valuable products and with extended lifetimes for good durability. Highly selective catalysts will help to reduce the energy consumption required for product separation and waste disposal processes in the chemical industry.

As is well known, the catalysts used for the oxidation of VOCs can be classified into three major groups: (1) *noble metals catalysts* (Papaefthimiou *et al.* 1997, 1998c, Tsou *et al.* 2005) are expensive and can be deactivated by sintering or poisoning (Liotta 2010) and alone they are not always selective enough (Ojala *et al.* 2011); (2) *metal oxide catalysts* (Barbero *et al.* 2006, Bastos *et al.* 2012), such as transition and rare earth metal oxides – the most commonly used metal-oxide catalysts include copper oxide, manganese dioxide, iron oxide, nickel oxide, chromium oxide and cobalt oxide (Galvita *et al.* 2014; Garcia *et al.* 2010; Huang *et al.* 2010; Morales *et al.* 2013; Solsona *et al.* 2011; Xia *et al.* 2009); and (3) *mixed-metal catalysts* (Gangwal *et al.* 1988; Garcia *et al.* 2006) – the performance of metal-oxide catalysts can be improved by combining two or more oxides to introduce a synergistic effect for the removal of VOCs (Yu *et al.* 2010, Morales *et al.* 2006, Liotta *et al.* 2008, Vasile *et al.* 2013). Table 3 presents examples of the catalysts used for the oxidation of VOCs reported in the open literature.

Table 3. Some reported catalysts for the oxidation of VOCs.

Catalysts	VOCs	References
Pd/Nb_2O_5	Toluene	Rooke et al. 2015
Au/CeO_2-ZrO_2	Propane	Ali et al. 2015
Pd/Co_3O_4	Xylene	Wang et al. 2015
Pt/Al_2O_3	n-butanol	Sedjame et al. 2014
Pd/ Al_2O_3	o-Xylene	Huang et al. 2008b
Pd/Co_3O_4	o-Xylene	Wang et al. 2013b
Au/Fe_2O_3	Toluene	Han et al. 2014
Pt/CeO_2	n-butanol	Sedjame et al. 2014
Nb_2O_5	Toluene	Rooke et al. 2015
Co_3O_4	Propane	Solsona et al. 2008
CuO	Ethyl acetate	Chen et al. 2013
Co_3O_4	1, 2-Dichloroethane	de Rivas et al. 2012
$PtCu/Al_2O_3$	Dimethyldisulfide	Darif et al. 2016
Au/Al_2O_3	Dimethyldisulfide	Nevanperä et al. 2016
$PtPd/Al_2O_3$-CeO_2	Perchloroethylene	Pitkäaho et al. 2011
V_2O_5/TiO_2-CeO_2	Methanol+methylmercaptan	Mouammine et al. 2013
Cu/TiO_2	Dichloromethane	El Assal et al. 2013

1.3.1 The oxidation of S-VOCs.

Reduced sulfur (TRS) compounds – such as DMS, DMDS, methyl mercaptan (MM) and H_2S – are the main constituents of the emissions of the pulp and paper industry. These compounds are malodorous and can have potentially serious effects on the quality of the environment and human health (EPA 2005, EPA 1997). According to the VOC definition, DMS and DMDS belong to the group of S-VOCs. More detailed information on the impacts of S-VOCs is given in Subsection 1.2.2.

The thermal and catalytic oxidation can manage emission streams that have high concentrations of VOCs and S-VOCs. High cleaning efficiency can be achieved with incinerators at operating temperatures higher than 600 °C (Muzenda *et al.* 2013).

The deactivation of the catalysts cannot be prevented, or at least it poses substantial challenges in the design and operation of a large-scale catalytic process. A catalyst may be poisoned by several contaminants present in the feed. In the case of S-VOC catalysts, the surface and pores may be poisoned, especially by sulfur present in the feed, and/or the catalysts can be exposed to sintering, resulting in a decrease in the active surface which lowers the catalytic activity.

More detailed information about different deactivation mechanisms will be presented in Chapter 2.

The choice of the most optimal catalyst is based on the activity, selectivity and stability. The most used catalysts for the treatment of VOCs and S-VOCs contain noble metals, such as Pt and Pd (Yu Yao 1984, Burch 1994, Rossiin 1989, Katona *et al.* 1991), but unfortunately these noble metal–based catalysts are susceptible to poisoning by the sulfur compounds that exist and are formed during the S-VOCs' oxidation reactions. Catalysts based on metal oxides are generally inexpensive, such as catalysts containing copper oxide and metallic molybdenum, and they are well known for their low temperature activity and resistance against sulfur (Wang *et al.* 1997, Wang *et al.* 1998, Wang *et al.* 2002, Kharas 1992, Kucherov *et al.* 1995, Neyestanaki *et al.* 1995, Severino *et al.* 1986). According to the previous studies, the activity and stability of the copper-based catalysts, such as $CuO/\gamma\text{-}Al_2O_3$, can be promoted by molybdenum for oxidative decomposition $(CH_3)_2S_2$ (Wang *et al.* 1998). Accordingly, the $CuO\text{-}MoO_3/\gamma\text{-}Al_2O_3$ catalyst shows higher activity and resistance towards deactivation by sulfur compounds than $CuO\text{-}Cr_2O_3/\gamma\text{-}Al_2O_3$. In comparison to other non–copper based catalysts, the sulfur deactivation of catalysts, such as MnO/Fe_2O_3 and Cr_2O_3/Al_2O_3, during the oxidation of low input concentrations (100 ppm) of S-VOCs like DMS or DMDS has been studied (Wang *et al.* 1997, Wang *et al.* 1998, Wang *et al.* 2002, Chu *et al.* 2003). The results showed that both Cr_2O_3/Al_2O_3 and MnO/Fe_2O_3 catalysts are susceptible to catalytic poisoning, especially at operating temperatures below 350 °C. For these reasons, Cu based catalysts were chosen in the present study to be the catalysts in the catalytic oxidation of DMDS.

1.4 The aims of the study

The main aim of this study is to generate new knowledge on the catalytic oxidation of S-VOCs. To reach this objective, DMDS is used as a model molecule since it is regularly present in industrial effluents and it is more difficult to oxidize than the other S-VOCs observed in the emissions of pulp mills, for instance $(CH_3)_2S$ and CH_3SH. In the development of the most advantageous catalytic materials that are active, selective and durable, it is necessary to tackle the main obstacle to S-VOC catalytic oxidation – the poisoning caused by sulfur. We are actively seeking to understand the deactivation phenomenon by sulfur in order to gain more information on how to develop sulfur tolerant catalysts. The detailed objectives of the thesis are listed below:

- To develop economical catalytic materials for the total oxidation of DMDS that are active, selective and sulfur resistant
- To study the phenomena related to sulfur deactivation and to develop materials that have a good sulfur resistance
- To establish the correlations between the different textural and structural properties and the redox and acid-base properties of the catalysts and the catalytic performances of the materials.

Sulfur deactivation is studied based on the catalysts that are aged industrially under S-VOC oxidation conditions and the accelerated ageing tests performed on the laboratory scale. The objectives of this study in relation to achieving the aims are summarised in Figure 2.

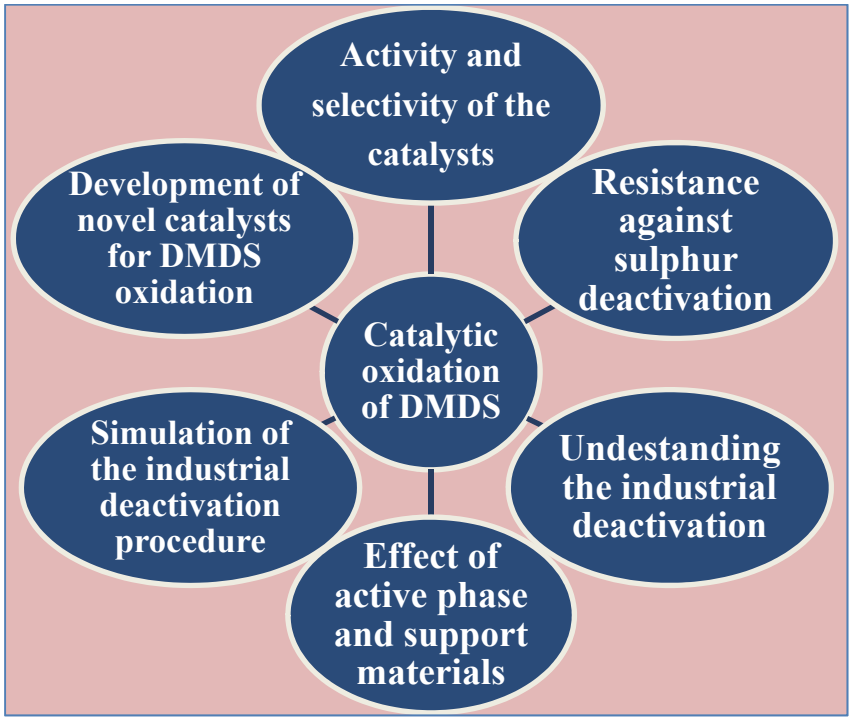

Fig. 2. The scope of the thesis.

2 Catalyst deactivation

Heterogeneous catalysts are exposed to one of the major problems related to the loss of catalytic activity with time-on-stream, i.e. deactivation. This process is both chemical and physical in nature and occurs simultaneously with the main catalytic reactions. Deactivation can be unavoidable but it can be slowed down and sometimes prevented, and some of its consequences can be avoided (Forzatti *et al.* 1999). Different causes for catalyst deactivation and the physico-chemical changes related to various deactivation processes will be discussed in the following sections.

Four classes of deactivation mechanisms were named by Bartholomew (2001) – i.e. poisoning, coking or fouling, sintering and phase transformation – although other classifications also exist. Other mechanisms for deactivation include masking and the loss of the active elements via volatilization, erosion and attrition (Bartholomew 2001).

2.1 Poisoning

Poisoning (Oudar *et al.* 1958, Maxted 1951, Hegedus *et al.* 1980, Hegedus *et al.* 1984, Butt *et al.* 1982, Barbier *et al.* 1985, Bartholomew 1987, Delmon 1987, Rostrup-Nielsen *et al.* 1987) is the loss of activity due to the strong chemisorption of impurities present in the feed stream on the active sites of catalysts. An example of poisoning is when the catalysts based on platinum supported on alumina are deactivated by sulfur poisoning. The study of Chang *et al.* (1997) showed that the deactivation of a catalyst may be due to the adsorption of H_2S and the formation of new compounds (reconstruction) like sulfates and sulfides (PtS). Poisons like sulfur may cause significant deactivation even at very low concentrations due to the formation of strong and irreversible metal-S bonds. Sulfur chemisorbs onto and reacts with the active catalyst sites, preventing reactants' access (the geometric effect) or modifying the adsorptivity of the other species essentially by the means of the electronic effect, so that the catalyst performance is definitively altered (Forzatti *et al.* 1999). Usually, a distinction is made between poisons and inhibitors (Haber *et al.* 1995). Poisons can be selective or non-selective. In the latter the poison chemisorption occurs in a uniform manner, independent of the nature of the surface sites on the catalyst. As a result, the net activity of the surface is a linear function of the amount of poison chemisorbed. In the case of selective poisoning, the characteristics of the active

sites (e.g. the acid strength) affect the chemisorption of a poisoning compound, and accordingly the strongest active sites will be poisoned first. This may lead to various relationships between catalyst activity and the amount of poison chemisorbed (Grove 2003).

Poisons can be also classified as reversible or irreversible. In the first case, the poison is not too strongly adsorbed and if it is removed from the feed, catalyst activity is regained. In the case of irreversible poisoning, activity cannot be regained and there is irreversible damage (Forzatti *et al.* 1999).

Sulfur-containing compounds (e.g. H_2S, SO_2, S-VOCs: DMS and DMDS) are potential poisons for all the catalytic processes employing metals as the primary active phase (Grove 2003). These poisons are generally considered temporary, although their effect can be permanent depending on e.g. the process conditions and ease of regeneration. Platinum group metal (PGM) catalysts react easily with H_2S to form sulfides and with SO_2 to form sulfates. As mentioned previously, sulfur can be a significant deactivation agent even at very low concentrations due to the formation of strong metal-S bonds that prevent the access of the reactants to the active sites. As a consequence, non-selective side reactions can occur in the presence of stable metal-adsorbate bonds, which can be a reason for the surface chemistry modifications (Dunleavy 2006).

2.2 Coking

Coke formation mechanisms have been studied and reported in several reviews (Rostrup-Nielsen and Trimm 1977, Trimm 1983). For catalytic reactions involving hydrocarbons (or even carbon oxides), the formation of coke results when some side reactions occur on the catalyst surface and carbonaceous by-products deactivate the catalyst, either by covering the catalyst surface or by pore blocking. A distinction is made between coke and carbon. Usually carbon is considered as the product of CO disproportionation ($2CO \rightarrow C + CO_2$), while coke is referred to as the material originated by the decomposition (cracking) or condensation of hydrocarbons (Forzatti *et al.* 1999).

2.3 Sintering

Sintering generally refers to the loss of active surface via structural modifications of the catalyst. This is usually a thermally activated physical process. Sintering may occur both in supported and unsupported catalysts. The reduction of the

active surface area is caused by the agglomeration and coalescence of small metal crystallites into larger ones with lower surface-to-volume ratios in the case of supported metal catalysts. Two different but quite general mechanisms have been proposed for the sintering of unsupported metal catalysts, i.e. the atomic migration model and the crystallite migration model. In the first case, metal atoms escape from a crystallite and then they transport across the surface of the support (or in the gas phase), causing an increase in the crystallite size since larger crystallites are more stable, small crystallites reduce in size and the larger ones increase and thereby a decrease in surface area takes place. For the second mechanism, sintering occurs due to the crystallites' migration along the support surface, resulting in the collision and coalescence of two crystallites (Forzatti *et al.* 1999).

There are early studies on the effects of heating on the metal dispersion of the supported catalysts. The research of Wanke and Flynn (1975) showed that by using a Pt/η- Al_2O_3 catalyst, after 70 h in air at 700 °C the dispersion of Pt decreased dramatically (a change of 97%). Other experiments with these types of catalysts showed similar results (Wanke & Flynn 1975). As is known, the sintering of metals and oxides can be affected by temperature. This effect is mainly physical in terms of the driving forces for the dissociation and diffusion of the surface atoms, which are both relative to the absolute melting point temperature (T_{mp}) (Morris 2015). Thus, by increasing the temperature, the mean lattice vibration of surface atoms increases. When the Hüttig temperature ($0.3T_{mp}$) is attained, the dissociation of the less strongly bound surface atoms at the edges and corner sites occurs and they diffuse freely over the surface. At the Tamman temperature ($0.5T_{mp}$), the atoms in the bulk become mobile as well. Consequently, the sintering rates are considerable if the temperature is over the Hüttig temperature and very high near the Tamman temperature, and, therefore, the Hüttig or Tamman temperatures are related to the relative thermal stability of metals or metal oxides (Moulijn 2001).

2.4 Solid-state transformation

Solid-state transformation can be understood as an extreme form of sintering, occurring at high temperatures and leading to the change of the crystalline phase. This deactivation may happen for both supported metal catalysts and metal oxide catalysts. In the first case we can observe the incorporation of the metal into the support, at temperatures near 1000 °C. In the case of metal oxide catalysts or

supports, the transformation of one crystalline phase into a different one can occur, like the conversion of γ- Al_2O_3 to δ-Al_2O_3, with a decrease in the specific surface area from about 150 m^2g^{-1} to less than 50 m^2g^{-1} (Forzatti *et al.* 1999).

2.5 Other types of deactivation

Masking or blocking pores is caused by e.g. the physical deposition of substances on the catalyst that block the access of the reactants. Masking may occur during, for example, hydrotreating processes, where metals in the feedstock deposit on the catalyst's external surface or, in the case of automotive exhaust converters, by the deposition of P and Si compounds (Forzatti *et al.* 1999).

Catalysts may also suffer from the loss of the active phase via volatilization, e.g. Cu in the presence of Cl with the formation of volatile $CuCl_2$ or the formation of volatile carbonyls by the reaction of metals with CO (Bartholomew 1984).

The deactivation may be also mechanical by nature. The loss of catalytic material due to attrition in moving or fluidized beds is a serious source of deactivation where the catalyst is continuously scraped away. Also, the loss of wash-coat on the monolith honeycomb catalysts may occur, especially when the gases are flowing at high linear velocities and/or when rapid changes in temperature occur (Forzatti *et al.* 1999).

2.6 Deactivation mechanisms relevant to S-VOC oxidation

The most probable deactivation mechanisms that can occur in S-VOC catalysts are sintering, in the case of noble metal catalysts working at high temperatures, and certainly poisoning by sulfur since sulfur is present in the feed with the reactants and also can be emitted as a reaction product in the form of SO_2. The molecules of SO_2 can also easily be oxidized to SO_3 in the presence of a highly active catalyst and oxidative conditions. It is known that the active site of noble metal oxidation catalysts, e.g. Pt/Al_2O_3, is PtO_x particles. In the gas stream SO_2 converts to SO_3 with excess oxygen and then PtO_x reacts with SO_3 to form less active species (Bartholomew and Fuentes 1997). Also the reaction of SO_3 with the γ-Al_2O_3 support that produces $Al_2(SO_4)_3$ is a serious cause of the deactivation of alumina-supported catalysts in several catalytic processes (e.g. diesel exhaust abatement and SCR). In these cases, TiO_2 or SiO_2 supports are used rather than Al_2O_3 and in diesel or automotive exhaust gas treatment the alumina catalyst is stabilized by the addition of BaO, SrO or ZrO_2 (Bartholomew and Farrauto 2006,

Peter-Hoblyn *et al.* 1999, Manson 2000, Deeba *et al.* 2000, Dry 1981, Huber *et al.* 2001, Busca *et al.* 1998).

2.7 Regeneration

Regeneration means the restoring of the activity of a deactivated catalyst, at least partly, in which case the complete replacement of the catalyst is not immediately needed. In real applications the effects of poisons cannot usually be completely avoided but can be reduced, for example by a purification system designed to protect the catalyst. Non-optimized purification may lead to unnecessary costs associated with the loss of process economics and catalyst regeneration or replacement. These can be insignificant compared to an unscheduled production loss at a major catalytic unit (Morris 2015).

The possibility to regenerate a catalyst depends on the reversibility of the deactivation process. For example, carbon and coke formation is rather easily reversed through gasification with hydrogen, water or oxygen. Sintering on the other hand is generally irreversible, although metal re-dispersion is possible in certain cases. Some poisons or foulants can be selectively removed by chemical washing, mechanical treatments, heat treatments or oxidation (Heck *et al.* 1995, Trimm 2001). The decision to regenerate/recycle or discard the entire catalyst depends largely on the rate of deactivation. If deactivation is very rapid, as in the coking of cracking catalysts, repeated or continuous regeneration becomes an economic necessity. The disposal of catalysts containing non-noble heavy metals (e.g. Cr, Pb or Sn) is environmentally problematic and should be the last choice (Trimm 2001).

The catalysts used in the oxidation of S-VOCs most probably suffer from poisoning by sulfur, and much of the previous literature has focused on the regeneration of the sulfur-poisoned catalysts used in hydrogenation and steam reforming (Bartholomew *et al.* 1982, Rostrup-Nielsen 1971). Less literature is focused on the regeneration of the sulfur-poisoned catalysts used in the oxidation of S-VOCs. The regeneration of sulfur-poisoned noble metals in air is more easily accomplished than with steam, although it is frequently attended by sintering. (Maxted 1951). It was reported that sulfur-aged Pd catalysts can be partly regenerated under a reducing atmosphere, such as H_2 (Lamper *et al.* 1997, Hoyos *et al.* 1993, Arosio *et al.* 2006, Leprince *et al.* 2004). Another example of regeneration was proposed for the sulfur-poisoned Pd/Al_2O_3 noble metal monolith catalyst used in the oxidation of CO and hydrocarbons (CH_4, C_2H_6 and C_3H_8). In

order to regenerate the catalyst, the gas stream was changed to a reducing atmosphere (N_2). As a result, the sulfates on PdO_x particles [$PdSO_4$] are quickly reduced and released from the catalyst as SO_2 at 400 °C (Hu and Williams 2007). However, more research should be dedicated to how the regeneration of poisoned S-VOC oxidation catalysts could be carried out.

3 Materials and methods

In this chapter the methods used in the preparation of catalysts and supports are detailed and different physico-chemical techniques for their characterizations are described. Part of the described characterization methods were also used in connection with studying industrially aged metallic monolith catalysts.

3.1 The synthesis of catalytic materials

The self-made catalysts used in this work are in powder form and their preparation involves three stages: support preparation, deposition of the active phase and thermal treatment to activate the catalytically active species. Three types of metal oxides were prepared by a sol-gel method – i.e. Al_2O_3, SiO_2 and Al_2O_3-SiO_2 – which were then used as supports for three catalytically active materials: Pt, Cu and Pt-Cu.

Nowadays, the most active catalysts are those that present a very large number of metal sites of nanoscale grains dispersed on a high surface area support. For this type of a catalyst, three techniques are mainly used in preparation: liquid impregnation (Fazle Kibria *et al.* 2002, Nagaraju *et al.* 2002, Ago *et al.* 2004), the sol-gel method (Kukovecz *et al.* 2000, Valiente *et al.* 2000, Shen *et al.* 2004) and co-precipitation (Avdeeva *et al.* 1999, Meier *et al.* 1999, Peigney *et al.* 1999).

The disadvantages of all these methods of preparation are that the methods consist of many steps and involve the use of a solvent. This requires the inevitable stages of drying, calcining and reduction, which create uncertainty about the reproducibility of the synthesis of the final catalyst. In addition, the use of any solvent other than water implies environmental restrictions and the cost of their eventual elimination and reprocessing (Perego and Villa 1997).

The existing special interaction between the metal and its support plays a vital role in the synthesis of catalysts. It affects the morphology, dispersion and the electronic properties of the active phase, and therefore the course that gives the active sites in the desired catalysts (Vander Wal *et al.* 2001). The metal-support interaction occurs via a charge transfer between the metal and the support. This can originate from different reactions (Vander Wal *et al.* 2001): oxidation/reduction, Lewis acid/base and donor/acceptor reactions. The density, nature and properties of the surface of the support functions control the quality of the metal-support interaction and affect the catalytic properties by influencing the electronic structure and the dispersion of the active phase (Scokart *et al.* 1982).

In addition to the intrinsic properties of metals and materials, the catalyst preparation method, and more specifically the experimental conditions (temperature, pressure, the presence of a solvent), can affect the physical or chemical properties of the support during the implementation of the contact with the active phase and thereby can affect and modify interactions and catalytic properties (Rojas 2013).

In this thesis work the sol-gel method is used in the preparation of supports. It was chosen from among others because of certain advantages. The sol-gel method is a process that results in the continuous transformation of a solution into a hydrated solid precursor (a hydrogel). Sol-gel methods have been acknowledged for their flexibility, which allows control of the texture, composition, homogeneity and structural properties of the finished solids. The applications of the sol-gel method to catalyst preparation were reviewed in 1992 by Cauqui and Rodriguez-Izquierdo. This method offers a range of possibilities to prepare tailored materials, such as dispersed metals, oxide catalysts and chemically modified supports (Schwarz 1995). There are some disadvantages to the sol-gel process, such as the cost of the raw materials or chemicals may be high and cracking often occurs during drying (Carter & Norton 2007).

The three support materials used in this work – namely Al_2O_3, SiO_2 and Al_2O_3-SiO_2 – were prepared by a sol-gel method. The details of the preparation are described in the following subsections.

3.1.1 Preparation of the Al_2O_3 support

The procedure for the preparation of the alumina support comprises three steps; the preparation of boehmite gel, drying and calcination. The preparation of Al_2O_3 started with the synthesis of boehmite gel, which was made following the description of Yoldas (1975). During the synthesis, a known mass of aluminium tri-sec-butoxide ($Al[OCH(CH_3)C_2H_5]_3$, 97%, Alfa Aesar) was mixed with ultrapure water corresponding to the molar ratio $n(H_2O)/n(Al) = 100$. The mixture was then homogenized under stirring at 60 °C for 1 h. Then, a volume of hydrochloric acid (HCl), accounting for 1 mol-% of Al, was added to catalyse the peptization process. The temperature was programmed at 80 °C and the mixture was maintained at this temperature with stirring for 2 h. During the synthesis, the beaker was covered with a watch glass to reduce the water evaporation. The resulting xerogel was then dried overnight at 120 °C in a ventilated oven. The

white solid, called boehmite, was then ground and calcined at 550 °C for 5 h with a heating rate of 5 °Cmin^{-1}.

3.1.2 Preparation of the SiO_2 support

The SiO_2 sol was prepared by the reactions of hydrolysis and the condensation of tetraethoxysilane (Si $(OC_2H_5)_4$, 98%, Aldrich) in the presence of concentrated nitric acid (HNO_3, 90%, Aldrich). The amounts of reactants used in the preparation (in molL^{-1}) were as follows: n(TEOS)/n(EtOH)/n(H_2O)/n(HNO_3) is equal to 1/8/6/0.3. In the next preparation stage, the mixture was stirred for 3 h, and then it was dried at room temperature for about three months and finally calcined at 550 °C with a temperature rise of 5 °Cmin^{-1}.

3.1.3 Preparation of the alumina-silica support Al_2O_3-SiO_2

The gel $(Al_2O_3)_{0,8}$-$(SiO_2)_{0.2}$ was also synthesized according to the procedure described by Yoldas (1975) but modified with a step for adding the silica dopant. For this purpose, aluminium tri-sec butoxide ($Al(O\text{-}sC_4H_9)_3$, 97%, Aldrich) was introduced into a beaker and ultrapure water was added following the molar ratio n(H_2O)/n(Al) = 100. The mixture was homogenized with stirring at 60 °C for 1 h. Then, a few drops of hydrochloric acid (HCl, 37%, Merck) were added to catalyse the peptization process. The acid was introduced along with the silicon precursor, tetraethoxysilane ($Si(OC_2H_5)_4$, 98%, Aldrich). Then the temperature was raised to 80 °C and maintained for 2 h. During the preparation, the reaction mixture was kept under stirring and the beaker was covered with a watch glass to limit the water evaporation. In these synthesis conditions (excess water, acid and 80 °C), hydrated silicon doped boehmite (AlO(OH)-Si-nH_2O) was obtained.

The obtained xerogel, that has a whitish appearance, was dried in a ventilated oven at 120 °C overnight. The solid (white, transparent) that was formed was then ground and calcined in an oven at 550 °C for 5 h with a temperature rise of 5 °Cmin^{-1}.

3.1.4 Preparation of the monometallic catalysts

The wet impregnation method was chosen for depositing the active phase on the supports. This procedure ensures the homogeneity of the adsorbed phase through the contact that is made in the same way at any point on the surface.

Monometallic catalysts prepared during our work were 0.3% Pt/Al_2O_3 and 10% Cu/Al_2O_3.

To prepare the wanted monometallic catalysts, a known quantity of a support calcined at 550 °C was placed in a beaker and then impregnated with a volume of metal precursor solution. In the case of Pt, the objective was to deposit 0.3% by weight of Pt metal relative to one gram of the final catalyst. For that purpose, a needed mass of hexachloroplatinic acid ($H_2PtCl_6 \cdot xH_2O$, Alfa Aesar, 99.9%) was dissolved in ultrapure water. In the case of the copper oxide catalyst, the objective was to deposit 10% by weight of Cu metal relative to one gram of the final catalyst, and for that reason, the needed mass of copper nitrate ($Cu(NO_3)_2 \cdot 3H_2O$, Sigma Aldrich, 99.9%) was dissolved in ultrapure water too. In both cases of impregnation, the mixture was stirred using a mechanical stirrer for 24 h and then dried on a sand bath at 60 °C. This temperature was selected in order to avoid the decomposition of the precursor salt.

To activate the catalysts, two steps are usually necessary: calcination and reduction. The calcination treatment transforms the precursor metal salts into metal oxides. The reduction is done to change the metal oxidation state to zero, if needed. In the present work, only calcination was used. After drying at 60 °C, the sample was calcined in an oven at 550 °C for 5 h with a temperature rise of 5 $°C min^{-1}$.

3.1.5 Preparation of bimetallic catalysts

Bimetallic catalysts were prepared by co-impregnation of the supports by simultaneously introducing the two metal precursors of copper and platinum (the same used in the preparation of the monometallic catalysts). Otherwise, the same procedure was followed as in the case of monometallic catalysts.

3.2 Catalyst characterization

The catalysts were analysed using different characterization methods to study the textural and structural properties in order to verify the composition and other characteristics of the materials and to gain information to explain their catalytic performance.

3.2.1 Optical emission spectrometry with inductively coupled plasma

Optical emission spectrometry with inductively coupled plasma (ICP-OES) is used to analyse a large number of elements with very good detection limits of the order of ppb. In the current work, the technique was used to determine the metal content of monometallic and bimetallic catalysts. The inductive plasma may be generated by directing the energy of a high frequency generator to a suitable gas, usually argon (Rouessac 2007).

The ICP-OES apparatus consists of a light source, a spectrometer, a detector and a computer for data processing. The apparatus used in the current study was a Perkin Elmer Optima 2000 DV device. The plasma used was an argon plasma, which can be operated at the temperatures between 6 000 to 10 000 K.

Before the analysis, the catalysts were dissolved in aqua regia (a mixture of concentrated nitric and hydrochloric acids). The sample was then transported to the centre of the plasma torch, where the elements of the sample were atomized and ionized at a high temperature. The photons that were emitted at specific wavelengths were analysed by a UV-visible spectrometer. The radiation energy was then converted by a photomultiplier. The detection limits of the ICP analysis for most elements is less than 0.005 mgL^{-1}, the accuracy of the apparatus is about 1–3% and the analytical range is from trace (μgg^{-1}) to main (%) components (PIS 2013).

3.2.2 X-ray fluorescence

X-ray fluorescence (XRF) is an atomic spectral property, generally recognized as a very precise method that is presently exploited to provide qualitative and quantitative information on the elemental composition of all types of samples. The principle of operation involves irradiating the sample, either with an X-ray beam or by bombardment with particles (such as electrons with sufficient energy) in order to monitor the resulting XRF emitted by the sample (Rouessac 2007).

The amount of certain elements, such as the sulfur content on the catalysts, was analysed by using XRF. The measurements were performed using a PANalytical Axios instrument. This apparatus allow the simultaneous measurement of up to 28 elements, with a minimum of a two-second measurement per sample.

About 100 mg of the samples were ground into fine powders and then mixed with 8 g of flux, 66:34. The final samples were taken to a melting machine operated at 1150 °C and then the produced samples were analysed.

3.2.3 X-ray diffraction

The X-ray diffraction (XRD) measurements were primarily used to identify the different formed phases of the prepared crystalline material and also to provide information on unit cell dimensions. The diffractograms were obtained at room temperature with a powder diffractometer, BRUKER-5500, using a Cu anode tube ($\lambda K\alpha 1$ = 1.5406 Å) and operating at 40 kV and 30 mA with a graphite monochromator, which eliminates the K_β radiation (1.5186 Å) and the possible fluorescence. The sample was placed in a sample holder rotating on its vertical axis so that the crystallites were oriented in a random manner. The diffraction patterns were recorded in the angular range of the diffraction beam 2θ between 5°, 10° and 90° with a step of 0.025° and an acquisition time of one second per step.

The average crystallite size is determined using the Scherrer formula:

$$d = \frac{K\lambda}{\beta \cos\theta} \quad (1)$$

where d is the average crystallite size (Å), λ is the wavelength of X-radiation ($(\lambda K\alpha 1)$ = 1.5406 Å), K is the Scherrer constant (= 0.94), θ is the Bragg angle and β is the corrected integral width of the apparatus effects: $\beta = \sqrt{\beta^2 exp + \beta^2 app}$ (in Radians).

The β_{app} value is obtained after the analysis under the same conditions with a standard powder of LaB_6.

3.2.4 The measurement of specific surface area and pore volume

BET (Brunauer, Emmett and Teller) analysis provides precise specific surface area evaluation of materials by nitrogen multilayer adsorption, measured as a function of relative pressure using a fully automated analyser. The technique includes external area and pore area evaluations to establish the total specific surface area in m^2g^{-1} (Lucideon 2016).

The specific surface area and pore volume (V_p) of the supports and catalysts were determined from the isotherms of dinitrogen physisorption at the boiling temperature of the adsorbate using a Micromeritics ASAP 2020 apparatus. The specific surface areas of the samples were determined by the BET method. This method relies on the physical adsorption of multiple layers of the dinitrogen molecules at 77 K (liquid nitrogen's boiling temperature) on the sample surface. The amount of adsorbed gas increases with pressure. Using the adsorption isotherm, the amount of gas adsorbed as a monolayer can be determined. Then, calculations can be performed via knowing the area occupied by one nitrogen molecule (Lucideon 2016). Pore-size distributions were estimated using the Barret, Joyner and Halenda (BJH) method, based on the empirical Lecloux-Pirard standard isotherm and cylindrical pore geometry.

To perform the measurements, a known mass of the sample in the order of 200 to 400 mg was introduced into the measuring cell and then the cell was degassed at 350 °C for 4 h in a vacuum to clean the surface of the sample. After degassing, the sample was weighed again in order to quantify the loss of mass due to outgassing. The cell was then placed in the measuring station and then into a Dewar of liquid nitrogen. Desorption was measured after heating the cell at room temperature.

3.2.5 Transmission electron microscopy

Electron microscopy is an essential characterization technique in the field of solid chemistry. It allows the obtaining of a mapping of the texture and structure, and provides the composition of the heterogeneous catalyst. The transmission electron microscopy (TEM) pictures taken in a bright field allow the estimation of the average size of the metal particles on the entire catalyst. The microscope can also be equipped with a spectroscopic analysis system by energy dispersive X-ray spectroscopy (EDS), to verify the chemical nature and quantify the examined particles (NanoComposix 2012).

To perform the analysis, about 10 mg of the sample was put in a beaker with some polar solvent. After that, the ultrasonication was turned on. The small particles were dispersed in the solvent and a micro pipette was used to take a very small drop and place the sample onto a Pt grid. The sample was left to dry for a short time before the analysis.

3.2.6 Scanning electron microscopy

A Zeiss Ultra Plus field emission scanning electron microscope (FESEM), equipped with energy-dispersive X-ray spectroscopy (EDS) at an accelerating voltage of 15.0 kV, was used to study the surface of the fresh, used and poisoned catalysts. Prior to the analysis, the samples were coaled to avoid the accumulation of charge.

3.2.7 Temperature programmed reduction

The reduction of the different reducible species present on the catalyst was measured as a function of temperature by chromatographic monitoring of the consumption of reducing gas (1% H_2 in Ar). This analytical method was used to have more information on the metal–metal interaction of the studied catalysts. The hydrogen consumption in the studied samples was used to determine the starting oxidation state of the cation if its final state was well known.

The general reaction of the reduction of a metal oxide is as follows:

$$MO + H_2 \rightarrow M\,(0) + H_2O \qquad (2)$$

where *MO* is the metal oxide and *M (0)* is the metal at a reduced state.

In the temperature programmed reduction (TPR) experiments, a sample with a mass of 150 mg was placed in a U-shaped quartz tube. The analysis took place as follows: a gas mixture consisting of 1% hydrogen diluted in argon is used in examination of the sample with a flow rate of 50 $mLmin^{-1}$. The amount of hydrogen consumed was measured as a function of temperature by using a thermal conductivity detector.

A qualitative evaluation of the results can be done by examining the temperature maxima for hydrogen consumption. Furthermore, the integration of different signals allows carrying out a quantitative study of the reducibility properties of the samples**.**

3.2.8 X-ray photoelectron spectroscopy

X-ray induced photoelectron spectroscopy (XPS) is a surface analysis technique used to determine the chemical composition of the studied material. This

technique also provides information on the oxidation state of certain elements deposited on the surface (PE 2016).

XPS analyses were performed using a spectrometer Thermo Fisher Scientific Escalab 250xi XPS System equipped with a non-monochromatic X-ray aluminium source (Al Kα = 1486.6 eV).

During XPS analysis, photons (Al Kα) are directed onto the sample to be analysed. The interaction between photons and targeted atoms causes the ejection of core or valence electrons, characteristic of the atom and the solid. If the energy provided by photons is sufficient, the electrons leave the surface and can be collected by an analyser, which measures their kinetic energies (E_K). Electrons are classified and counted based on either their binding energy (E_B) or their kinetic energy (E_K) (PE 2016).

In XPS analysis, the electrons ejected from an insulating or semiconductor material result in the appearance of a positive potential. This charge effect slows down the electrons and changes their kinetic energy. At the spectrum level, it is reflected by an energy shift of the same amount for all the peaks. Therefore, the reference energy needs to be chosen that will allow the correction of the range of kinetic energy (or binding) (TFS 2013).

The static charge of the studied samples was corrected by referencing all the binding energies at Al 2p (E_B = 72.6 eV) because the samples were not that contaminated with carbon, except for the catalyst 0.3Pt10Cu/Si; the charging effects were corrected using the C1s peak (285 eV).

3.2.9 Acidity measurements

The nature of acid sites was investigated using the adsorption of pyridine as the probe molecule and followed by a NEXUS FT-IR (Thermo Nicolet) instrument. Pellets of 16 mm diameter (the mass of the pellets was 20–30 mg) were placed on a sample holder in a glass cell connected to a vacuum pump system (a primary pump and a turbo molecular pump). The pre-treatment of samples was done overnight at 450 °C under vacuum to clean the catalyst surface. After the pre-treatment, the first spectrum was collected (the reference spectrum), and then 2 mbar of pyridine was introduced into the cell for 10 minutes following the removal of physisorbed pyridine under vacuum before collecting the new spectrum. The spectra were then taken after 20 min of heating the wafer at certain desorption temperatures from RT up to 450 °C with 50 °C intervals. The subtraction between each spectrum and the reference spectrum allows measuring

the area of the bands corresponding to the amount of pyridinium ions (1545 cm^{-1}) and coordinated pyridine (1454 cm^{-1}) (Zaki *et al.* 2001). The amount of Lewis and Brønsted acid sites per gram of samples ($\mu molg^{-1}$) can be calculated using the following mathematical expression:

$$Amount = (A \times 2|\varepsilon \times m) \times 100 \quad (3)$$

where A is the surface of the band, 2 corresponds to the wafer surface in cm^2, ε is the molar extinction coefficient (1.28) and m is the mass of the pellet.

3.3 Evaluation of the catalytic performance in the oxidation of S-VOCs (DMDS)

3.3.1 Tests for the catalytic oxidation of DMDS

The experimental device used (Figure 3) allows the study of the activity of different catalysts in the total oxidation of DMDS. The catalytic tests were performed at ambient pressure in a quartz tube reactor. To prevent corrosion by the reaction products, all materials used in the construction of the experimental setup were resistant to corrosion.

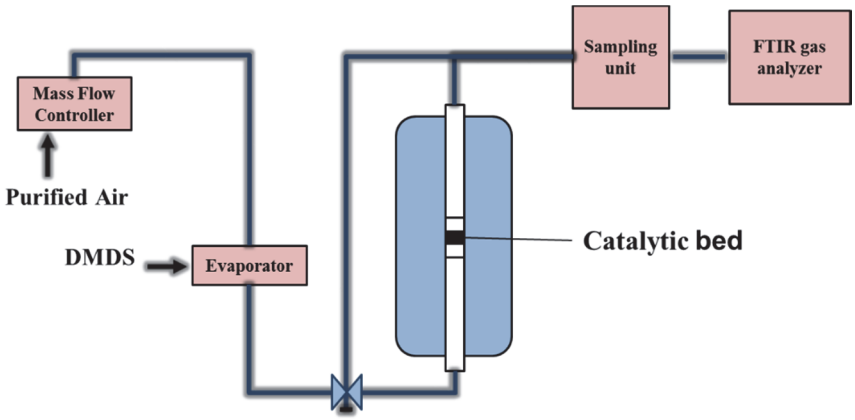

Fig. 3. The layout of the experimental setup used for the catalytic tests.

In the evaporator unit, the liquid phase DMDS was pumped into the heating device (T = 110 °C) using a syringe pump so that the DMDS evaporates and mixes with the air (1 $Lmin^{-1}$) coming through the mass flow controller. The concentration of 500 ppm of DMDS was used in the experiments.

The gas composition was measured with Fourier transform infrared spectroscopy (FTIR) (Gasmet, Model CR2000). The FTIR analyser was calibrated to detect the following compounds: DMDS ($C_2H_6S_2$), methyl mercaptan (CH_4S), sulfur dioxide (SO_2), sulfur trioxide (SO_3), DMS (C_2H_6S), ethyl mercaptan (C_2H_6S), formaldehyde (CHOH), carbon monoxide (CO), carbon dioxide (CO_2), methane (CH_4), methanol (CH_4O) and water (H_2O).

The conversion of DMDS and the yields of the main products are defined in the following way:

$$\text{Conversion } (\%) = \frac{Ci-Co}{Ci} \times 100, \quad (4)$$

$$CO_2\ (\%) = \frac{[CO_2]}{2xCi} \times 100, \quad (5)$$

$$CO\ (\%) = \frac{[CO]}{2xCi} \times 100, \quad (6)$$

$$SO_2\ (\%) = \frac{[SO_2]}{2xCi} \times 100, \quad (7)$$

where C_i is the initial feed concentration of DMDS (ppm), C_0 is the outlet concentration of DMDS (ppm), and [CO_2], [CO] and [SO_2] are the concentrations of the corresponding compounds in $molL^{-1}$.

3.4 Catalyst deactivation

Different industrial (1%Pt/Al, 1%Pt/Al-R1) and lab-made (0.3%Pt10%Cu/ Al_2O_3, 0.3%Pt10%Cu/$(Al_2O_3)_{0.8}(SiO_2)_{0.2}$) catalysts were exposed to an accelerated deactivation procedure that was developed based on the results of a study on industrial deactivation. The industrial ageing of the catalysts was done during the catalytic treatment of pulp mill S-VOC emissions.

3.4.1 Industrial deactivation

The industrial deactivation of the catalysts was done during pilot experiments at Stora Enso Oulu pulp mill between 2005 and 2006. In the pilot experiments, the chip bin emissions (about 10%) were treated in a catalytic incinerator of 500 m^3h^-

^{1} capacity. At that time the emission stream consisted of methanol, terpenic compounds, hydrogen sulfide, DMS, DMDS and methyl mercaptan. In addition, the industrial emission contained a significant amount of moisture and solids (content about 0.003 kgh^{-1}), the amounts of which were reduced by condensation and filtration before the catalytic incinerator (Ojala *et al.* 2005). For ageing purposes, the catalysts were placed inside an ageing rack (Ojala *et al.* 2006) that was positioned inside a regenerative catalytic incinerator. During the ageing, the incinerator temperature near to the ageing rack varied between 330 and 530 °C. During the downtimes, the incinerator was cooled down to a minimum temperature of -20 °C (since the pilot experiments were done during the wintertime). The period of the industrial ageing accounted for about two months, where the exact uptime was 1355 h, giving the incinerator about 88.5% of the utilization rate.

3.4.2 Accelerated poisoning

To simulate the long-term exposure of catalysts to the sulfur-containing compounds, the industrial and the lab-made catalysts were exposed to a reaction mixture containing SO_2 and water. The poisoning treatment and/or deactivation was carried out in a gas phase using a flow reactor.

The treatment was developed based on the study on industrial catalysts deactivation. The deactivation treatment was carried out under the following conditions: 100 ppm SO_2, 10% by volume H_2O and 10% by volume air balanced with N_2. The water flow was injected in the gaseous stream using a peristaltic pump at the same time as the SO_2 feeding, when a 400 °C reaction temperature was achieved. The tubular furnace was heated from the ambient temperature to 400 °C, with a temperature rise of 10 $°Cmin^{-1}$ under mixed nitrogen and air flow. After 5 h of treatment at 400 °C, the furnace was cooled down to room temperature under a stream of nitrogen and air (Figure 4).

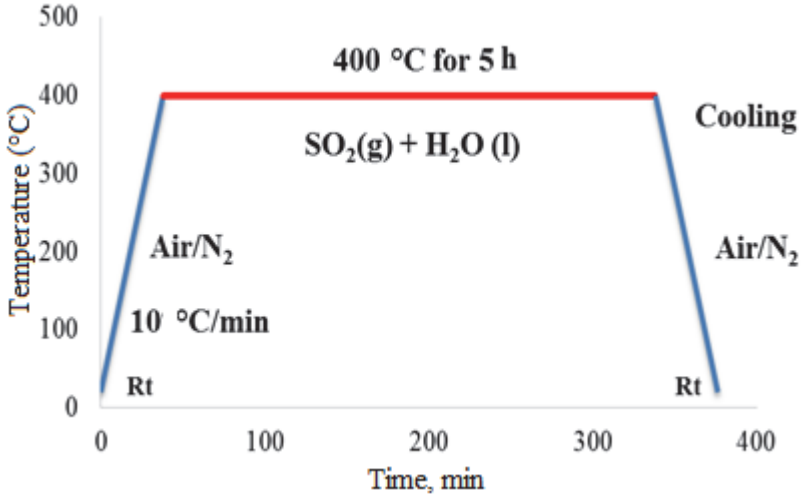

Fig. 4. The experimental setup for the poisoning tests.

4 Results and discussion

This chapter deals with all the results of the performance evaluation of the self-made and the monolithic catalysts (supplied from Ecocat-Dinex Ltd) in the oxidation of DMDS. For the self-made catalysts, the first set of the catalytic materials was alumina supported catalysts (10Cu/Al, 0.3Pt/Al and 0.3Pt10Cu/Al). In this study, Cu was chosen as the first monometallic active phase, since many previous studies in the oxidation of DMDS have shown its high activity and selectivity (Wang *et al.* 1997, Wang *et al.* 1998 and Wang *et al.* 2002). Since the selectivity of 10Cu/Al was not high enough at low temperature, Pt was used to enhance the 10Cu/Al catalyst selectivity, which is the reason why the monometallic 0.3Pt/Al was studied as well.

After the evaluation of these three catalysts, the research was then continued with the bimetallic active phase on different supports in order to prepare a potentially even more selective and durable catalyst for the oxidation of DMDS. The alternative catalytic support materials prepared were silica and silica doped alumina.

Another important factor that will be discussed in this chapter is the deactivation phenomenon caused by sulfur, which is a risk for all the used catalysts in the oxidation of S-VOCs. This study is based on the industrial deactivation results. Next, we will start with the characterization and activity tests of the self-made catalysts.

4.1 The characterization and activity tests of the self-made catalysts

The prepared supports and catalysts were analysed using different physico-chemical characterization methods in order to study their textural and structural properties in order to be able to evaluate their relation through their catalytic performance. Section 4.1 concentrates on the characterization of the self-made Al_2O_3, SiO_2 and $AlSi_{20}$ supported monometallic and bimetallic platinum and copper catalysts.

4.1.1 ICP-OES

The metal contents of the catalysts were evaluated by ICP-OES. The targeted catalyst composition was 0.3% by weight in the active phase (Pt) and 10% by

weight in the other active phase (Cu) with respect to the final mass of the catalyst. The results of ICP-OES analysis are summarized in Table 4 (The general accuracy of the ICP measurement used is +/- 1–3 %). It can be observed that the targeted levels of the active phase are met rather well. In the case of $AlSi_{20}$, less than the expected 20% of SiO_2 was found.

Table 4. The correlation between the experimental and theoretical content of platinum and copper in the monometallic and bimetallic catalysts, and the amount of SiO_2 in $AlSi_{20}$ derived from ICP-OES.

Catalysts	ICP / wt-%		
	Pt	Cu	SiO_2
Al_2O_3	-	-	-
$AlSi_{20}$	-	-	16
SiO_2	-	-	-
0.3Pt10Cu/Al	0.3	9	-
0.3Pt/Al	0.28	-	-
10Cu/Al	-	10	-
0.3Pt10Cu/$AlSi_{20}$	0.3	9	16
0.3Pt10Cu/SiO_2	0.28	8	-

4.1.2 XRD

The XRD analysis of the supports and catalysts calcined at 550°C was performed at room temperature. This technique allows the identification of crystalline phases in comparison with standard base ICDD (The International Centre for Diffraction Data), using the 2011 version which has over 160 000 references and is integrated into the operating system DiffracPlus (EVA). Using Scherrer's formula, based on the mid-height width of the most intense diffraction peak, the average sizes of crystallites have been estimated.

Supports Al_2O_3, SiO_2 and $AlSi_{20}$

The studied support materials are Al_2O_3 (denoted later as Al), $(Al_2O_3)_{0.8}(SiO_2)_{0.2}$ (denoted later as $AlSi_{20}$) and SiO_2 (denoted later as Si).
The X-ray diffractograms of the A1, Si and $AlSi_{20}$ supports are shown in Figure 5.

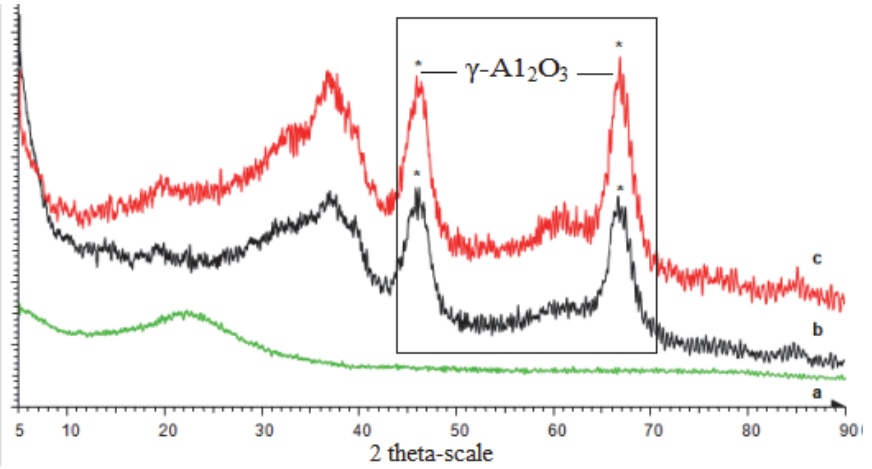

Fig. 5. The diffractograms of supports calcined at 550 °C, for Si (a), Al (b) and Al Si_{20} (c) with γ-Al_2O_3 (*) marked.

Based on the results, both $A1_2O_3$ and $AlSi_{20}$ support materials that were calcined at 550 °C are semi-amorphous, but the results highlight the presence of gamma-alumina in both of them, γ-$A1_2O_3$ (Reference ICDD 01-75-0921), characterized by two diffraction peaks located at 46.48 °C and 67.95 °C (Park *et al.* 2004). Regarding the SiO_2 support, the obtained diffractogram shows a completely amorphous phase with the presence of a broad peak for the low 2θ values. Therefore, it was not possible to determine the crystallite size of the sample.

Alumina supported catalysts

The diffraction pattern of the monometallic 0.3Pt/Al catalyst after the calcination treatment at 550 °C is shown in Figure 6.

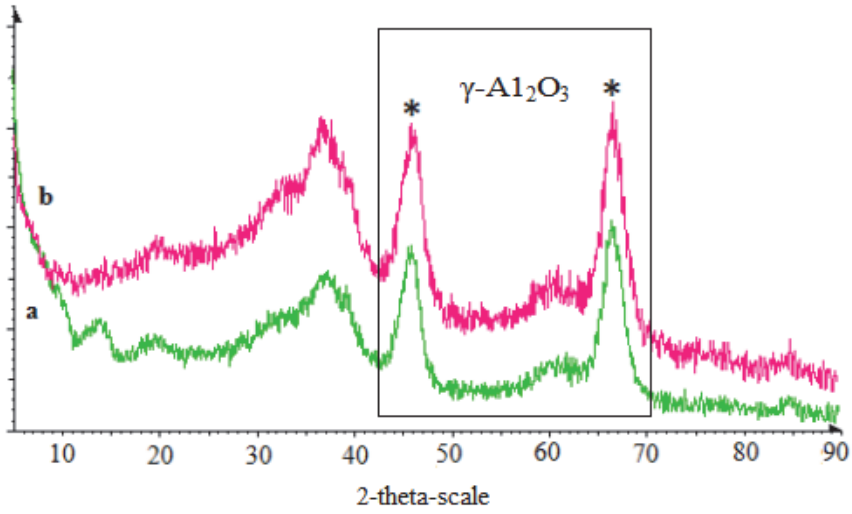

Fig. 6. The diffractogram for the 0.3Pt/Al catalyst (a) and the Al_2O_3 catalyst (b), with γ-Al_2O_3 (*) marked.

Figure
6 shows the XRD diffractogram of the 0.3Pt/Al catalyst. In the diffractorgam of 0.3Pt/Al, the same features are visible as there were for the pure Al_2O_3 support. The Pt phase is not detected because of its low content in the catalyst (0.3% by weight) and because of the very small particle size (in the order of 2 nm – determined later by TEM). The decrease in the peak widths of the support material after impregnation demonstrate the increase in the crystallite size of Al_2O_3 (see Table 5).

The two additional peaks (at 2θ = 34.88 °C and 38.18 °C) are observed in the case of the 0.3Pt10Cu/Al and 10Cu/Al catalysts (Figure 7). According to the ICDD database (41-0254), these peaks are found to be associated to the CuO crystal phase (Wang *et al.* 1998). The amorphous phase is also observed after the impregnation of copper.

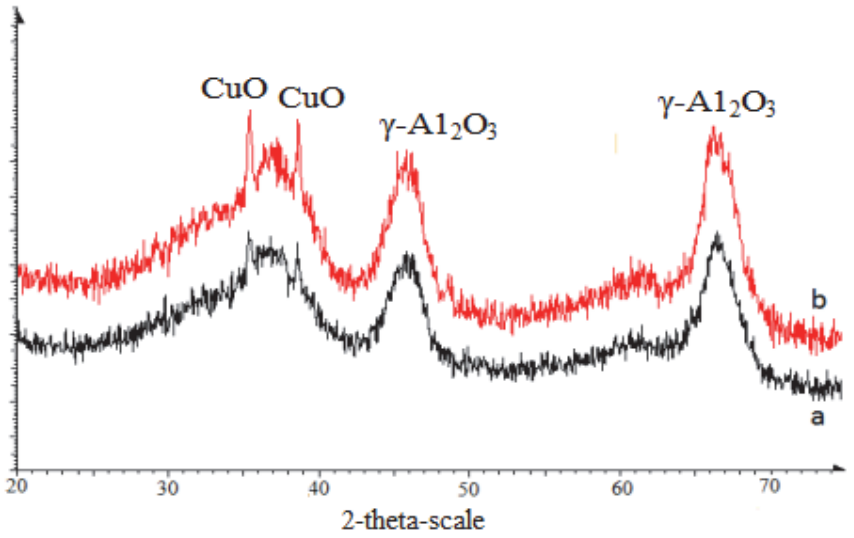

Fig. 7. The diffractogram for the 0.3Pt10Cu/Al catalyst (a) and the 10Cu/Al catalyst (b).

The details of the results of the XRD characterization are shown in Table 5. The crystallite sizes of the supports and catalysts were estimated when possible, using the Scherrer equation.

Table 5. The XRD results of the alumina support and alumina based catalysts.

Samples	Crystallite size (XRD) / nm	Phases (XRD)
Al_2O_3	2.18	γ - Al_2O_3 + amorphous phase
0.3Pt/Al_2O_3	2.2 for Al_2O_3	γ - Al_2O_3 + amorphous phase
10Cu/Al_2O_3	2.3 for Al_2O_3	γ - Al_2O_3 + CuO
	9 for CuO	
0.3Pt10Cu/Al_2O_3	6 for CuO	γ - Al_2O_3 + CuO
	2.3 for Al_2O_3	

After co-impregnation with platinum and copper, the crystallite size of γ-Al_2O_3 changed slightly from 2.18 to 2.3 nm. Moreover, the phase of tenorite (CuO), identified in the 0.3Pt10Cu/Al and 10Cu/Al catalysts, has a somewhat larger crystallite size (6–9 nm) but it still remains nanoscale.

Bimetallic 0.3Pt10Cu catalysts

The studied bimetallic catalysts were supported on three different support materials: Al, $AlSi_{20}$ and Si.

The diffractograms of the bimetallic Pt-Cu catalysts, shown in Figure 8, indicate the presence of γ-$A1_2O_3$ and copper oxide CuO phases characterized by two diffraction peaks at 2θ = 35.05 °C and 38.18 °C (Wang *et al.* 1998) according to the ICDD reference (01-089-2530). The CuO phase is also visible in the results of the 0.3Pt10Cu/Si catalyst. In the case of the 0.3Pt10CuO/$AlSi_{20}$ catalyst, the CuO diffraction peaks are not clearly identified. Furthermore, it should be noted that the three catalysts exhibit partially amorphous structure. The phase corresponding to Pt could not be detected by XRD due to low loading of Pt as in the case of monometallic catalysts.

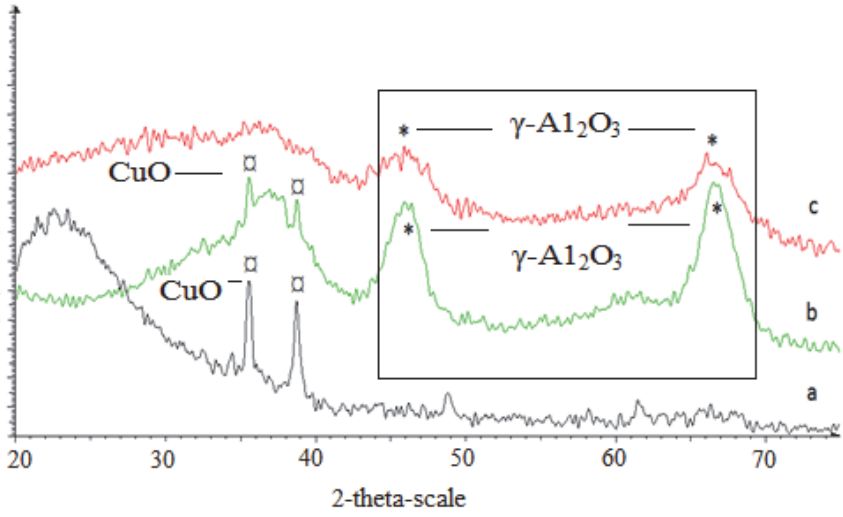

Fig. 8. The XRD diffractogram for the 0.3Pt10CuO/Si catalyst (a), the 0.3Pt10CuO/Al catalyst (b) and the 0.3Pt10CuO/$AlSi_{20}$ catalyst (c), with Al_2O_3 (*) and CuO (¤) marked.

The results of X-ray diffraction of bimetallic catalysts are grouped in Table 6. Also in the case of bimetallic catalysts, the phase of tenorite (CuO) identified in the catalysts (0.3Pt10Cu/Al and 0.3Pt10Cu/Si) has a slightly larger particle size (6–11 nm) than the support's oxide that exhibited a crystallite size of around 2 nm, as shown above in Table 5.

Table 6. The XRD results of the different supports and catalysts.

Samples	Crystallite size (XRD) / nm	Phases (XRD)
0.3Pt10Cu/ Al	CuO (6) Al_2O_3 (2.3)	γ - Al_2O_3 + CuO
0.3Pt10Cu/$AlSi_{20}$	nd	γ -Al_2O_3
0.3Pt10Cu/Si	11 for CuO	amorphous phase + CuO

The small crystallite sizes of the support materials or in the catalysts can result in high specific surface areas, which will be verified in the content of the following subsection.

4.1.3 The measurement of specific surface area and pore volume

The specific surface area of the supports and catalytic materials as well as their pore volumes were determined by the physical adsorption of liquid nitrogen at 77 K. The obtained isotherms of the Al_2O_3 support and the 0.3Pt/Al, 10Cu/Al (Figure 9) and 0.3Pt10Cu/Al catalysts (Figure 10) are Type IV (Gregg *et al.* 1982, Sing *et al.* 1985, Lin *et al.* 2009, Popat *et al.* 2012), corresponding to mesoporous materials. They also exhibit hysteresis of type H2, generally attributed to interconnected pores (Mason 1982, Mason 1983) and to a non-uniform size distribution.

The BJH results show a mesopore distribution (Type IV isotherm) for the 0.3Pt/Al catalyst with an average pore diameter of 6.9 nm and a pore volume of 0.43 cm^3g^{-1} (Table 7). For the second monometallic catalyst, 10Cu/Al (and according to the BJH results), it was found that the pore average diameter was 7.4 nm and the pore volume was 0.38 cm^3g^{-1}. The bimetallic catalyst 0.3Pt10Cu/Al has an average pore diameter of 7.2 nm and a pore volume of 0.37 cm^3g^{-1}.

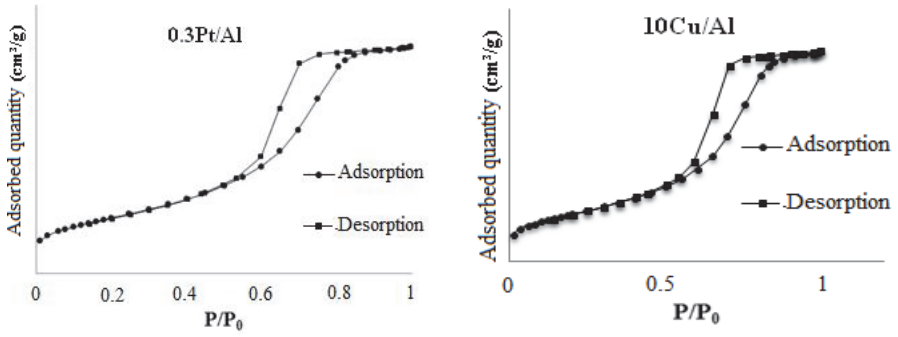

Fig. 9. The adsorption–desorption isotherms of liquid nitrogen for the 0.3Pt/Al and 10Cu/Al catalysts.

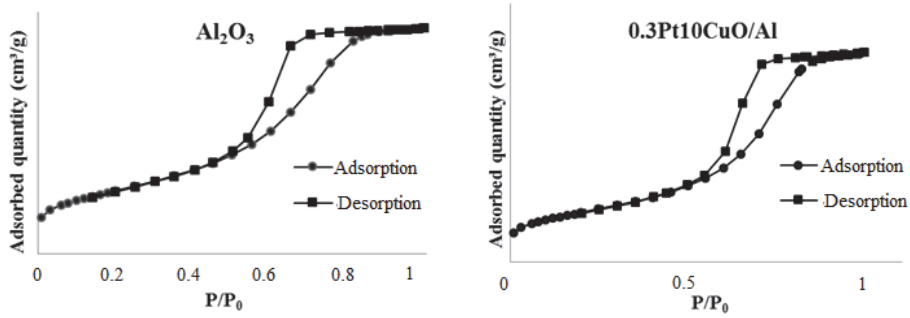

Fig. 10. The adsorption–desorption isotherms of liquid nitrogen for the Al_2O_3 support and the 0.3Pt10Cu/Al catalyst.

The addition of SiO_2 as a dopant in the support did not significantly change the isotherms and hysteresis forms since the same isotherm type (Type IV) and hysteresis type (H2) were found again (Figure 11), indicating the presence of a good interconnectivity of the pores (Yuan *et al.* 2006, Sangwichien *et al.* 2002).

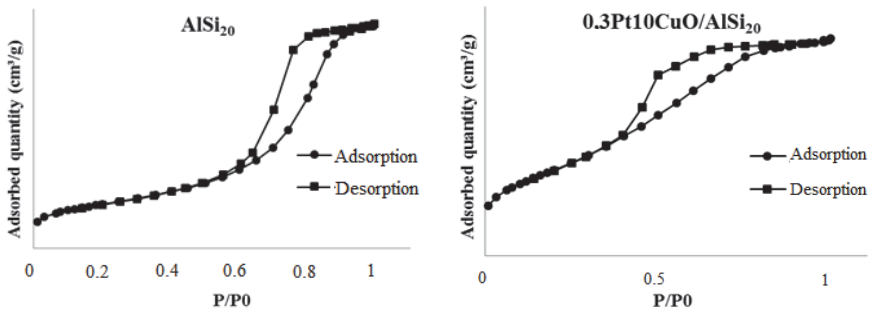

Fig. 11. The adsorption–desorption isotherms of liquid nitrogen for the 0.3Pt10Cu/AlSi$_{20}$ catalyst and the AlSi$_{20}$ support.

Regarding the SiO_2 support, it has a Type I isotherm, according to the IUPAC classification, which stays the same after depositing platinum as an active phase (Figure 12). This type of isotherm is assigned to microporous materials, which present a very large external surface.

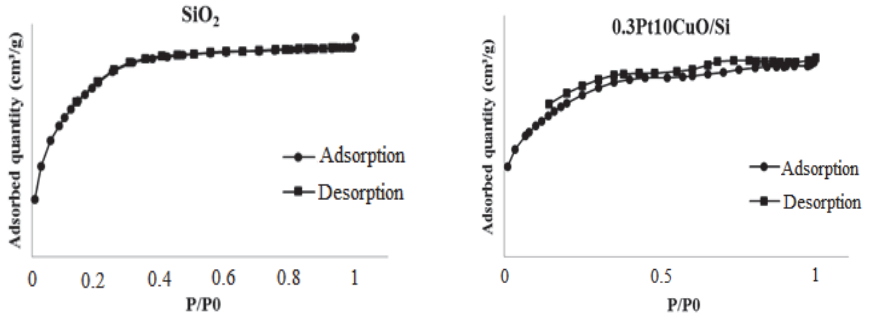

Fig. 12. Isothermal adsorption–desorption of liquid nitrogen for the 0.3Pt10Cu/Si catalyst and the SiO_2 support.

The SiO_2 and Al_2O_3 supports develop very large specific surface areas, in the order of 540 and 290 m^2g^{-1} respectively, in accordance with the crystallite sizes or the amorphous nature of the materials identified by XRD. The addition of 20% SiO_2 by weight to the alumina support leads to the S_{BET} value of 400 m^2g^{-1}.

The deposition of the Pt-Cu active phase on the various prepared supports decreased the surface area in all the cases, but the decline is much more

pronounced in the case of SiO_2. This can be explained by the surface area decrease caused by the blockage of silica micropores and by the reduction of pore accessibility after the deposition of Cu particles (in the order of 11 nm, as estimated from the diffraction pattern, and thus of much larger crystallite size than the micropores as microporous materials typically have < 2 nm pore size).

In general, the supports have a larger pore volume, which naturally decreases after the deposition of the active phase. The pore diameters estimated are in agreement with the obtained isotherm types. The results grouped in Table 7 show that the pore volume of the calcined silica decreased from 0.38 cm^3g^{-1} to 0.03 cm^3g^{-1} after the co-impregnation, also showing the decrease in surface area.

Table 7. The BET-BJH results for the supports and catalysts.

Catalysts	Surface area (BET) / m^2g^{-1}	Pore volume cm^3g^{-1}	Pore diameter nm
Al_2O_3	290	0.43	6.0
$AlSi_{20}$	400	0.43	6.9
SiO_2	540	0.38	1.94
$0.3Pt/Al_2O_3$	260	0.43	6.9
$10Cu/Al_2O_3$	206	0.38	7.4
$0.3Pt10Cu/Al_2O_3$	210	0.37	7.2
$0.3Pt10Cu/AlSi_{20}$	150	0.16	4.2
0.3Pt10Cu/Si	55	0.03	2.1

To get a more visual view of the particle sizes of the bimetallic catalysts, TEM measurements were performed.

4.1.4 TEM

The monometallic and bimetallic catalysts were characterized using TEM in order to study the morphology of the catalyst surface and the particle sizes of the active phases.

Monometallic catalysts.

The TEM results for the monometallic 0.3Pt/Al and 10Cu/Al catalysts are presented in Figure 13.

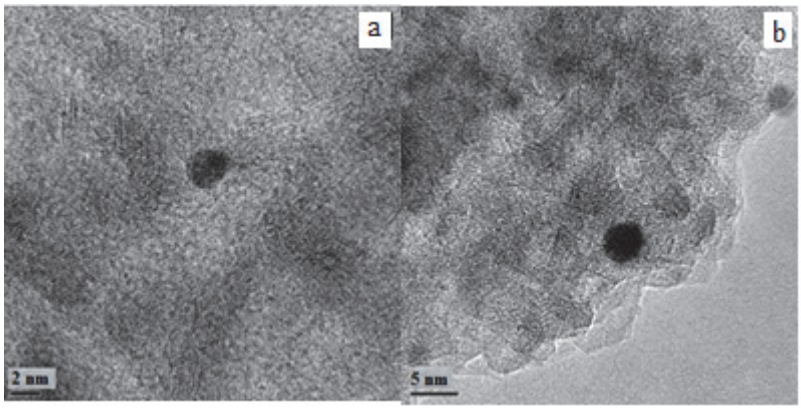

Fig. 13. TEM images of the 0.3Pt/Al catalyst (a) and the 10Cu/Al catalyst (b).

The TEM image in Figure 13a shows that the active phase of Pt was well dispersed on the catalyst support for the 0.3Pt/Al catalyst because the estimated average size of the particles at the surface was about 2 nm. For the 10Cu/Al catalyst, the same average particle size was estimated for the Cu particles (Figure 13b).

Bimetallic catalysts

The morphology and composition of the catalysts were examined by TEM coupled with EDS. Figure 14 shows the results obtained for the samples, i.e. for 0.3Pt10Cu/Al, 0.3Pt10CuO/$AlSi_{20}$ and 0.3Pt10Cu/Si.

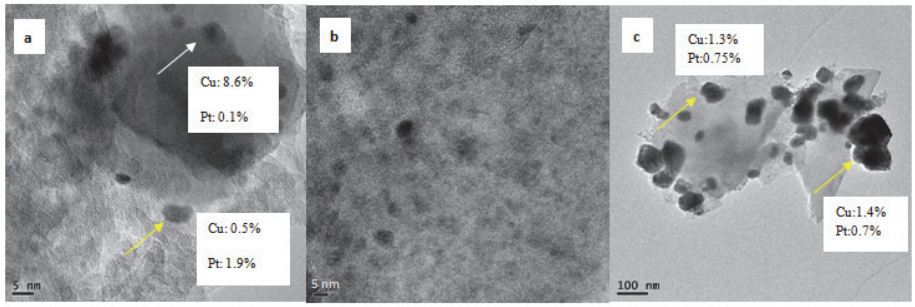

Fig. 14. TEM images of the 0.3Pt10Cu/Al catalyst (a), the 0.3Pt10Cu/$AlSi_{20}$ catalyst (b) and the 0.3Pt10Cu/Si catalyst (c).

In the catalysts supported on simple oxides, as was the case for Al_2O_3 and SiO_2, Pt is intimately linked to the Cu particles. Indeed, most of Pt is either dispersed on Cu, forms an alloy (Pt-Cu) or does both. Subsequent analyses by XPS elucidate this point further. From the TEM images it can be observed that there might be an interesting interaction between Pt and Cu species. It is important to note that the Cu and Pt particles are in nanometrically sized in the range of 2–3 nm in the case of the 0.3Pt10Cu/Al catalyst, however, they are much larger in the case of the 0.3Pt10Cu/Si catalyst, being around an average of 30 nm. This result is also in agreement with the drastic reduction of the specific surface area from 540 m^2g^{-1} for the SiO_2 support to 55 m^2g^{-1} after impregnation of the active phase. The addition of 20% SiO_2 to the Al_2O_3 support does not markedly increase the size of Cu particles compared to what was observed for the 0.3Pt10Cu/Al catalyst. Indeed, the TEM image (Figure 14b) clearly shows the presence of Cu particles, having a size of about 5 nm, which are well dispersed on the amorphous $AlSi_{20}$ support. In the sample 0.3Pt10Cu/$AlSi_{20}$ the Pt particles were not visible; they were perhaps covered by copper.

4.1.5 TPR

TPR experiments were conducted to examine the reducibility of different prepared catalysts.

Monometallic catalysts supported on Al_2O_3

No reduction peak was observed in the case of alumina support calcined at 550 °C due to its stability at high temperatures. Concerning the platinum-containing catalysts, it is important to take into consideration that Pt is reduced at lower temperatures. The small amount of hydrogen consumed during the experiment does not, however, help to determine the exact platinum reduction state.

In the TPR profile of the 0.3Pt/Al catalyst (Figure 15), the single peak found begins to appear at room temperature and it vanishes at 165 °C. It has been reported in the literature (Carvalho *et al.* 2004, Reyes *et al.* 1996) that the peaks centred at 190 °C can be attributed to the reduction of amorphous PtO_X species, while the enlargement may suggest strong interactions with the support. However, it was very difficult to make the conclusions regarding platinum based on the low temperature H_2 consumption observed because the content of Pt is only 0.3%, which corresponds to a very low consumption of H_2.

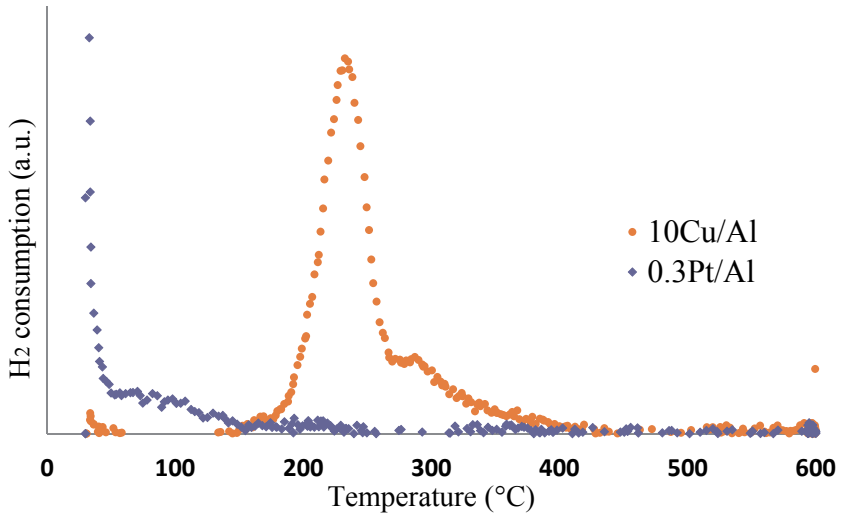

Fig. 15. The TPR profiles of the 0.3Pt/Al and 10Cu/Al catalysts.

The TPR profile of 10Cu/Al (Figure 15) showed a peak related to the H_2 uptake at 233 °C with a shoulder at around 287 °C. According to the literature (Lamonier *et al.* 2008), the peak at the low temperature region can be attributed to the reduction

of several well-dispersed copper oxide species that cannot be detected by XRD. The higher temperature peak at about 287 °C is attributed to the reduction of the CuO bulk phase, which can be detected by XRD.

Bimetallic catalysts supported on alumina, silica and $AlSi_{20}$

The TPR results presented in Figure 16 indicate that the reduction of the 0.3Pt10Cu/Si catalyst starts at about 127 °C, which is in accordance with the previous finding of Kazachkin *et al.* (2008). The TPR profile of the 0.3Pt10Cu/Si catalyst shows only one broad reduction peak, at about 190 °C. This peak can be assigned to the reduction of Cu oxides. It is known that the reduction of Cu oxides is promoted by the presence of the noble metal, such as Pt (Aristizabal *et al.* 2011, Epron *et al.* 2001), which is also visible in our case. This finding also signifies that Cu and Pt species are close to each other, as observed by TEM. The improved reducibility observed in this case can be explained by the presence of platinum, which is needed to provide an abundant source of dissociated hydrogen which in turn will contribute to the reduction of copper oxide because of the spillover. In addition, it is expected that copper oxide species reduce rapidly because of other reasons. It was reported that silica promotes the spillover of hydrogen as well, due to its large storage capacity of hydrogen after H_2 dissociation on the metal surface (Anderson 1975). Therefore, there would not be a hydrogen deficiency in the neighbourhood of copper particles (Kazachkin *et al.* 2008).

The 0.3Pt10Cu/Al and 0.3Pt10Cu/$AlSi_{20}$ catalysts both exhibited a maximum temperature (T_{max}) in the range of 220–280 °C for the reduction of copper. These peaks can be observed at a lower temperature than those generally observed for monometallic copper catalysts (at least for 10Cu/Al_2O_3 in our case), which may indicate that in these cases the reduction of Cu oxides is also promoted by the presence of Pt. The differences in the reduction profiles are clearly indicative of the different supports used.

The 0.3Pt10Cu/Al catalyst was reduced at lower temperatures (220 °C) compared to the 0.3Pt10Cu/$AlSi_{20}$ catalysts (280 °C). In addition, the hydrogen consumption at 280 °C could be ascribed to the reduction of the oxidized copper species that are not interacting with platinum (Epron *et al.* 2002), which is confirmed by the TEM-EDS analysis. Another explanation is that the lower reduction temperature of a catalyst supported on alumina is related to the crystalline CuO (Yu *et al.* 2011) and the higher one is observed for the reduction

of amorphous CuO on alumina-silica supported catalyst, the phases of which are indicated by the XRD results.

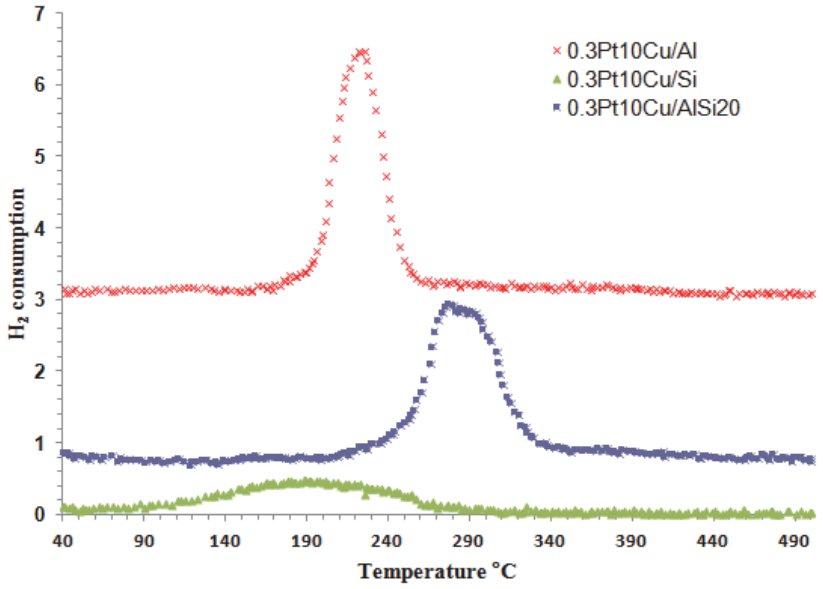

Fig. 16. The TPR profiles of the 0.3Pt10Cu/Al, 0.3Pt10Cu/AlSi$_{20}$ and 0.3Pt10Cu/Si catalysts.

Regarding H_2 consumption calculations, a value of 0.5 has been found in the case of the 0.3Pt10Cu/Si catalyst, which is less than the expected value (1). It means that a part of the active phase is either in an oxide form, or it is already at the beginning of the TPR measurement in a reduced form as a solid solution of Pt-Cu for example and/or a metal oxide part, for some reason, was not available for the reduction. Similarly, in the case of the 0.3Pt10Cu/Al catalyst, the H_2 consumption calculated for the bimetallic species gave a value of 0.87, which is lower than the expected value (1). After the addition of silica in alumina, platinum and copper oxide species were principally completely reduced and the value of the H_2 consumption gave 0.95 in comparison with the expected value (1).

As discussed previously, the studied catalysts showed different reduction behaviours, and concerning the structural characteristics, the TEM results of the 0.3Pt10Cu/AlSi$_{20}$ and 0.3Pt10Cu/Al catalysts showed smaller copper particles. Sales *et al.* (2005) reported that the CuO reduction temperature of the 0.3Pt10Cu/Al catalyst depends on the particles size and their interactions with the

support. Another study made by Epron *et al.* (2002) reported that copper oxide particles in a bimetallic catalyst are assumed to be well dispersed and interact strongly with the support, which is the most likely explanation for their higher reduction temperature. From the TPR results, it can be considered that the copper particles' size is larger on 0.3Pt10Cu/Si (which displays lower temperature reduction) than on 0.3Pt10Cu/Al and 0.3Pt10Cu/$AlSi_{20}$. This conclusion is consistent with the observed TEM results.

4.1.6 Analysis of acid-base properties

The adsorption using pyridine as the basic probe molecule, is one of the most frequently used methods for the characterization of surface acidity, and being a weak base, it would be held only by the stronger Lewis acid sites. An absorption band near to 1540 cm^{-1} is characteristic of pyridinium ions, while a spectral difference in the region of 1640 to 1580 cm^{-1} and 1500 to 1440 cm^{-1} allows physically adsorbed pyridine to be differentiated from pyridine coordinated to Lewis acid sites. Pyridine is usually considered to be a better probe for acidity measurement than NH_3 because it does not adsorb on weak acid sites and besides, it is more stable toward dissociative adsorption on certain sites (Bhatia 1989).

The use of IR spectroscopy to detect the adsorbed pyridine (Py) allows distinguishing between the acid sites. Figure 17 presents in situ infra red (in sity IR) spectra of pyridine adsorption on the γ-Al_2O_3, SiO_2 and $AlSi_{20}$ supported catalysts, evacuated at 150 °C and after the subtraction of the background spectrum. The spectra were obtained in the range of 1700–1400 cm^{-1}. In general, the presence of Lewis acid sites was observed and no traces of Brønsted sites were found. These results are comparable with the ones found by Thomas T. Onfroy *et al.* (2005). In their study, they only found the presence of Lewis acid sites by using lutidine, which could detect Lewis and Brønsted sites.

Figure 17c shows the chemisorbed Py on Si, after degassing at 150 °C. The band νCCN at 1613 cm^{-1} that corresponds to the Lewis acid sites (LPy species) is not observed, indicating that pyridine is weakly attached on the surface. Farrauto *et al.* (1997) also reported that the acidic proton – referring to 1575 cm^{-1} (ν8b) that is due to HPy^+ and LPy – was not found on the silica, even when using another probe molecule like ammonia. Figure 17b indicates the existence of different types of Al-OH groups isolated in the case of Py adsorption on Al at 150 °C. Unlike in the case of Si, the corresponding νCCN vibration induces a strong band at 1612 cm^{-1} (ν8a) with a shoulder at 1622 cm^{-1} (ν8a) that is due to

the strong Lewis acid sites (LPy species) and a band at 1490 cm^{-1} (ν19a) that is assigned to coordinately bound pyridine and hydrogen bonded pyridine, in addition to bands at 1578 and 1450 cm^{-1} assigned to the formation of HPy species (Zaki *et al.* 2001, Urban 199). The chemisorption of Py on $AlSi_{20}$ at 150 °C, shown in Figure 17a, leads to the formation of LPy species involving coordinatively unsaturated Al^{3+} on the octahedral sites (identified by the bands at 1610 cm^{-1}) and the tetrahedral sites (recognised by the band at 1623 cm^{-1}). The adsorption of Py on $AlSi_{20}$ is not distinguished by the formation of any additional species, except of a slight shift of the band at 1578 to 1576 cm^{-1} related to the formation of HPy species in addition to the registration of high Lewis acidity for the catalyst supported on $AlSi_{20}$, as shown in Table 8.

As was mentioned previously, we could not find the presence of any acid sites in the 0.3Pt10Cu/Si sample, which may be due to the presence of weak acid sites that cannot be detected by pyridine.

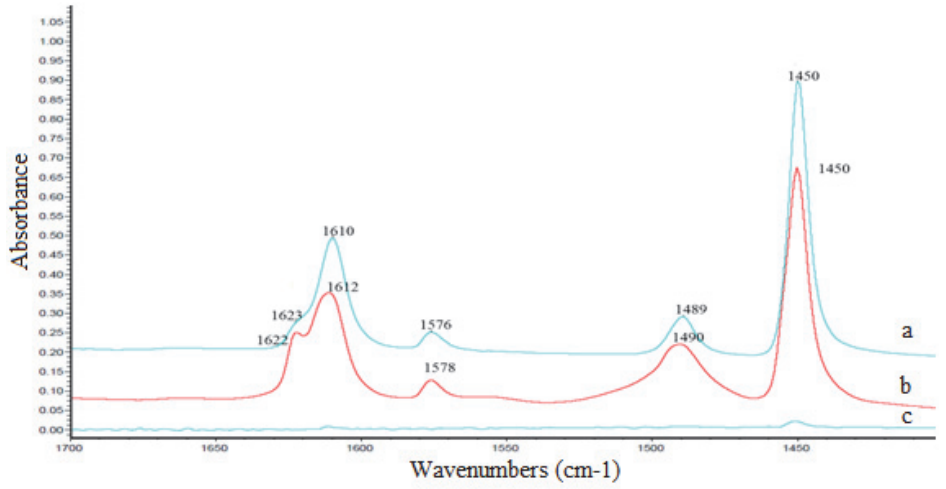

Fig. 17. The IR spectra of pyridine adsorbed on the 0.3Pt10Cu/$AlSi_{20}$ catalyst (a), the 0.3Pt10Cu/Al catalyst (b) and the 0.3Pt10Cu/Si catalyst (c).

Table 8. The specific Lewis acidity of the studied catalysts.

Samples	0.310Pt10Cu/Al b	0.3Pt10Cu/AlSi$_{20}$ a	0.3Pt10Cu/Si c
The total quantity of Lewis acid after 150 °C (μmolg^{-1})	490	720	9
The total quantity of Lewis acid by m^2 of catalyst (μmolm^{-2})	2.3	4.8	0.2

4.1.7 XPS

Monometallic catalysts

Regarding the 0.3Pt/Al catalyst (Figure 18), only two different platinum species were found. The binding energy of Pt4d$_{5/2}$ showed a component at around 314.7 eV that can be associated to Pt (0), and at higher energy at around 318.9 eV associated to Pt (II).

In the case of the 10Cu/Al catalyst (Figure 18), the most intense peak (Cu 2p$_{3/2}$) of the Cu 2p line at a binding energy of around 934 eV and the appearance of satellite lines on each component of the Cu 2p are conclusive that copper is present as CuO on the surface of the catalysts (Tsenga *et al.* 2010).

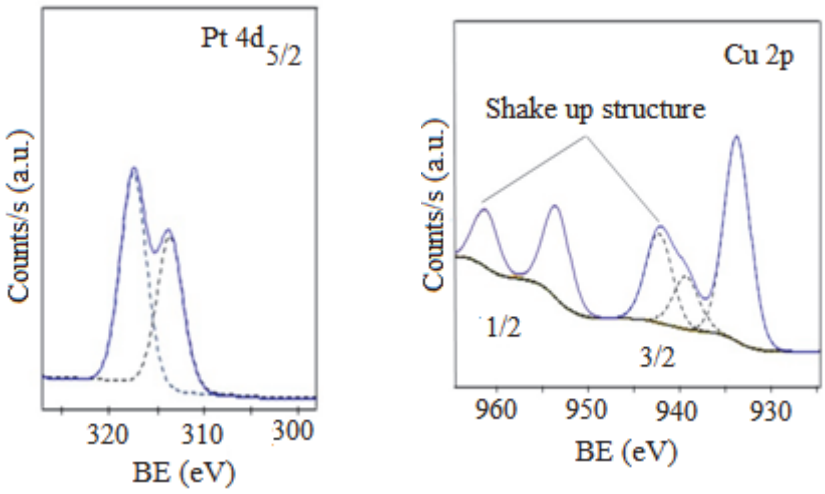

Fig. 18. Pt 4d of 0.3Pt/Al and Cu 2p of 10Cu/Al.

Bimetallic catalysts

XPS of different Pt-Cu catalysts were measured with the aim of identifying the oxidation state of copper and platinum species. The fresh catalysts were also compared to the catalysts used in the DMDS oxidation.

The XPS results of the Pt $4d_{5/2}$ core-level (Table 9) showed the presence of three different platinum species in the case of the fresh 0.3Pt10Cu/Al catalyst (Figure 19Aa). These species are Pt (0), oxidized platinum species PtO_2 and Pt (0) that belong to the Pt-Cu alloy or to the intermetallic compound (Gómez *et al.* 2014). This finding confirmed the presence of particles containing both Pt and Cu found by the TEM-EDS measurements and TPR as well.

The sample used in the DMDS oxidation (Figure 3, subsection 3.3.1) showed the Pt $4d_{5/2}$ peak (Table 9), which could be resolved after the curve fitting procedures into two components with binding energies of 312.7 eV assigned to Pt (0) belonging to the Pt-Cu alloy or to the intermetallic compound (Gómez *et al.* 2014) and another with a binding energy of 318 eV (Figure 19Ab) that can be ascribed as PtO_x or as likely to be PtO_2 species (Bouwman *et al.* 1977).

The XPS results of the fresh 0.3Pt10Cu/$AlSi_{20}$ catalyst (Figure 19Ba) indicated that Pt is present in an oxidized form (PtO) (Corro *et al.* 2006). After the catalytic test in the DMDS oxidation (Figure 19Bb), the binding energies of the $Pt4d_{5/2}$ revealed two components with binding energy of around 315 eV, which is assigned to Pt (0), and another of around 318.5 eV, which shows that Pt is also present also in PtO_x form.

For the catalyst 0.3Pt10Cu/Si (Figure 20), the decomposition of the spectra to individual components of the Pt 4f core level revealed the presence of PtO_x species in the bimetallic catalysts. The peak components with BE of Pt $4f_{7/2}$ and Pt $4f_{5/2}$ at around 74.1 and 77.4 eV respectively, reveal that the Pt species on the surface of the catalyst exist as PtO_2 (Peuckert *et al.* 1984).

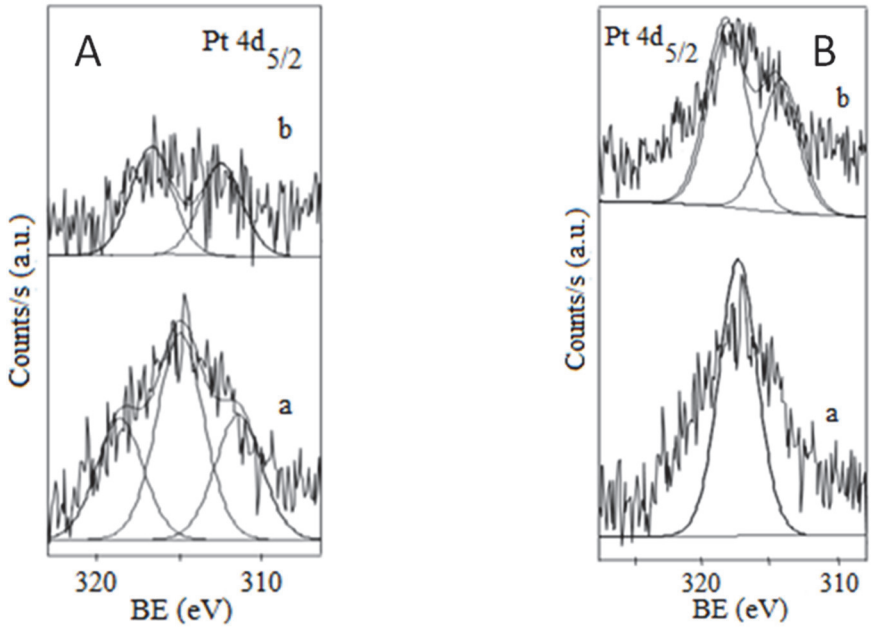

Fig. 19. Pt 4d of fresh (a) and used (b) 0.3Pt10Cu/Al (A) and 0.3Pt10Cu/$AlSi_{20}$ (B).

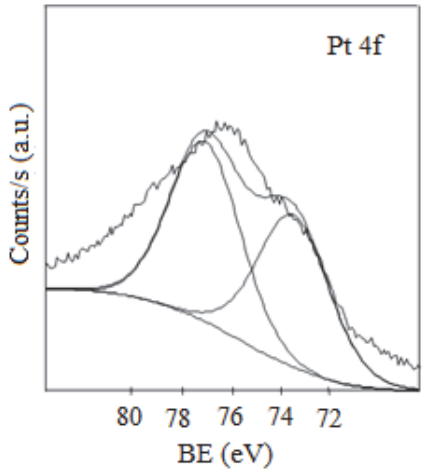

Fig. 20. Pt 4f of fresh 0.3Pt10Cu/Si.

Concerning copper, in all the fresh and used (0.3Pt10Cu/Al, 0.3Pt10Cu/$AlSi_{20}$) catalysts (Figure 21 and Figure 22), the most intense peak (Cu $2p_{3/2}$) of the Cu 2p

line at a binding energy of around 933.68–933.8 eV and the appearance of the satellite lines on each component of the Cu 2p (Tseng *et al.* 2010) (Table 9) show that copper is present in the form of CuO in all the catalysts.

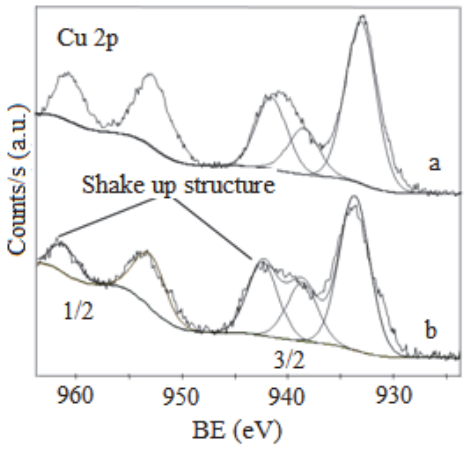

Fig. 21. Cu 2p of fresh 0.3Pt10Cu/Al (a) and used 0.3Pt10Cu/Al (b) .

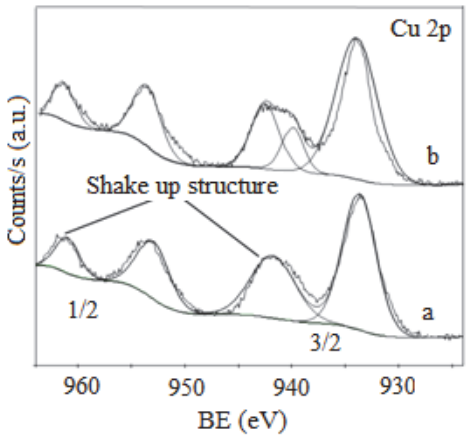

Fig. 22. Cu 2p of fresh 0.3Pt10Cu/AlSi$_{20}$ (a) and used 0.3Pt10Cu/AlSi$_{20}$ (b).

The XPS dispersion (Table 10) of copper on Al and $AlSi_{20}$ surfaces when observed for the corresponding catalysts is also confirmed by the close atomic ratios of Cu/Al (0.1) and Cu/$AlSi_{20}$ (0.083), obtained from XPS with respect to the calculated values Cu/Al (0.17) and Cu/$AlSi_{20}$ (0.15) derived from their nominal composition.

In the 0.3Pt10Cu/Si catalyst, the calculated Cu/Si atomic ratio based on XPS, was higher (0.13) than the bulk value derived from its chemical composition (0.09), indicating the presence of an overlayer of copper species. The higher value of the surface Cu/Si ratio for the silica supported catalyst indicates the potential presence of aggregates of copper on the surface, which is in line with the TEM that showed the existence of large particles of copper species on the SiO_2 support.

The Pt/Si surface ratio for the same sample, summarized in Table 10, is higher than the calculated value derived from its chemical composition (Pt/Si = 0.007). This dissimilarity between the XPS and theoretical Pt/Al ratios could be explained by TEM-EDS. According to the TEM results, no Pt particles were seen to exist alone on the support SiO_2 but only on the large particles of Cu, and thus, Pt could be far away from the Si species of the support, which could be the reliable reason for this difference in the surface ratio of Pt/Si. In spite of this, the variations in the calculated Pt/Al ratios indicate that changes have occurred in Pt surface concentrations between fresh and used catalysts.

Table 9. Characterization of fresh and used catalysts by XPS.

Samples	Pt $4f_{7/2}$ (eV)	Pt 4d (eV)	Cu $2p_{3/2}$ (eV) CuO	Pt species
0.3Pt10Cu/Si fresh	74.1		933.7	PtO_2
0.3Pt10Cu/$AlSi_{20}$ fresh		317.2	933.68	PtO
0.3Pt10Cu/$AlSi_{20}$ used		315	934	Pt (0)
		318.5		PtO_x
0.3Pt10Cu/Al fresh		315.2	933.8	Pt (0)
		318.9		PtO_2
		312.6		Pt-Cu
0.3Pt10Cu/Al used		312.7		Pt-Cu
		318		PtO_2

Table 10. The surface atomic ratios of fresh and used catalysts by XPS.

Sample	Pt/Si	Cu/Si	Pt/Al	Cu/Al	Si/Al	S/catalyst
0.3Pt10Cu/Si fresh	0.01	0.1				
0.3Pt10Cu/$AlSi_{20}$ fresh			0.004	0.083	0.165	
0.3Pt10Cu/Al fresh			0.0033	0.1		
0.3Pt10Cu/$AlSi_{20}$ used			0.0036	0.066	0.165	0.012
0.3Pt10Cu/Al used			0.002	0.059		0.029

After the use of the catalysts in the DMDS oxidation (as described in the Subsection 3.3.1) a remarkable change in the surface dispersion of the active phase occurred in the case of 0.3Pt10Cu/Al. According to the XPS measurement (Table 10), the atomic ratio of Pt/Al (0.002) and Cu/Al (0.059) decreased, indicating that the surface of the used catalyst was exposed to certain chemical poisoning, most probably to that of sulfur species coming from the by-products or from the DMDS feed. In the case of 0.3Pt10Cu/$AlSi_{20}$, the decrease in the dispersion of Pt (0.0036) and Cu (0.066) was noticed as well, but it was not as high as in the case of the 0.3Pt10Cu/Al catalyst. Besides, the elemental concentration of sulfur on the surface of 0.3Pt10Cu/Al was higher (0.029) than that found in the case of the 0.3Pt10Cu/$AlSi_{20}$ catalyst (0.012). Concerning the surface concentration of Si on aluminium oxide, it remained the same (0.165). This finding supports the assumption that silica doping increases the resistance of alumina against sulfur.

4.2 Catalytic oxidation of DMDS

To obtain more information on the performance of the different catalytic materials used in this study, their activities were evaluated in the total oxidation of DMDS. At the beginning, the effect of the active metal, Pt, Cu or bimetallic Pt-Cu supported on alumina were studied. Then, the focus was directed to the bimetallic catalyst that is supported on alumina, silica and silica-doped alumina.

4.2.1 The catalytic performance of alumina supported catalysts

At the beginning, the activities of 0.3Pt/Al, 10Cu/Al and 0.3Pt10Cu/Al (self-made) were studied. The aim was to discover the effect of adding a very small amount of platinum on the copper catalyst.

The results related to the T_{90} for DMDS and yields of the total oxidation products are presented in Table 11 and Figure 23. One can observe that with the addition of only 0.3 wt-% of Pt, the DMDS was totally oxidized at a slightly lower temperature than in the case of the copper supported alumina catalyst, however, the difference was almost insignificant. Nevertheless, the 0.3Pt10Cu/Al catalyst provides a higher yield of CO_2 and SO_2 at a lower temperature than the two monometallic catalysts. The improvement in the selectivity of the catalysts after the addition of Pt was more significant than the improvement in the activity.

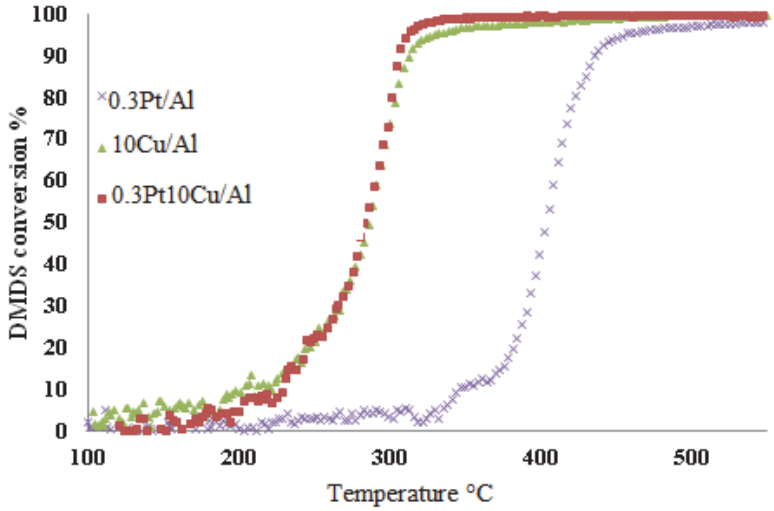

Fig. 23. Light-off curves in DMDS oxidation over the 0.3Pt/Al, 10Cu/Al and 0.3Pt10Cu/Al catalysts (DMDS 550 ppm, m = 100 mg, RT – 550 °C, 5 °Cmin^{-1}).

Table 11. T_{100}, SO_2 and CO_2 yields at 400–500 °C for the DMDS oxidation over the prepared catalysts.

Studied catalysts	0.3Pt/Al	10Cu/Al	0.3Pt10Cu/Al
SO_2 Yield (%)	19	11	100
CO_2 Yield (%)	1.5	1	100
T_{100} (°C)	520	380	320
$T_{Appearance}(CO_2)$ (°C)	450	450	220
$T_{Appearance}(SO_2)$ (°C)	350	230	200

There are a few possible explanations for the observed increase in the performance of the bimetallic catalyst for the total oxidation of DMDS. First of all, the addition of Pt species in the catalyst increases the number of active sites for the catalytic oxidation of DMDS. However, as can be seen, the effect of adding 0.3 wt-% of Pt on alumina or Cu/Al is very low in terms of T_{50}. Due to the low loading, the increase in the number of active sites is not very high for adsorbing DMDS molecules and helping them to react. Furthermore, when comparing 0.3Pt/Al and Al_2O_3, the T_{100} of DMDS has not changed.

Another potential possibility is that the metal-metal interactions on the surface of the 0.3Pt10Cu/Al catalyst could improve the activity and selectivity of

the catalyst. This is more probable since a close contact between Cu and Pt was observed in the TEM-EDS analysis, TPR experiments and XPS results as well. Another important result is that Pt improved the selectivity of the bimetallic 0.3Pt10Cu/Al catalyst towards the formation of the desirable reaction products, i.e. CO_2 and SO_2. According to the results in Table 11, the 0.3Pt10Cu/Al catalyst showed higher selectivity and 100% yield towards the formation of SO_2 and CO_2 at lower temperatures.

The synergistic effect between Pt and Cu may be due to the simple presence of both in the catalyst (complementary effect) or it is due to the strong metal-metal interactions between the two species. To test this hypothesis, another catalytic test was performed with a mechanical mixture of PtO + CuO + Al_2O_3 in accordance with the composition of the 0.3Pt10Cu/Al catalyst prepared by co-impregnation (Figure 24).

The catalytic activity of the mechanical mixture was observed to be less than that of the co-impregnated catalyst but it still remained higher than that of the monometallic 0.3Pt/Al catalyst. This result shows that the presence of both Cu and Pt is important for high performance but the existence of a contact and strong interactions between the Pt and Cu species significantly improve the catalytic activity. Concerning the selectivity, the yield of SO_2 and CO_2 formation moved to higher temperatures in the case of the mechanical mixture, and thus the selectivity of the catalyst was affected as well.

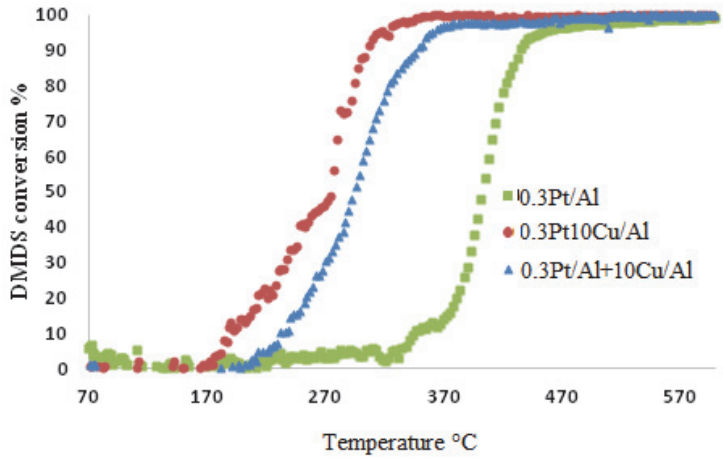

Fig. 24. Light-off curves in DMDS oxidation over the mechanical mixture of 0.3Pt/Al+10Cu/Al and its comparison to 0.3Pt10Cu/Al and 0.3Pt/Al (DMDS 550 ppm, m = 100 mg, RT – 550 °C, 5 °Cmin^{-1}).

To check the influence of the Pt content on the catalytic performance of the PtCu/Al catalysts, three catalysts with different Pt loadings were prepared. Figure 25 shows the results of catalytic tests over xPt10Cu/Al catalysts where x = 0.3, 0.5 and 1 wt-%. The results demonstrate that there was no significant difference in activity between the 0.3Pt10Cu/Al and 0.5Pt10Cu/Al catalyst (BET = 184 m^2g^{-1}) - only a few degrees change to the lower T_{50} temperature was observed. With increasing the loading of the noble metal to 1% Pt (the S-BET of 1Pt10Cu/Al = 183 m^2g^{-1}), it was found that the T_{50} was reached at about 282 °C, which does not show remarkable improvement. However, the T_{100} was attained at higher temperature, at around 420 °C, since the T_{100} temperature difference that was recorded between 1Pt10Cu/Al and 0.3Pt10Cu/Al increased to 100 °C. This may be due to the encapsulation of noble metal oxide by the metal oxide. The different platinum concentrations above 0.3% in the catalyst can lead to Pt encapsulation by CuO after calcination, which means there is little benefit from the active phase. Another explanation is that higher concentrations of Pt particles can lead to larger particle sizes (Kriston 2014). Therefore (and according to these results), only a small loading of the noble metal Pt is sufficient to obtain an

effective catalyst with substantially good synergy between the Pt and Cu species in the oxidation of DMDS.

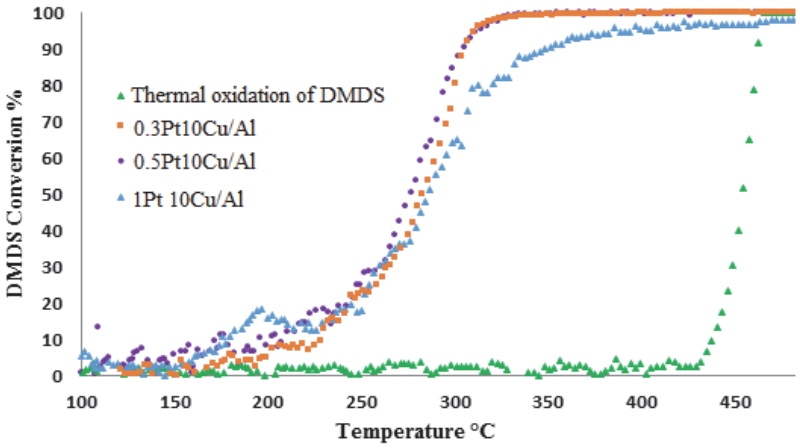

Fig. 25. The effect of platinum loading on the catalytic activity of the Pt-Cu based catalyst.

According to the TEM analysis of 1%Pt10Cu/Al, Pt particles were found deposited on the support without any interaction with copper particles (Figure 26.a), however when inspecting another area of the catalyst, some Pt particles were found deposited on the surface of Cu diffuse areas (Figure 26.b) where Cu species are widely dispersed and spread out in high quantities, probably causing the agglomeration of the small Pt species.

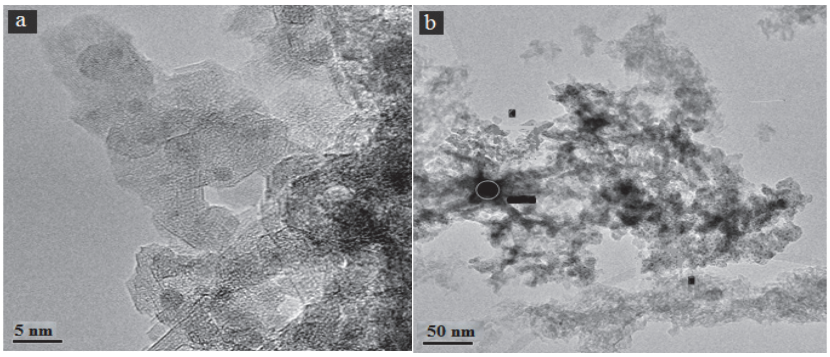

Fig. 26. TEM images of 1Pt10Cu/Al.

In order to have a first overview of the stability of the tested catalysts for the total oxidation of DMDS, the material balance of sulfur was checked, based on the following equation (Eq. 8).

$$CH_3 - S - S - CH_3 + \frac{11}{2} O_2 \rightarrow 2\,SO_2 + 2\,CO_2 + 3\,H_2O \qquad (8)$$

The calculation of the sulfur balance was done to find out if all the fed sulfur exits in the outlet gas mixture. The sulfur balance results grouped in Table 12 confirm that the studied catalysts have catalysed the total oxidation of DMDS in terms of sulfur, meaning that all the sulfur contained in the feed DMDS was found at the end of the reaction in the catalytic oxidation product stream as sulfur dioxide (SO_2). The molar concentration of sulfur after the reaction was calculated at a slightly higher temperature than the total conversion of DMDS observed for 10Cu/Al and 0.3Pt10Cu/Al because the maximum formation of SO_2 was observed at a slightly higher temperature. Furthermore the amount of sulfur at the outlet was somewhat higher than expected. The reason for that could be that the catalyst was adsorbing sulfur at some point at lower temperatures and then, when the temperature was increased, SO_2 started to desorb from the catalyst surface. For Pt/Al, the molar concentration of sulfur is calculated at a temperature slightly lower than the T_{100} of DMDS, the temperature of which corresponds to the maximum production of SO_2. This is also an interesting observation, since it is known that the Pt catalyst can also oxidize sulfur-containing compounds to SO_3,

which leads to H_2SO_4 formation that enhances catalyst deactivation as well as the corrosion of construction materials of the industrial incinerator (Kröcher *et al.* 2009). When the formed reaction by-products were studied it was seen that the reaction proceeds in general via a similar route over these three tested catalysts. The catalytic reaction of DMDS leads to the formation of HCOH, SO_2 and H_2O, and finally to the oxidation of HCOH to CO_2 and H_2O.

Table 12. The sulfur balance of DMDS oxidation over the prepared catalysts at the temperature that corresponds to the maximum formation of the reaction products.

Tested Catalysts	0.3Pt/Al	10Cu/Al	0.3Pt10Cu/Al
DMDS (T_{50}/T_{100}) (°C)	400/530	282/380	280/320
T (where the S balance is calculated) (°C)	510	396	350
n(S) in (10^{-5} molL^{-1})	1.7	1.8	2.2
n(S) out (10^{-5} molL^{-1})	1.7	1.9	2.4

As a conclusion for this subsection the addition of a small amount of platinum seems to be beneficial for the copper catalysts, especially in terms of selectivity, but it may also bring certain advantages to the catalyst related to the resistance to sulfur. Next, the attention will be turned to study the doped alumina support for bimetallic catalyst.

4.2.2 The catalytic performances of the Al_2O_3, $AlSi_{20}$ and SiO_2 supported bimetallic catalysts

In order to evaluate the role of the support, the catalytic performances of the 0.3Pt10Cu/Al, 0.3Pt10Cu/$AlSi_{20}$ and 0.3Pt10Cu/Si catalysts in DMDS oxidation were evaluated. The test results are shown in Figure 27 for the three different catalyst samples.

It can be observed in general that the oxidation of DMDS is obviously influenced by the nature of the support of the tested catalysts. Besides this, the DMDS light-off curve indicates no significant competition between the catalytic and the thermal oxidation.

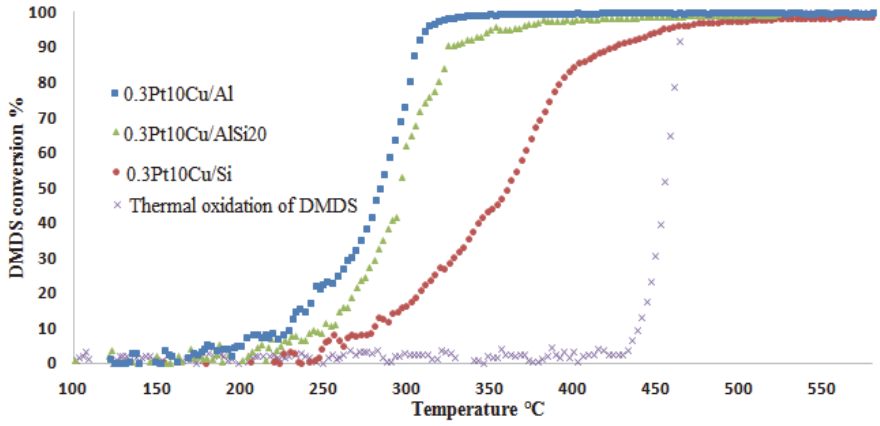

Fig. 27. Light-off curves in DMDS oxidation over 0.3Pt10Cu/Al, 0.3Pt10Cu/$AlSi_{20}$ and 0.3Pt10Cu/Si catalysts (DMDS 550 ppm, $m_{Catalyst}$ = 100 mg, RT – 550 °C, 5 °Cmin^{-1}).

According to Figure 27, all the studied catalysts reached close to 100% DMDS conversion but, nevertheless, the 0.3Pt10Cu/Si catalyst was remarkably less active than the alumina-containing catalysts. Over the catalyst supported on $AlSi_{20}$, about 100% DMDS conversion was reached at 440 °C. The reaction products detected were SO_2, CO_2 and H_2O with only a slight formation of CO, indicating rather good selectivity towards total oxidation products. The catalyst supported on Al_2O_3 showed slightly better activity in terms of lower oxidation temperature than the 0.3Pt10Cu/$AlSi_{20}$ catalyst. Other studies proved the same results (Wang *et al.* 1997, Wang *et al.* 2002) in DMDS oxidation when using the CuO/γ-Al_2O_3 catalyst. The final catalysts were confirmed as active catalysts for the oxidation of DMDS at lower concentrations, varying between 84 ppm to 450 ppm (Wang *et al.* 1997, Wang *et al.* 2002).

According to the DMDS oxidation reaction, as was mentioned previously, the catalytic oxidation of DMDS should finally lead to the formation of CO_2, SO_2 and H_2O. In general, concerning the selectivity of the studied catalysts towards the wanted oxidation products, the significant formation of CO as an incomplete oxidation product was observed in addition to small amounts of some organic intermediate products such as methanol (CH_3OH) and formaldehyde (CH_2O). All the catalysts showed high selectivity towards SO_2 formation. Table 13 summarizes the formed reaction by-products in $molL^{-1}$ and shows that the by-product content at the end of the catalytic reaction over 0.3Pt10Cu/$AlSi_{20}$

matched well the theoretical values and only traces of CO were formed. However, in the case of 0.3Pt10Cu/Al and 0.3Pt10Cu/Si, about 0.9 and 0.8 $molL^{-1}$ of CO were observed respectively. The results also showed that 0.3Pt10Cu/$AlSi_{20}$ had almost similar activity to 0.3Pt10Cu/Al in DMDS oxidation, but the formation of CO_2 and SO_2 is closer to the targeted values.

Table 13. A comparison of the catalytic reaction products at the outlet stream for the 0.3Pt10Cu/Al, 0.3Pt10Cu/$AlSi_{20}$ and 0.3Pt10Cu/Si catalysts.

Samples	0.310Pt10Cu/Al	0.3Pt10CuO/$AlSi_{20}$	0.3Pt10CuO/Si	Expected values
CO ($molL^{-1}$) 10^{-5}	0.9	**0.2**	0.8	≈ 0
CO_2 ($molL^{-1}$) 10^{-5}	2.8	**2.4**	1.6	2
SO_2 ($molL^{-1}$) 10^{-5}	2.2	**2.0**	2.6	2

Figure 28 and Figure 29 show the evolution of the intermediates and desired products of the DMDS oxidation over 0.3Pt10Cu/Al and 0.3Pt10Cu/$AlSi_{20}$ respectively. Both catalysts follow the same behaviour in general, however, we found a clear difference regarding in which way each catalyst leads to the formation of the desirable reaction products.

According to the results, the 0.3Pt10Cu/Al catalyst (Figure 28) does not advance the reaction towards the formation of CO_2 as fast as in the case of the $AlSi_{20}$ supported catalyst. It was found that somewhat before 450 °C, the 0.3Pt10Cu/$AlSi_{20}$ catalyst (Figure 29) has promoted the oxidation of CO and HCOH to CO_2, but in the case of the 0.3Pt10Cu/Al catalyst, only a small formation of CO_2 is observed and the concentrations of HCOH and CO (measured in ppm) have not begun to decline.

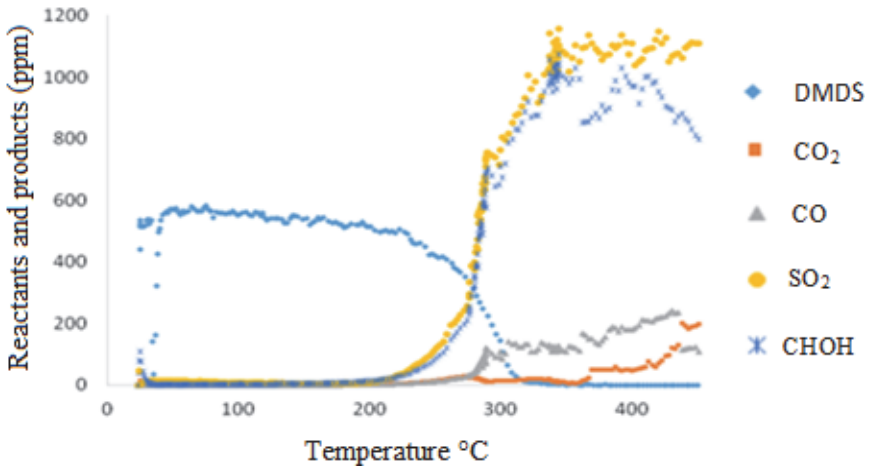

Fig. 28. The evolution of reactant and intermediate products during the oxidation of DMDS over 0.3Pt10Cu/Al.

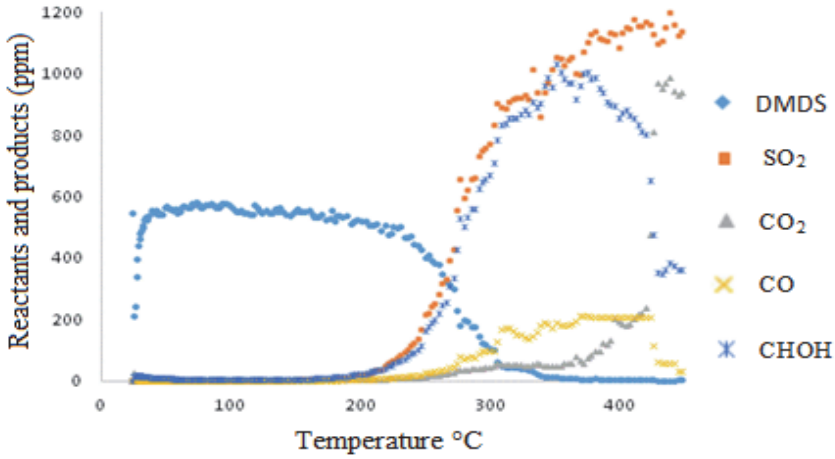

Fig. 29. The evolution of reactant and intermediate products during the oxidation of DMDS over 0.3Pt10Cu/$AlSi_{20}$.

To conclude, the addition of less than 20% of SiO_2 to the Al_2O_3 support leads to almost to the same catalytic activity as that reached over the pure alumina supported catalyst but it remarkably enhances the selectivity of the 0.3Pt10Cu/$AlSi_{20}$ catalysts in terms of SO_2, CO_2 formation while avoiding the

formation of a high concentration of CO. These findings indicate strongly that the $AlSi_{20}$ supported catalyst would be the most active, selective and stable catalyst in the oxidation of DMDS among the studied materials. Next, the attention will be turned to confirm the stability assumption of the doped alumina support.

4.2.3 The durability of the 0.3Pt10Cu/Al and 0.3Pt10Cu/$AlSi_{20}$ catalysts

The catalytic oxidation of S-VOCs does not only necessitate high activity but also the ability to direct the reaction to yield the desired reaction products. The over-oxidation of sulfur to form SO_3, leading to H_2SO_4 formation, should especially be avoided and a theoretical maximum of SO_2 formation should be aimed for. In addition, due to the presence of sulfur, the stability of the catalyst plays an important role. However, stability improvement is expected by using the Al_2O_3-SiO_2 support since it has been found that the amorphous Al_2O_3-SiO_2 phase increases the resistance of the supported catalyst against sulfur poisoning (van Veen *et al.* 1999, Robinson *et al.* 1999). For this reason, and based on the activity experiments, the most active catalyst (i.e. 0.3Pt10Cu/Al) and the most selective catalyst (i.e. 0.3Pt10Cu/$AlSi_{20}$) were chosen for a long-term stability test in DMDS oxidation at a constant temperature of 400 ºC. For the 0.3Pt10Cu/$AlSi_{20}$ catalyst (Figure 31), according to the established results, no evident decrease in the catalyst performance was detected during the stability test. The DMDS conversion stayed stable at about 99%. In the activity of 0.3Pt10Cu/Al (Figure 30), a decrease of 3% was observed already after 6 h on stream. Moreover, there was no noticeable decline in the selectivity towards SO_2 during the stability test for either of the catalysts.

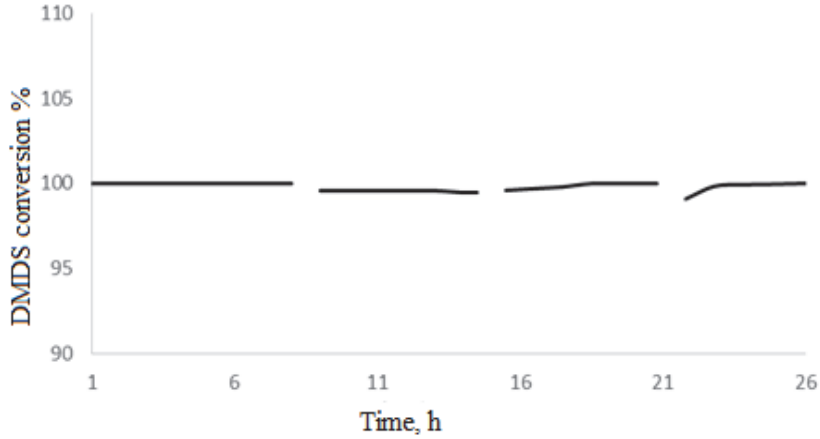

Fig. 30. The stability of the 0.3Pt10Cu/AlSi$_{20}$ catalyst in the oxidation of DMDS (at 400 °C with 550 ppm DMDS).

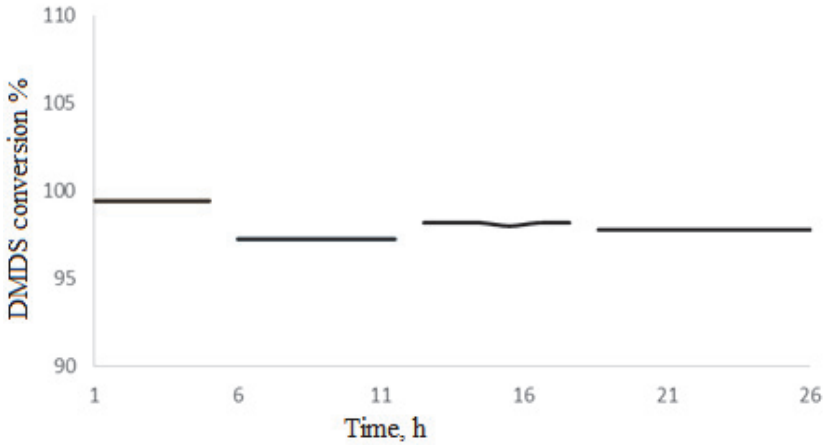

Fig. 31. The stability of the 0.3Pt10Cu/Al catalyst in the oxidation of DMDS (at 400 °C, with 550 ppm DMDS).

Once the stability tests of 30 h were over, the light-off tests were carried out again for the 0.3Pt10Cu/AlSi$_{20}$ and the 0.3Pt10Cu/Al catalysts (Figure 32) in order to compare the behaviour of the fresh and aged catalysts. According to the results, the catalytic activity of the studied catalyst seems to be promoted after the ageing

experiments in the temperature range of 150–290 ºC, which may be due to the rearrangement of the catalytically active surface. At a higher temperature range, it was observed that the DMDS conversion over 0.3Pt10Cu/AlSi$_{20}$ was slightly decreased, as well as the T_{90} value which was shifted from 320 ºC for the fresh catalyst to 400 ºC for the used one (Table 14). The T_{50} value shifted to lower temperatures, i.e. from 298 ºC to 225 ºC. Furthermore, the selectivity was observed to be stable towards the SO_2 (100% yield) and CO_2 (98–99%) formation in addition to a slight formation of CO, i.e. about 6% (Table 15). However, the carbon balance was observed to exceed 100%, which can be explained by the adsorption and the accumulation of DMDS on the catalyst surface at the beginning of the reaction. When temperature was increased, the catalyst started to release the accumulated DMDS at the same time as the recently adsorbed DMDS, which affected the carbon balance calculation.

Regarding the 0.3Pt10Cu/Al catalyst, the displayed results in Figure 32 prove that the activity was changed and deteriorated severely. The T_{50} value was shifted to a higher temperature, from 285 ºC to 330 ºC (Table 14), as was the T_{90} value that shifted from 310 ºC to over 500 ºC.

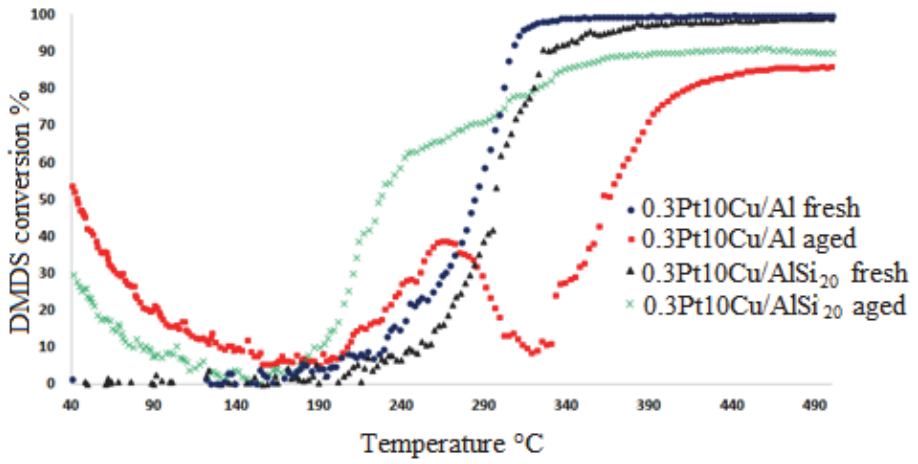

Fig. 32. Light-off curves in DMDS oxidation over 0.3Pt10Cu/Al and 0.3Pt10Cu/AlSi$_{20}$ before the ageing and after 30 h on stream.

Table 14. The T_{90} and T_{50} values for DMDS oxidation over the fresh and used (after stability tests) catalysts.

Studied catalysts	0.3Pt10Cu/Al	0.3Pt10Cu $AlSi_{20}$	0.3Pt10Cu/Si
T_{90} for fresh (°C)	310	320	480
T_{50} for fresh (°C)	285	298	362
T_{90} for used (°C)	≥ 500	400	_
T_{50} for used (°C)	330	225	_

In addition, a decline in the selectivity towards CO_2 was observed. The yields of CO_2 and CO were measured at the end of the stability tests (Table 15). Furthermore, not only CO was observed during the catalytic oxidation experiment but some other by-products were formed too, e.g. DMS (C_2SH_6). According to the XPS analysis, an alumina supported catalyst was vulnerable against the deactivation due to sulfur. Furthermore, there was a noticeable accumulation of sulfur on the alumina supported catalyst surface as well as a decrease in the Pt and Cu surface dispersion on the support. However, the $AlSi_{20}$ supported catalyst showed resistance against sulfur. The XPS analysis indicated a low concentration of sulfur on the surface of the catalyst after the stability test, as well as higher dispersion of Pt and Cu species compared to the alumina supported catalyst. Thus, less than 20% of SiO_2 provided a potential resistance and tolerance towards sulfur poisoning.

Table 15. The SO_2, CO_2 and CO yields for the 0.3Pt10Cu/Al and 0.3Pt10Cu/$AlSi_{20}$ catalysts after the stability tests.

Samples	0.3Pt10Cu/Al	0.3Pt10Cu/$AlSi_{20}$
SO_2 (%)	100	100
CO_2 (%)	69	98
CO (%)	21	6

Earlier, we mentioned the improvement caused by the amorphous nature of alumina-silica support proposed by van Veen and Sie, and Robinson *et al.* (van Veen and Sie 1999, Robinson *et al.* 1999). An additional explanation could be that the addition of SiO_2 onto γ-Al_2O_3 decreased the surface basicity and increased the surface acidity of the catalyst, providing good conditions to enhance desorption of SO_2 molecules from the surface of the catalyst after its formation in the DMDS oxidation reaction. A number of different groups have concluded from their

studies that strong SO_2 adsorption could occur at basic sites (Dalla Lana *et al.* 1993, Karge *et al.* 1984, Pacchioni *et al.* 1994).

4.3 Studies on the industrial deactivation of monolithic catalysts 1Pt/Al and 1Pt/Al-R1

This section is devoted to the study of catalyst deactivation via understanding the deactivation of the industrially aged 1Pt/Al monolithic catalyst and simulating the industrial deactivation by an accelerated deactivation procedure. The other catalyst, 1Pt/Al-R1, will not be studied and characterized in detail in this thesis due to the related confidentiality. It is brought into this section to reinforce the evaluation of the efficiency and representativeness of the developed rapid deactivation procedure.

The deactivation study was carried out with the help of several characterization methods and by verifying the actual activities of different samples in the total oxidation of DMDS (using the wash-coat part from the metallic 1Pt/Al and 1Pt/Al-R1 monoliths). The accelerated laboratory-scale deactivation procedure is performed using SO_2-H_2O as the poisoning atmosphere (Figure 4, see also the Subsection 3.4.2).

4.3.1 Characterization studies on monolithic industrially aged 1Pt/Al and 1Pt/Al-R1 catalysts

This section is devoted to comparing the textural and structural properties of the 1Pt/Al and 1Pt/Al-R1 catalysts and to studying the effect of the support, since the two catalysts have the same active phase but different support materials.

Elemental analysis by XRF

The elemental analysis by XRF is performed for the industrially aged 1Pt/Al and 1Pt/Al-R1 catalysts to determine the weight percentage of sulfur in different samples. The results obtained are summarized in Table 16.

Table 16. Elemental analysis by XRF.

Catalysts	S wt-% (XRF)
1Pt/Al industrially aged	17
1Pt/Al-R1 industrially aged	17

According to the XRF results, a high amount (17%) of sulfur was found in the case of both the industrially aged 1Pt/Al and 1Pt/Al-R1 catalysts, meaning that both catalysts were most probably exposed to significant poisoning by sulfur compounds.

The measurement of specific surface area and pore volume

The specific surface areas of the catalytic materials, as well as their pore volumes, were determined by nitrogen adsorption. The BET surface area and pore volume (based on the BJH method) for fresh and industrially aged catalysts are presented in Table 17.

The results of the specific surface area measurements of the catalysts showed that the surface area of 1Pt/Al-R1 decreased significantly, i.e. by about 75%, during the industrial ageing but not as severely as in the case of 1Pt/Al which had a BET decrease of about 96% (Table 17). This reduction in the BET surface area could be caused by a sintering phenomenon caused by crystal growth on the surface of the industrially aged catalyst or sintering of the support itself. This change in the structure of the catalysts can to some extent cause physical deactivation when the active surface of the catalyst decreases by structural changes (Russell *et al.* 2011, Bartholomew 2001). Typically, thermal deactivation occurs when the temperature rises unexpectedly, causing sintering of the precious metals and catalytic materials (Cavataio *et al.* 2009, Neyestanaki *et al.* 2004). In the case of the Al_2O_3 support, sintering occurs during phase transformation from γ to θ at high temperatures (at around 1000 °C or lower in the presence of water), resulting in a loss of surface area (Hayes and Kolaczkowski 1997). This assumption is proven later by the XRD measurement results.

Concerning the noble metals, and especially Pt, sintering usually occurs at lower temperatures than for the metal oxides (at over 600 °C) (Neyestanaki *et al.* 2004). In conclusion to both cases, the precious metal coating may have been sintered or coagulated to form larger particles with a lower surface area and/or there might have been a phase change in the support material and then a decrease in the surface area. Moreover, it was noticed that the different support material of 1Pt/Al-R1 has a stabilizing effect, most probably since it contains silicon oxide as one of the support compounds, which is known for its good interaction with the active phase (Darif *et al.* 2016).

Table 17. The BET-BJH results of the fresh, used and poisoned self-made and industrial catalysts.

Catalysts	Surface area (BET) m^2g^{-1}	Total pore volume cm^3g^{-1}	Pore diameter nm
1Pt/Al fresh	188	0.44	9.18
Pt/Al industrially aged	8	0.01	5.11
1Pt/Al-R1 fresh	191	0.3	6
1Pt/Al-R1 industrially aged	48	0.04	3.3

It was also found that both the catalysts showed a decrease in the total pore volume and pore diameter after industrial deactivation.

XRD analysis

According to the XRD results, Pt was not detected in the industrially aged 1Pt/Al (Figure 33) and 1Pt/Al-R1 (Figure 34) catalysts. The appearance of a new phase was detected in the case of the support, as the XRD showed the presence of θ-alumina (ICDD 00-023-1009). The γ-alumina (ICDD 00-050-0741) has transformed at high temperatures into the θ-phase, resulting in a loss of surface area, which was proved previously by the decrease in the specific surface area. Moreover, this phase transformation is associated with the loss of H_2O and with increasing the temperature that can thereafter cause a gradual loss of the internal pore network structure (Matori *et al.* 2012).

Another result found by the XRD analysis is related to the decrease in the intensity of Al_2O_3 peaks, which explains the formation of new phases on the industrially aged catalysts, i.e. aluminum sulfates (ICDD 01-081-1835) that can be explained by the non-selective poisoning when sulfur is deposited on the alumina support by forming new compounds and masking the pores. This is another cause for the deactivation since aluminum sulfates are not active in DMDS oxidation and when they block the pores, they also decrease the specific surface area of the support. The aluminium sulfate formation is a type of chemical deactivation. The chemical deactivation may be considered as a poisoning process wherein the catalytic oxidation performance decreases due to the chemisorption of undesirable elements on the active metal and the catalyst support (Bartholomew 2001, Winkler *et al.* 2009). The poisoning species, such as sulfur (S), may exist in the reactants or the reaction products in the form of organic or inorganic compounds. It has also been reported earlier that the formation of

$Al_2(SO_4)_3$ on the surface of Pt/Al_2O_3 (if SO_2 or sulfur compounds exist in the gas feed) can block catalyst pores and lower the catalyst's oxidation activity (Peter-Hoblyn *et al.* 1999, Manson 2000, Deeba *et al.* 2000).

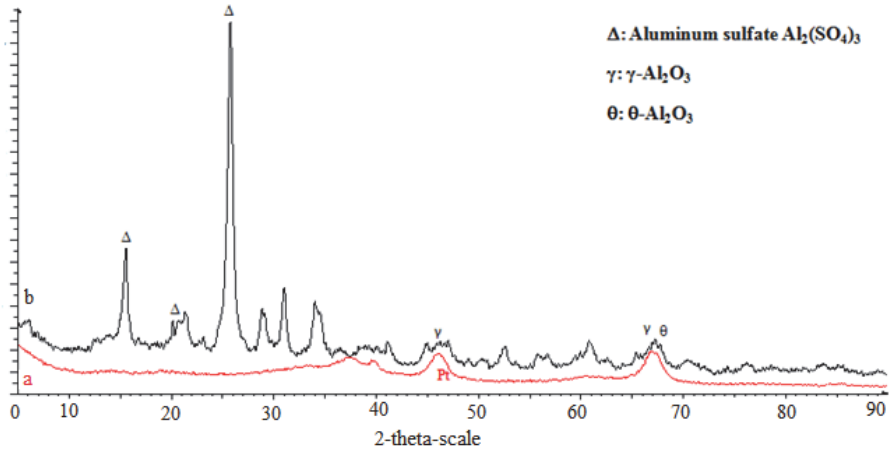

Fig. 33. XRD diffractograms of the fresh 1Pt/Al catalyst (a) and the industrially aged. 1Pt/Al catalyst (b).

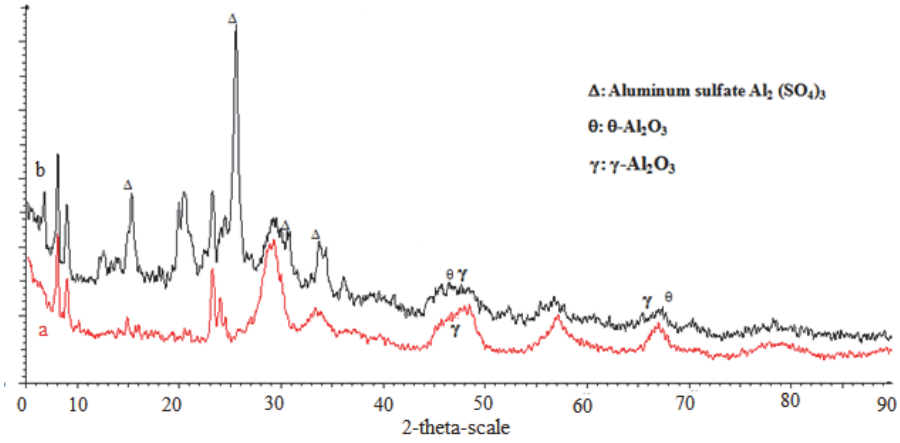

Fig. 34. XRD patterns for the fresh 1Pt/Al-R1 catalyst (a) and the industrially aged 1Pt/Al-R1 catalyst (b).

FESEM

To get an overview about the existence and the deposition of sulfur on the industrially aged 1Pt/Al and 1Pt/Al-R1 catalysts, FESEM images with elemental mapping were made. Figure 35 shows that some overlapping of S, O and Al exists. This confirms the fact that new compounds, such as aluminium sulfate, have been formed on the surface of the alumina support.

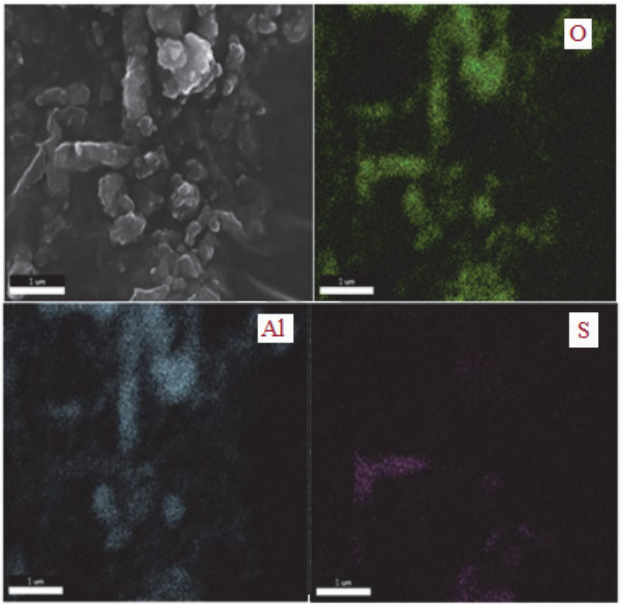

Fig. 35. Elemental mapping by FESEM for O, Al and S species on the surface of the industrially aged 1Pt/Al catalyst.

For the 1Pt/Al-R1catalyst (Figure 36), we found that the small areas of Pt species are located in the same region where Al is and this is presented in the FESEM images. Another finding is that the support material of this catalyst essentially consists of Al-Si oxide. Moreover, it was found that there is an overlapping of S, O and Al on the catalyst, which can explain the appearance of sulfates in the XRD analysis.

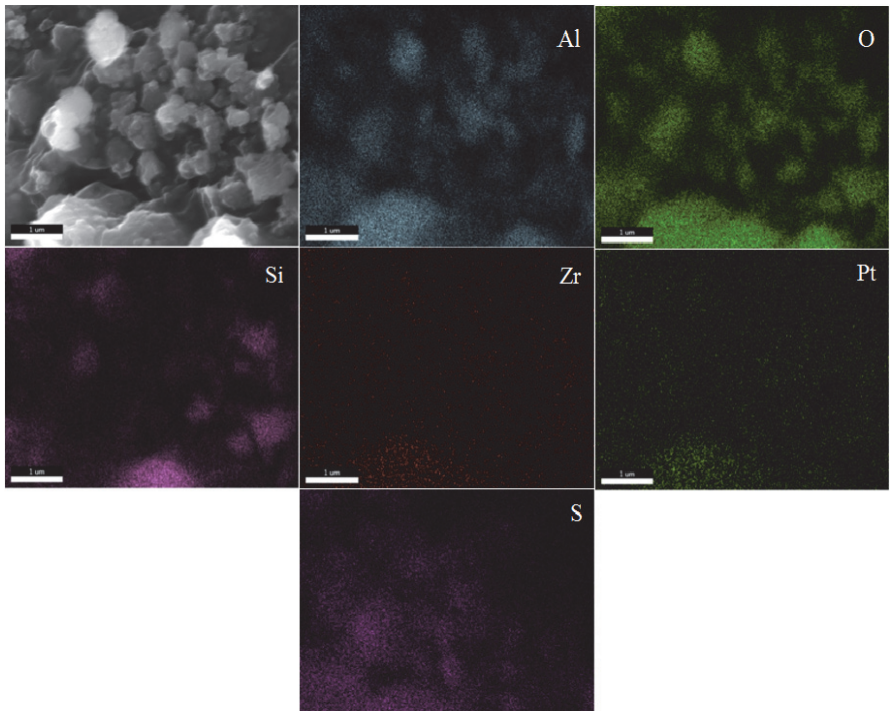

Fig. 36. Elemental mapping by FESEM for O, Al, Pt, Si, Zr and S species on the surface of the used 1Pt/Al-R1 catalyst.

TEM

After the industrial ageing, we expect some sintering of Pt. To test this assumption, TEM analyses were made to reveal information on the structure of fresh and industrially aged 1Pt/Al catalysts, including the characterization of Pt particle architecture and the assessment of their sizes.

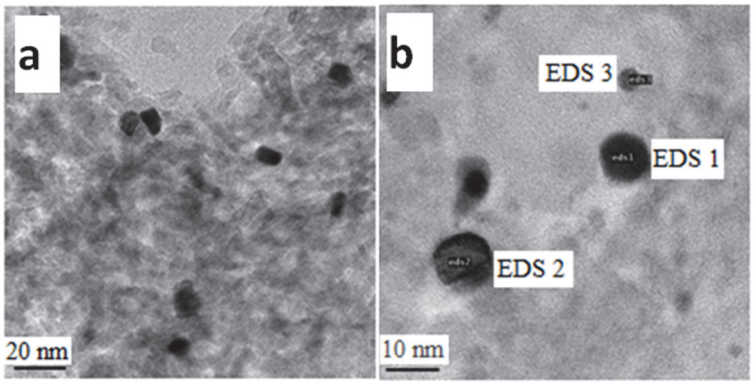

Fig. 37. TEM of the fresh 1Pt/Al catalyst (a) and the industrially aged 1Pt/Al catalyst (b).

For the fresh 1Pt/Al catalyst, the TEM results (Figure 37a) showed that Pt particles seem to be fairly uniform in size, in the order of 7 nm, and relatively well dispersed. Concerning the industrially aged 1Pt/Al catalyst (Figure 37b), the Pt particles were found to not be homogeneously uniform on the surface of the catalysts and some of the Pt particles were sintered and were measured to be about 10 nm. Moreover the TEM coupled with EDS analysis, showed that sulfur is deposited not only on the support, but also on the active phase. Table 18 shows details of these results.

Table 18. EDS measurements for different Pt particles on the surface of the used Pt/Al catalyst.

EDS analysis	O	Al	S	Pt	Total (Atom-%)
EDS 1 on a Pt particle	48.65	29.27	10.36	11.72	100
EDS 2 on a Pt particle	58.67	32.02	3.83	5.48	100
EDS 3 on a Pt particle	59.13	30.04	6.77	4.07	100

XPS

The XPS spectra of different fresh and industrially aged 1Pt/Al catalysts were analysed in order to identify and compare the oxidation states of the active species on the surface.

The decomposition of the spectra of individual components of Pt $4d_{5/2}$ showed the presence of a single type of platinum in the case of the fresh catalyst

1Pt/Al (Figure 38a). Indeed, the spectral peak (Pt $4d_{5/2}$) with EB at around 315.8 eV is associated with metallic platinum, Pt (0). However, concerning the industrially aged 1Pt/Al catalyst, the decomposition of the Pt $4d_{5/2}$ spectral levels showed the presence of two platinum species (Figure 38b). The spectral peak ($Pt4d_{5/2}$) of BE at around 315 eV is associated with the chemical state of Pt (0), but the last peak at 318.5 eV corresponds to the platinum species interacting with the ionic SO_2^{-4} of the metallic interface of the support (Duong *et al.* 2005).

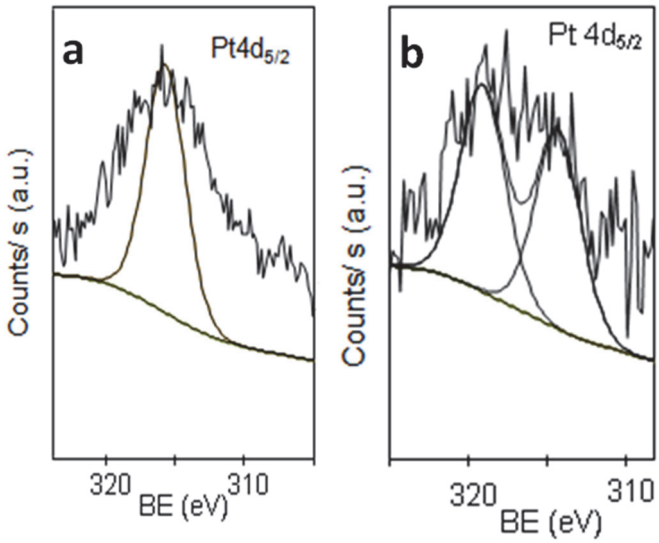

Fig. 38. Pt of the fresh 1Pt/Al catalyst (a) and the industrially aged 1Pt/Al catalyst (b).

Regarding O 1s, the spectral decomposition of individual components of the O 1s level showed the presence of three oxygen species in the case of the fresh 1Pt/Al catalyst (Figure 39a). Both spectral peaks (O 1s) with BE at around 530 and 531 eV are associated with the oxygen atoms in the oxide network and the last peak, at 532 ± 0.3 eV, comes from surface oxygen, such as hydroxyl groups (Kim *et al.* 2010). For the industrially aged 1Pt/Al catalysts, the decomposition of the spectra of individual components of the O 1s level showed the presence of two oxygen species (Figure 39b). The spectral peak (O 1s), with BE at around 530.5 eV, is associated with the oxygen atoms in the oxide network and the last peak, at 532.4 eV, could be derived from oxygen in the sulfated groups $Al_2(SO_4)_3$.

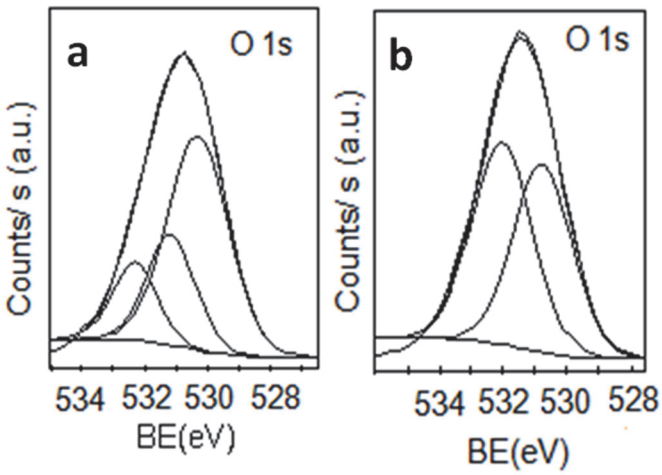

Fig. 39. O 1s of the fresh 1Pt/Al catalyst (a) and the and the industrially aged 1Pt/Al catalyst (b) .

Concerning the S element – and according to the decomposition of the individual components of the spectral levels S 2p of the industrially aged 1Pt/Al catalyst (Figure 40) – the binding energy of the S $2p_{1/2}$ = 168.8 eV and S $2p_{3/2}$ = 167.5 eV showed that sulfur is only present in the form S^{6+} (Kohler *et al.* 1982, Ku *et al.* 1981, Briggs *et al.* 1990, Wagner *et al.* 1999). Thus, it can be deduced that sulfur is present in a single form and in a single type of sulfate in the surface structure of the concerned catalysts, as shown by the presence of a single transition S $2p_{1/2}$ and a single S $2p_{3/2}$.

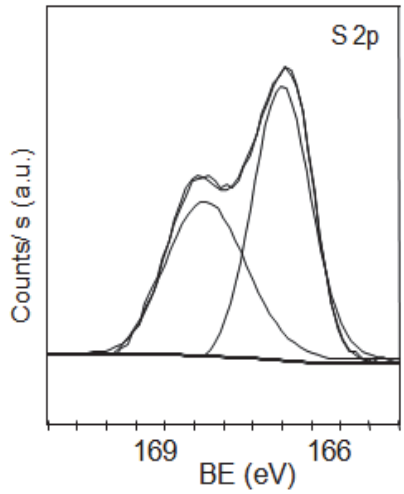

Fig. 40. S 2p of the industrially aged 1Pt/Al catalyst.

Based on what has been found previously by the performed characterization methods, the deactivation of the studied catalysts was clear because of sulfur poisoning, Pt sintering on the surface of the catalyst and phase transformation induced thermally at high temperatures or at somewhat lower temperatures in the presence of water or impurities.

After going through all the previous results, the chemical type of deactivation was especially chosen for simulation in this study. To reach the sintering of the support, a thermal ageing procedure should be done before the chemical poisoning by sulfur since carrying out the chemical deactivation at 400 °C in the presence of water did not lead to exactly the same result as that of the industrial ageing. An accelerated laboratory-scale deactivation procedure was performed using SO_2-H_2O as the poisoning feed for both fresh 1Pt/Al and 1Pt/Al-R1 catalysts. The conditions of the used poisoning treatment are presented in Figure 4.

4.3.2 Characterization studies of monolithic laboratory aged 1Pt/Al and 1Pt/Al-R1 catalysts

Elemental analysis by XRF

The elemental analysis by XRF was performed for the laboratory aged 1Pt/Al and 1Pt/Al-R1 catalysts to determine the weight percentage of sulfur. The results obtained are summarized in Table 19.

Table 19. Elemental analysis by XRF.

Catalysts	S wt-% (XRF)
1Pt/Al, laboratory aged	0.9
1Pt/Al-R1, laboratory aged	2

According to the XRF results, the higher sulfur concentration (2%) was registered for the 1Pt/Al-R1 catalyst and 0.9% of sulfur was found in the case of the laboratory aged 1Pt/Al catalyst.

The measurement of specific surface area and pore volume

The specific surface areas of the catalytic materials, as well as their pore volumes, were determined by nitrogen adsorption. The results obtained are collated by the BET and BJH methods. The BET-BJH results of the fresh and laboratory aged 1Pt/Al and 1Pt/Al-R1 catalysts are presented in Table 20.

According to Table 20, the specific surface areas of the laboratory aged 1Pt/Al and 1Pt/Al-R1 catalysts decreased by more than 50% during the ageing, which is in line with the decrease of the total pore volume. The only difference noticed in this study was that the pore diameter increased instead of decreasing, as in the case of the industrially aged 1Pt/Al and 1Pt/Al-R1 catalysts. In comparison to the results observed for the industrially aged catalysts, the accelerated deactivation treatment of 5 h does not induce as severe decrease in BET as the industrial ageing did. The higher decrease of specific surface area could be realized with thermal treatment at high temperature before chemical deactivation.

Table 20. BET-BJH results for the fresh and laboratory aged Pt/Al-R1 catalysts.

Catalysts	Surface area (BET)/ m^2g^{-1}	Total pore volume cm^3g^{-1}	Pore diameter nm
1Pt/Al fresh	188	0.44	9.2
Pt/Al-R1 laboratory aged	90	0.24	10.6
Pt/Al-R1 fresh	191	0.3	6
Pt/Al-R1 laboratory aged	88	0.2	7.2

It is good to mention here, that the XRD measurements of the catalysts that had undergone accelerated deactivation treatment did not show clear differences or the formation of new phases on the catalysts. This may be due to the low sulfur loading and lower temperature.

FESEM

To get an overview about the existence of sulfur on the laboratory aged 1Pt/Al and 1Pt/Al-R1 catalysts, FESEM images with elemental mapping were made. Figure 41 shows that some overlapping of S, O and Al exists. This confirms the fact that new compounds, such as aluminum sulfate, have been formed on the surface of the 1Pt/Al catalyst.

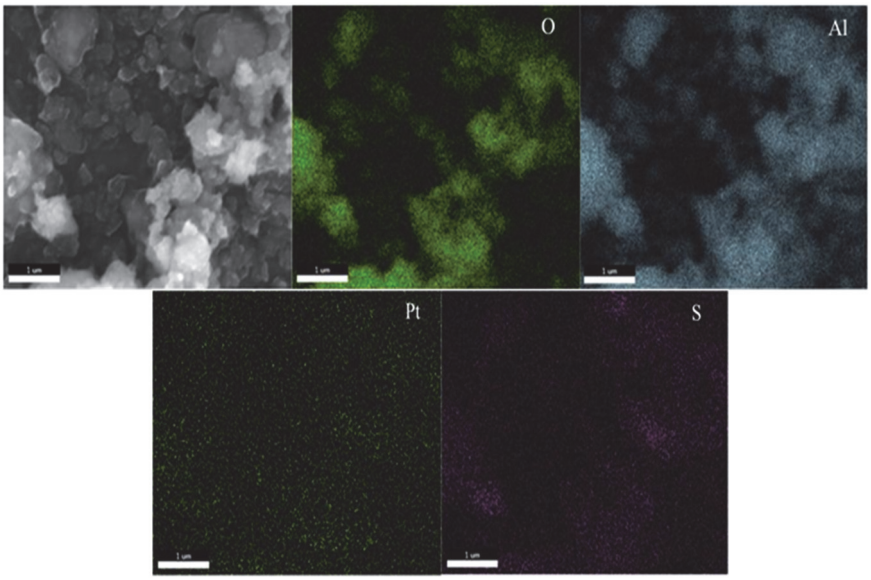

Fig. 41. Elemental mapping by FESEM for O, Al, Pt and S species on the surface of the laboratory aged 1Pt/Al catalyst.

Concerning the laboratory aged 1Pt/Al-R1 catalyst (Figure 42) there is an appearance of sulfur but at a lower concentration than that found in the case of the industrially aged catalyst, as the previous XRF results have confirmed. The sulfur species were found in the regions of Al and O, which could also indicate the formation of new sulfate phases.

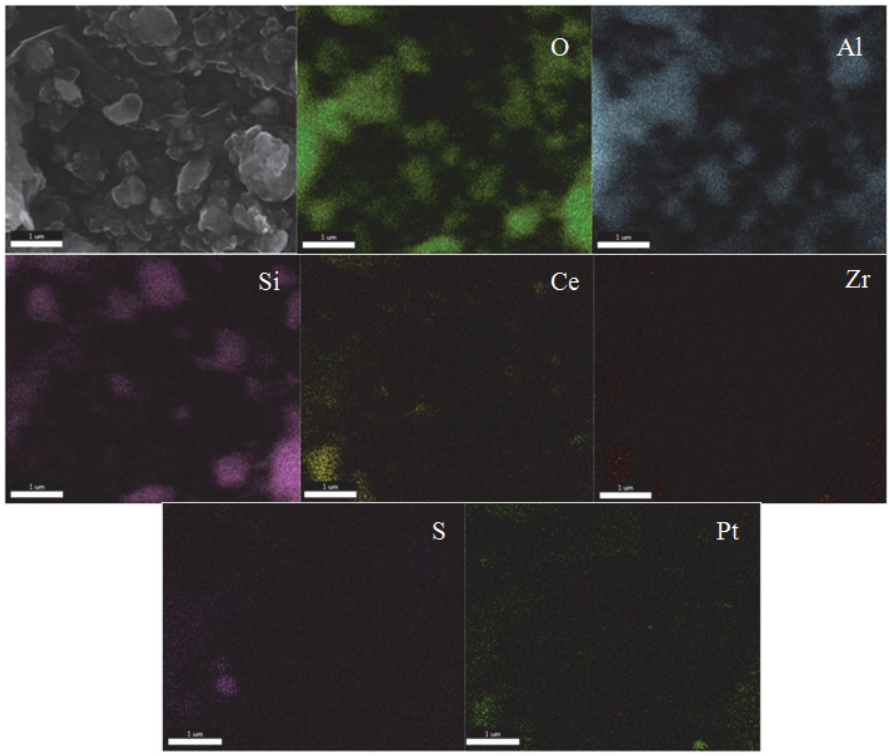

Fig. 42. Elemental mapping by FESEM for O, Al, Pt, Si, Zr, Ce and S species on the surface of the laboratory aged 1Pt/Al-R1 catalyst.

According to what was found earlier, sulfur was clearly seen on the surface of the catalysts that had undergone the accelerated deactivation procedure.

TEM

Temperature was controlled carefully during the accelerated ageing treatment and it was 400 °C. At such temperatures, no severe thermal deactivation of alumina was expected and, in fact, no other phases than γ-Al_2O_3 were observed in the XRD analysis. However, the $T_{Hüttig}$ for PtO and T_{Tamman} for PtO_2 phases are exceeded, indicating a slight possibility for an increase in the particle size. In order to confirm this, TEM measurement was done for the 1Pt/Al catalyst that had undergone the accelerated deactivation (Figure 43).

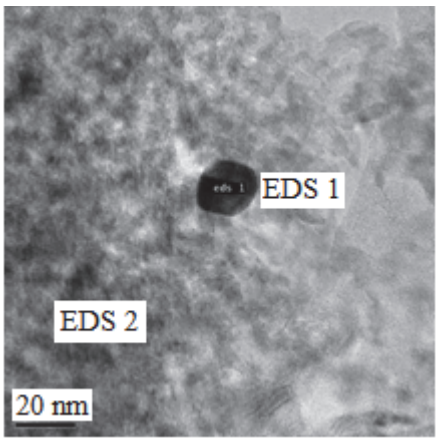

Fig. 43. TEM Pt image of the laboratory aged 1Pt/Al.

Figure 43 shows the TEM image of the 1Pt/Al catalyst after accelerated deactivation. Some of the Pt particles seem to be sintered and their size was measured to be around 20 nm, which proves what was expected based on the $T_{Hüttig}$ and T_{Tamman} temperatures. The results of TEM-EDS measurements presented in Table 21 showed that sulfur appears on the active phase and the support.

Table 21. EDS measurements for different Pt particles on the surface of the poisoned Pt/Al catalyst.

EDS analysis	O	Al	S	Pt	Total (Atom-%)
EDS 1 on a Pt particle	59.39	32.76	1.58	6.27	100
EDS 2 on the support	63.95	36.01	0.02	0.01	100

XPS

The XPS spectra of the 1Pt/Al catalysts after accelerated deactivation were analysed in order to identify and compare the oxidation states of the active species on the surface.

The decomposition of the spectra of individual components of Pt $4d_{5/2}$ showed the presence of two platinum species (Figure 44). The BE of the peak ($Pt4d_{5/2}$) at around 315 eV is associated with the chemical state of Pt (0), but the

last one, at 318.5 eV, could correspond to the platinum species interacting with the ionic SO_2^{-4} of the metallic interface of the support (Duong *et al.* 2005), which is the same result found in the case of the industrially aged 1Pt/Al catalyst. It can be concluded that this deactivation procedure has not been comparable to the industrial deactivation quantitatively in terms of sulfur content but as the XPS results showed, it is qualitatively comparable.

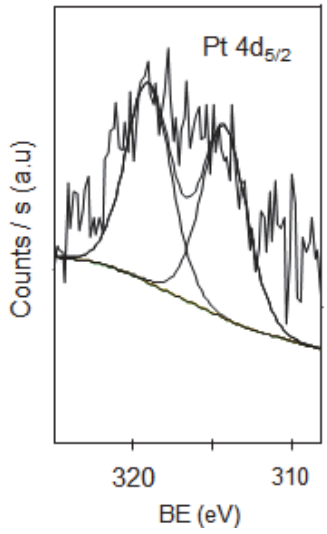

Fig. 44. The Pt of the laboratory aged 1Pt/Al.

In the next subsection, the catalytic performances of the fresh, industrially aged and laboratory aged 1Pt/Al and 1Pt/Al-R1 catalysts are evaluated in the oxidation of DMDS.

4.3.3 Activity performance comparison of the fresh, industrially aged and laboratory aged 1Pt/Al, 1Pt/Al-R1 catalysts

To study the performance of fresh, industrially aged and catalysts that had undergone accelerated deactivation, activity tests were carried out for 1Pt/Al and 1Pt/Al-R1. The conversions of DMDS over the 1Pt/Al and 1Pt/Al-R1 catalysts are shown in Figure 45 and Figure 46 respectively. The results show that the accelerated deactivation treatment affected the activity of both the catalysts.

The fresh 1Pt/Al catalyst seems to be relatively active in the catalytic oxidation of DMDS, but at high temperatures T_{90} = 426 °C compared to the self-made bimetallic catalysts, as the results from Figure 45 and Table 22 show. In the case of the industrially aged catalyst, it was noticed that its catalytic performance in DMDS oxidation decreased in terms of T_{50} and T_{90}. This behaviour indicated that the active surface of the catalyst has been modified in some way, which prevents the catalyst from working as efficiently as the fresh one in the oxidation of DMDS. The explanation for this was found before by the results of the XRD, BET, XRF and XPS studies. The results showed the existence of other new species, such as aluminium sulfates and the formation of new alumina phases on the surface of the studied catalyst, thereby decreasing the specific surface area.

After performing the accelerated deactivation procedure in the laboratory, the catalytic performance of the 1Pt/Al catalyst in the oxidation of DMDS was evaluated as well. The summarized results shown in Figure 45 and Table 22, that the sulfur ageing affected the activity of the 1Pt/Al catalyst in a negative way. According to the BET-BJH data, the surface area of Pt/Al only decreased by 52% (with a 95% decrease in the case of the industrially aged catalyst) and yet the catalytic results were relatively close to each other. This finding can allow us to consider the success of simulating the industrial aging of the catalysts; even the decrease in the specific surface area was remarkably noticebale after industrial ageing. According to the XPS results, it was found that the presence of Pt (0) and Pt (IV) species in the metal surface of the Pt based catalyst can provide an environment in which SO_2 interactions can happen faster (Corro *et al.* 2003, Darif *et al.* 2016).

Table 22. A comparison of the light-off temperatures T_{50} and T_{90} in the oxidation of DMDS over fresh, industrially aged and laboratory aged 1Pt/Al catalysts.

Catalyst	Treatment	T_{50}	T_{90}
Pt/Al	Fresh	375	426
	Industrially aged	404	454
	Laboratory aged	392	440

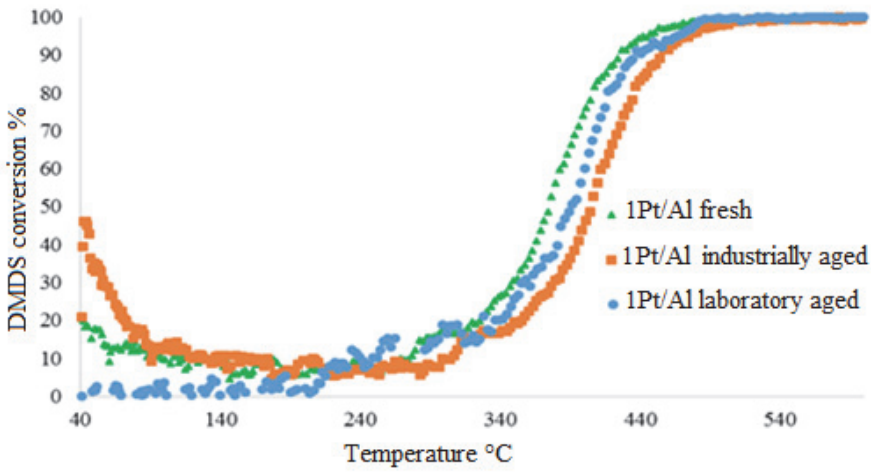

Fig. 45. Light-off tests for DMDS oxidation over fresh, industrially aged and laboratory aged 1Pt/Al catalysts.

Concerning the fresh 1Pt/Al-R1 catalyst, it was more active in the oxidation of DMDS than the 1Pt/Al catalyst. The observed T_{90} was 380 °C, as Figure 46 and Table 23 show. This is probably due to the used support material that was different than that used in 1Pt/Al. In the case of the industrially aged 1Pt/Al-R1 catalyst, it was noticed that the catalytic performance in DMDS oxidation decreased in terms of T_{50} and T_{90}. The earlier presented XRD, BET, XRF and FESEM measurements showed the sintering of the Pt species, the existence of new species (such as aluminium sulfates) and the formation of new phases e.g. θ-Al_2O_3 on the surface of the studied catalyst, similar to the 1Pt/Al catalyst.

Table 23. A light-off temperature comparison (T_{50} and T_{90}) in the oxidation of DMDS over fresh, industrially aged and laboratory aged 1Pt/Al-R1catalysts.

Catalyst	Treatment	T_{50}	T_{90}
Pt/Al-R1	Fresh	317	380
	Industrially aged	379	450
	Laboratory aged	371	438

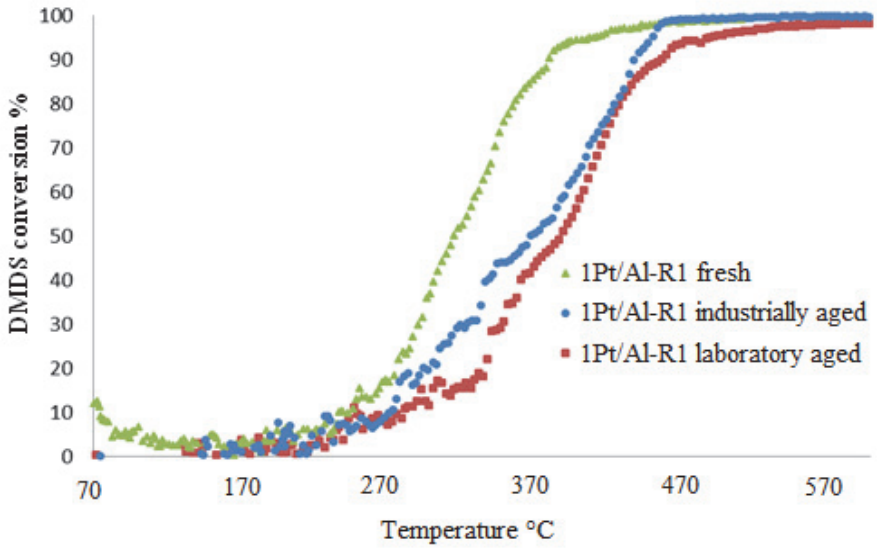

Fig. 46. Light-off tests in DMDS oxidation over fresh, industrially aged and laboratory aged Pt/Al-R1 catalysts.

After the accelerated deactivation treatment in the laboratory, the catalytic performance of the 1Pt/Al-R1 catalyst in the oxidation of DMDS was affected in a negative way too. According to the BET-BJH data, the surface area of 1Pt/Al-R1 decreased by 54% (with a decrease of 75% in the case of the industrially aged catalyst) and still the results of the light-off tests for the industrially aged catalyst and the catalyst after accelerated deactivation procedure were relatively close to each other. Thus, we can confirm that the industrial deactivation was simulated at least in a qualitative way.

4.4 The accelerated deactivation of self-made bimetallic catalysts

The best catalysts in terms of catalytic activity and stability (0.3Pt10Cu/Al and 0.3Pt10Cu/$AlSi_{20}$) were chosen to be treated and studied in more detail after the accelerated ageing procedure.

4.4.1 Characterization of the laboratory aged 0.3Pt10Cu/Al and 0.3Pt10Cu/$AlSi_{20}$ catalysts

The deactivation study was carried out with the help of several characterization methods in order to explore the structural and textural changes of the catalyst surface after the developed accelerated ageing in the laboratory.

Elemental analysis by XRF

Elemental analysis by XRF was carried out to determine the weight percentages of sulfur in the different 0.3Pt10Cu/Al and 0.3Pt10Cu/$AlSi_{20}$ samples. The results obtained are summarized in Table 24.

Table 24. Elemental analysis of sulfur by XRF.

Catalysts	S wt-% (XRF)
0.3Pt10Cu/Al, laboratory aged	4
0.3Pt10Cu/$AlSi_{20}$, laboratory aged	2.7

The results show different sulfur content depending on the support material. We found 4 wt-% of sulfur in the case of the 0.3Pt10Cu/Al catalyst, but after the addition of less than 20% of SiO_2 into the Al_2O_3 support, the accelerated deactivation did not have the same effect. Only 2.7 wt-% of sulfur was found in the case of the 0.3Pt10Cu/$AlSi_{20}$ catalyst. It can be concluded that with this deactivation procedure it was not possible to quantitatively deposit the same amount of sulfur on the catalyst compared to industrial ageing. However, it was found (based on XRF results) that the $AlSi_{20}$ support retained less sulfur than the pure alumina support.

The measurement of specific surface area and pore volume

After performing the accelerated deactivation in the laboratory for the fresh 0.3Pt10Cu/Al and 0.3Pt10Cu/$AlSi_{20}$ catalysts, it was noted (Table 25) that the surface area of 0.3Pt10Cu/$AlSi_{20}$ decreased by only 38% while it was decreased by 42% in the case of the 0.3Pt10Cu/Al catalyst. This finding is in accordance with what was found from the XRF analysis, wherein the sulfur was not deposited on $AlSi_{20}$ to the same extent as it was in the case of the Al supported catalyst, proving that sulfur and its compounds block the porous structure of the support.

The self-made bimetallic Pt-Cu catalysts showed a relatively smaller BET decrease compared to the monolithic 1Pt/Al catalyst, most likely due to the existence of copper in the active phase next to the Pt surface. Most active metal oxides in the total oxidation are the semiconductors of type P. Conduction is produced from positive holes in these type of semiconductors, electrons are highly mobile and offer easy adsorption of oxygen in an anionic form on the surface, such as O^- (Spivey 1987). Copper is one of the semiconductor materials which is most commonly used. Both copper (I and II) are P-type semiconductor oxides and they have applications in the oxidation of VOCs (Lahousse *et al.* 1998), CO (Xu *et al.* 2001) and NO_x emissions (Kang *et al.* 2006). They also have very notable potential in the oxidation of sulfur containing VOCs since they have good resistance against deactivation caused by sulfur (Liao *et al.* 1982).

Table 25. The BET-BJH results of the fresh and laboratory aged 0.3Pt10Cu/Al and 0.3Pt10Cu/AlSi$_{20}$ catalysts.

Catalysts	Specific surface area (BET)	Pore volume	Pore diameter
	m^2g^{-1}	cm^3g^{-1}	nm
0.3Pt10Cu/Al, fresh	225	0.37	6.42
0.3Pt10Cu/Al, laboratory aged	130	0.26	7.28
0.3Pt10Cu/AlSi$_{20}$, fresh	290	0.57	7.59
0.3Pt10Cu/AlSi$_{20}$, laboratory aged	180	0.31	6.71

FESEM

FESEM was used to analyse the topographic microstructure and to perform the elemental mapping of the surface of the 0.3Pt10Cu/AlSi$_{20}$ and 0.3Pt10Cu/Al catalysts after accelerated deactivation.

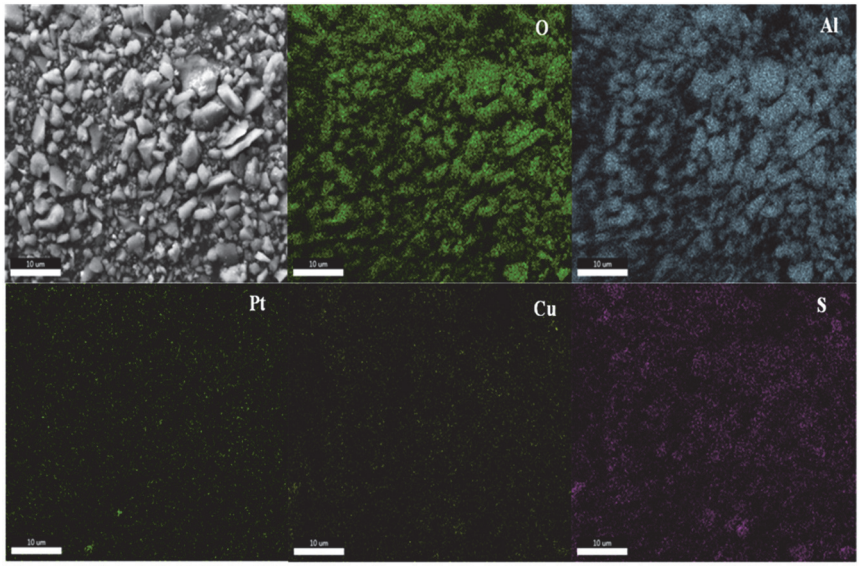

Fig. 47. Elemental mapping by FESEM for O, Al, Pt, Cu and S species on the surface of the 0.3Pt10Cu/Al catalyst after accelerated deactivation.

According to Figure 47, it can be seen that Cu and Pt were barely detected in very small areas. Another finding is that sulfur is found to be dispersed over the entire surface of the 0.3Pt10Cu/Al catalyst after accelerated deactivation.

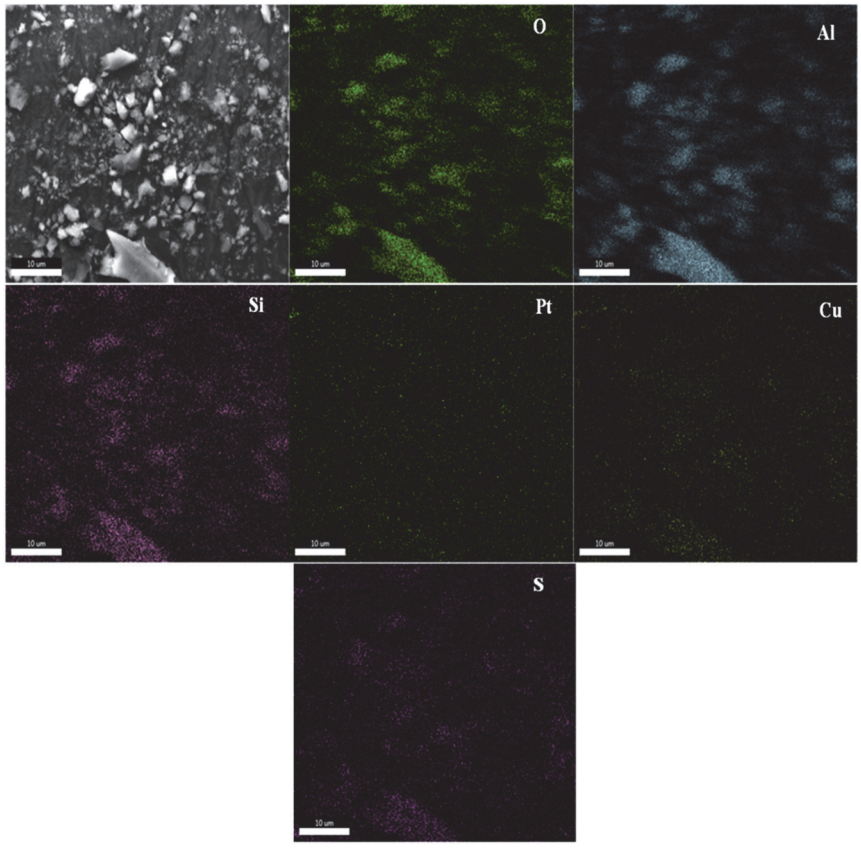

Fig. 48. Elemental mapping by FESEM for O, Al, Si, Pt, Cu and S species on the surface of the 0.3Pt10Cu/AlSi$_{20}$ catalyst after accelerated deactivation.

For the 0.3Pt10Cu/AlSi$_{20}$ catalyst (Figure 48), it was clearly seen that sulfur took the same localization as Si, Al, O and Cu on the surface of the aged catalyst, which allows us to say that sulfur is well dispersed on the catalyst surface but with a lower concentration than in the case of the 0.3Pt10Cu/Al catalyst.

TEM

After the accelerated deactivation, TEM analyses were made to reveal information on the existence of any Pt sintering. Figure 49 and Table 26 show the TEM images and EDS results of the catalysts.

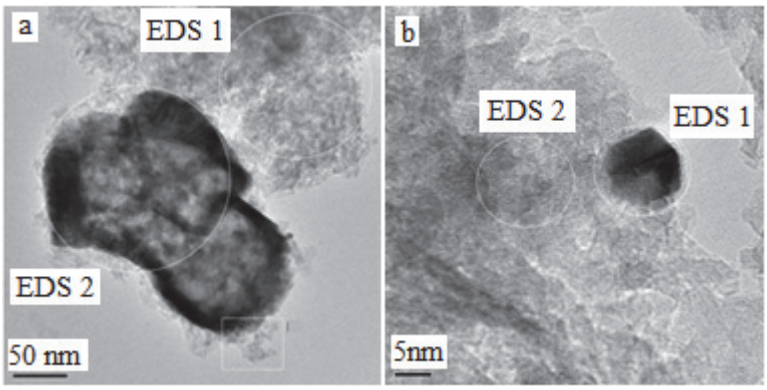

Fig. 49. TEM images of the 0.3Pt10Cu/Al catalyst (a) and the 0.3Pt10Cu/AlSi$_{20}$ catalyst (b) after accelerated deactivation.

Table 26. The EDS measurements of different Pt particles on the surface of the 0.3Pt10Cu/Al and 0.3Pt10Cu/AlSi$_{20}$ catalysts after accelerated deactivation.

EDS analysis	O	Al	Si	S	Pt	Cu
EDS 1b on a Pt particle	45.58	32.86	2.04	0.00	15	4.51
EDS 2b on the support	58.14	34.75	3.78	0.42	0.07	2.84
EDS 2a on a Pt particle	47.10	11.98	--	3.09	5.12	32.7
EDS 1a on the support	59.25	37.09	--	0.78	0.00	2.88

Based on the TEM results, it was found that the particles on the surface of the aged 0.3Pt10Cu/Al catalyst were exposed to sintering, since the size of about 100 nm was found for Pt (Figure 49a) compared to the size for the fresh catalyst (3 nm). Moreover, according to Table 26, the aged 0.3Pt10Cu/Al catalyst exhibited relatively high sulfur content and sulfur was found to be present in both the active phase and the support material.

For the 0.3Pt10Cu/AlSi$_{20}$ catalyst that had undergone accelerated ageing, there was an appearance of bimetallic particles on the surface of the catalyst, as Figure 49b and EDS 1b in Table 26 show. The mixed Pt-Cu particle exhibited a bigger size (10 nm) compared to the fresh catalyst (5 nm), meaning that some particles were exposed to the sintering phenomena. Another important finding was that the sulfur content in this catalyst was much lower compared to the 0.3Pt10Cu/Al catalyst. Besides, no sulfur was found to be deposited on the surface of the active phase. These results are consistent with the previously presented XRF results and will be confirmed further by the coming XPS results.

The XPS measurements were the last characterization done for the fresh and laboratory aged 0.3Pt10Cu/Al and 0.3Pt10Cu/$AlSi_{20}$ catalysts.

XPS

Concerning both the 0.3Pt10Cu/Al and 0.3Pt10Cu/$AlSi_{20}$ catalysts, after the accelerated deactivation, the same results were found, i.e. the decomposition of the spectra of individual components of Pt $4d_{5/2}$ showed the presence of two platinum species in both cases (Figure 50a and 50b), the spectral peak ($Pt4d_{5/2}$) with a BE at around 315 eV is associated to the chemical state of Pt (0) and the last peak at 318.5 eV may correspond to the platinum species interacting with SO_2^{-4} on the support surface (Mishra 2002).

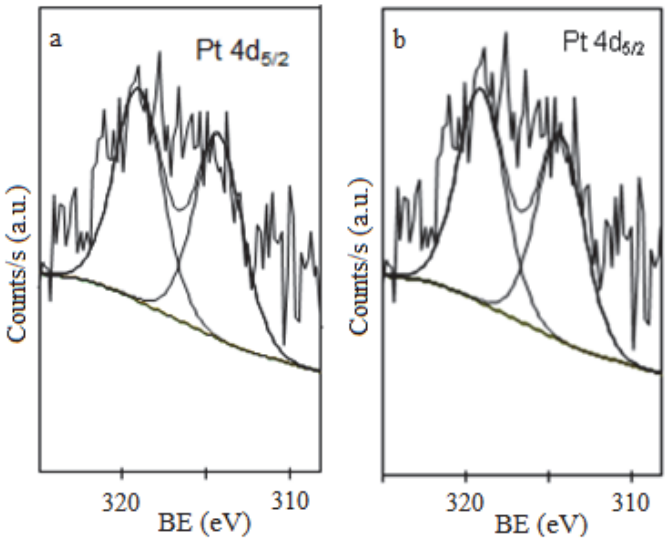

Fig. 50. Pt $4d_{5/2}$ of the laboratory aged 0.3Pt10Cu/Al catalyst (a) and 0.3Pt10Cu/$AlSi_{20}$ catalyst (b).

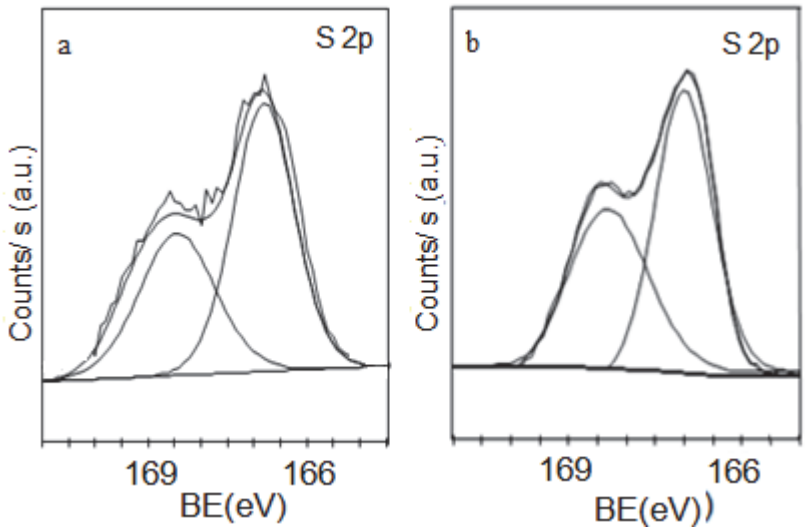

Fig. 51. S 2p of the laboratory aged 0.3Pt10Cu/Al catalyst (a) and 0.3Pt10Cu/AlSi$_{20}$ catalyst (b).

According to the decomposition of the individual components of S 2p (Figure 51), the binding energy of the S $2p_{1/2}$ at 168.9 eV showed that sulfur is only present in the form of S^{6+} (Kohler *et al.* 1982, Ku *et al.* 1981, Briggs *et al.* 1990, Wagner *et al.* 1999), proved by the presence of a single transition of S $2p_{1/2}$ and S $2p_{3/2}$.

After the 0.3Pt10Cu/Al and 0.3Pt10Cu/AlSi$_{20}$ catalysts were treated with the accelerated deactivation procedure, it was noted that the dispersion (the surface dispersion detected by XPS) of the active phase was remarkably changed in the case of 0.3Pt10Cu/Al (Table 27). The atomic ratio of Pt/Al (0.0022) and Cu/Al (0.09) decreased, indicating that the surface of the catalyst was exposed to some chemical poisoning and covered by sulfur, as the measurements show, this sulfur is most likely in the form of SO_2.

Table 27. Surface atomic ratios determined by XPS.

Catalysts	0.3Pt10Cu/Al fresh	0.3Pt10Cu/Al laboratory aged	0.3Pt10Cu/AlSi$_{20}$ fresh	0.3Pt10Cu/AlSi$_{20}$ laboratory aged
Cu/Al	0.13	0.09	0.16	0.12
Pt/Al	0.0033	0.0022	0.004	0.0035
S/Al	-	0.1	-	0.08

In the case of 0.3Pt10Cu/$AlSi_{20}$, the dispersion decrease (surface concentration detected by XPS) in the Pt/Al (0.0035) and Cu/Al (0.12) was detected as well, but it was not as severe as in the case of the 0.3Pt10Cu/Al catalyst. Furthermore, the concentration of the elemental sulfur of the 0.3Pt10Cu/Al surface was higher (0.1) than that found in the case of the 0.3Pt10Cu/$AlSi_{20}$ (0.08) catalyst. Besides this, the presence of Pt (0) and Pt (IV) species was observed. The metal surface can provide an environment in which the interaction of SO_2 can be faster. Another explanation which could be possible is that sulfate promotes the Pt mobility which leads to an agglomeration of Pt and a loss of the active surface, which ultimately leads to a stability loss. In addition, the platinum crystals cannot be properly re-scattered when sulfate is present on the catalyst surface (Hawkins 2016).

4.4.2 The activities of the 0.3Pt10Cu/Al and 0.3Pt10Cu/$AlSi_{20}$ catalysts before and after the accelerated deactivation

The catalytic performance of the 0.3Pt10Cu/Al and 0.3Pt10Cu/$AlSi_{20}$ catalysts was evaluated after they were treated with the accelerated deactivation procedure. Figure 52 shows the light-off curves of the fresh and laboratory aged 0.3Pt10Cu/Al and 0.3Pt10Cu/$AlSi_{20}$ catalysts.

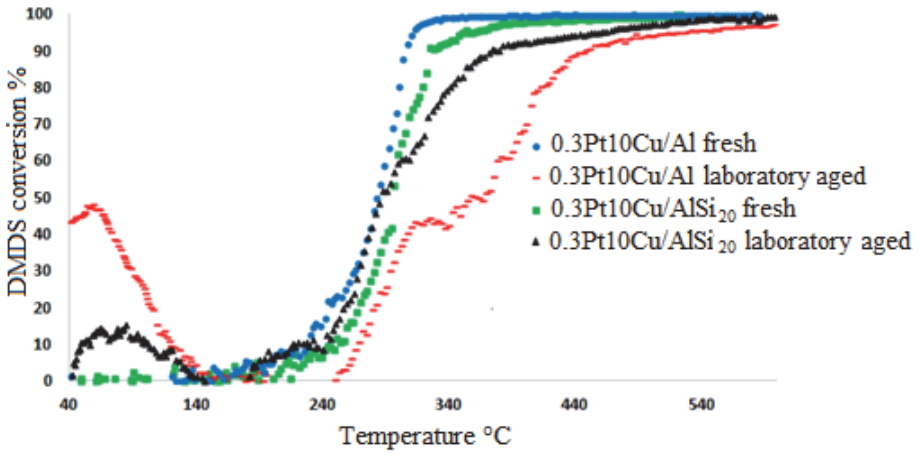

Fig. 52. Light-off tests for DMDS oxidation over the fresh and aged 0.3Pt10Cu/Al and 0.3Pt10Cu/$AlSi_{20}$ catalysts.

Figure 52 shows that the catalytic activity of 0.3Pt10Cu/Al seems to be improved after aging in the temperature interval from 40 to 140 °C. This change can be explained by the rearrangement of the active surface in the tested catalyst. However, the activity of the aged 0.3Pt10Cu/Al catalyst at higher temperature has decreased since T_{90} has moved from 310 °C to a temperature higher than 400 °C (Table 28). Regarding the 0.3Pt10Cu/$AlSi_{20}$ catalyst, it can be observed that at higher temperatures the conversion temperature of DMDS over 0.3Pt10Cu/$AlSi_{20}$ was slightly increased and the T_{90} value has moved from 320 °C in the case of the fresh catalyst to 360 °C in the case of the aged one (Table 28). Concerning the T_{50}, it moved to the lower temperature from 298 °C for the fresh catalyst to 286 °C for the laboratory aged catalyst.

Comparing the catalytic performance of the two catalysts after being aged in the laboratory by sulfur dioxide and water, it was found that the $AlSi_{20}$ support played a very important and protective role against the poisoning of the active surface. According to the XRF data, the sulfur content was found to be lower (2.7% S) than in the γ-Al_2O_3 supported catalyst (4% S). These results are in accordance with what was found in our previous work (Darif *et al.* 2016), where the improvement in the sulfur tolerance was achieved by using silica doped alumina support.

Table 28. T_{90} and T_{50} in DMDS oxidation over the fresh and laboratory aged 0.3Pt10Cu/Al and 0.3Pt10Cu/$AlSi_{20}$ catalysts.

Catalysts	0.3Pt10Cu/Al	0.3Pt10Cu/$AlSi_{20}$
T_{90} of fresh catalyst (°C)	310	320
T_{90} of laboratory aged catalyst (°C)	400	365
T_{50} of fresh catalyst (°C)	285	298
T_{50} of laboratory aged catalyst (°C)	330	286

According to other studies (Bond 1962, Golodets 1983, Beck *et al.* 1991), it has been reported that the most sensitive and vulnerable catalyst against sulfur is the one that contains high oxidation states of Pt on the surface. This is in agreement with what was observed related to the 0.3Pt10Cu/Al catalyst, which showed the presence of Pt^{4+}species and also a higher concentration of sulfur on its surface in comparison to the 0.3Pt10Cu/$AlSi_{20}$ catalyst that contained Pt^{2+} on the surface.

To summarize, the self-made catalysts showed an interesting catalytic performance. The improved catalytic activity and selectivity were not the only differences – also the durability or resistance of these catalysts against sulfur

poisoning was good. According to the results discussed earlier, it was found that the Pt-Cu sites were strongly involved in promoting the catalysts' performance in terms of activity and stability. As was shown, CuO is one of the metal oxides that are very active in the complete oxidation of S-VOCs. In addition, they have beneficial properties against catalyst deactivation by sulfur (Wang *et al.* 2002). The FESEM, XPS and XRF data of fresh and aged catalysts showed that sulfur is deposited on the catalyst surface during the accelerated deactivation procedure, which can be considered as the major cause of the catalyst deactivation. The same result was observed for the industrially aged catalysts even though sulfur was deposited in higher amounts. Another conclusion that can be extracted is that Pt sintering occurs after both industrial and accelerated ageing. This causes the loss of active surface and affects the catalytic activity.

5 Conclusions and perspectives

The main objective of this work was to find efficient and selective catalysts for the total oxidation of S-VOCs with a good resistance against catalyst deactivation. In this study the S-VOCs were modelled by the DMDS molecule. To reach the main objective, several parameters were studied, particularly the influence of the active phase, the influence of the nature of the support and, finally, the stability and the sulfur-caused deactivation, which are perhaps the main obstacle in developing catalysts for the oxidation of S-VOCs.

In Subsection 4.2.1, the focus was on the study of the influence of the type of active phase. Catalysts based on Pt, Cu and Pt-Cu and supported on Al_2O_3 were prepared (0.3Pt/Al, 10Cu/Al and 0.3Pt10Cu/Al) and characterized by various chemical and physico-chemical techniques. The monometallic 0.3Pt/Al and 10Cu/Al catalysts are both active in the total oxidation of DMDS but the 10Cu/Al catalyst reaches 100% conversion at a very low temperature – T_{100} = 380 °C – while in the case of 0.3% Pt/Al, the total conversion was at T_{100} = 530 °C. The bimetallic 0.3Pt10Cu/Al catalyst develops practically the same activity as 10Cu/Al. However, in terms of selectivity, the presence of Pt in the bimetallic catalyst leads the reaction towards the predominant formation of CO_2 and SO_2 at lower temperatures compared to the monometallic 10Cu/Al catalyst. The characterization of the 0.3Pt10Cu/Al catalyst by XPS and TPR helped to highlight the existence of the interaction between Pt and Cu, and the formation of the Pt-Cu solid solution, which may explain its better activity and selectivity in the oxidation of DMDS.

In Subsections 4.2.2 and 4.2.3, the focus was in the optimization of the catalyst support in order to make it resistant towards poisoning by sulfur compounds. For this, the alumina support was doped with 20 wt-% of SiO_2, known for its resistance to sulfur compounds. The study was conducted for the bimetallic catalysts supported on γ-Al_2O_3 (Al), $(Al_2O_3)_{0.8}(SiO_2)_{0.2}$ ($AlSi_{20}$) and SiO_2 (Si). The results of the different characterizations of the supports and catalysts and the tests in the total oxidation of DMDS generated many relevant conclusions. The activity, selectivity and stability of the catalysts in the oxidation of DMDS were found to be governed by the texture, the chemical structure and the reducibility of the catalysts. In terms of activity, the alumina supported 0.3Pt10Cu/Al catalyst presents the best activity in the oxidation of DMDS. As mentioned above, the direct interaction between Pt and Cu on the nanoscale could be a very likely explanation for its good performance. The $AlSi_{20}$ supported

0.3Pt10Cu/$AlSi_{20}$ catalyst also exhibits good catalytic activity and especially better stability compared to the 0.3Pt10Cu/Al catalyst in DMDS oxidation. The XPS analysis showed that the $AlSi_{20}$ support is more resistant to sulfur poisoning than pure alumina. Indeed, the content of sulfur on the surface of the 0.3Pt10Cu/$AlSi_{20}$ catalyst is lower compared to the catalyst supported on pure Al_2O_3. Besides this, the addition of less than 20 wt-% of SiO_2 increases the acidity of the 0.3Pt10Cu/$AlSi_{20}$ catalyst, making it more resistant and selective towards the formation of SO_2 and CO_2. Another important conclusion is that after the formation of SO_2 molecules during the oxidation reaction of DMDS, the desorption of SO_2 could happen effectively from the surface of the 0.3Pt10Cu/$AlSi_{20}$ catalyst. This can be related to the acidity of the surface of the $AlSi_{20}$ support, which could be a reason for it resisting sulfur poisoning.

Sections 4.3 and 4.4 dealt with the other important aim of this research: the study of catalyst deactivation. With the intention of simulating industrial deactivation (during S-VOC oxidation) and developing an accelerated deactivation procedure using gas mixtures of SO_2 + H_2O, several catalysts were compared, i.e. monolithic catalysts aged in an industrial pilot plant and self-made catalysts aged in the laboratory. The results showed that the self-made 0.3Pt10Cu/Al and 0.3Pt10Cu/$AlSi_{20}$ catalysts exhibited better performances in terms of stability or resistance against sulfur poisoning when compared to the 1Pt/Al and 1Pt/Al-R1 catalysts after accelerated deactivation. More importantly, it was found that the $AlSi_{20}$ support showed promising stability. In addition, sulfur and its compounds were observed on the catalyst surface based on the FESEM, XPS, XRD and XRF studies after industrial ageing, accelerated deactivation and more than 30 h S-VOC oxidation. Therefore, it can be concluded that sulfur compounds deposit/adsorb on the catalyst surface and react with the support and/or the active phase species forming new compounds, like aluminum sulfates. The existence of these new compounds can prevent the catalyst from functioning in the same, effective way as the fresh one, and the accumulation of sulfur poisons on the surface is an important cause for the loss or decline of the catalytic activity. Besides the chemical deactivation, thermal deactivation was observed after industrial ageing, shown by the alumina phase change from γ–Al_2O_3 to θ–Al_2O_3 and the sintering of active phases.

This work can generate a positive impact generally on the environment and human health, and it can especially provide an academic and societal impact since the sulfur-resistance of the catalysts has lately become a more important issue due to industrial activities that burn fossil fuels containing sulfur. The deactivation

phenomena occurring during the S-VOC oxidation are very similar to, for example, those of car exhaust gas catalysis. This research topic is therefore interesting for the S-VOC emitting companies (for example pulp mills and water treatment plants), catalyst and catalytic abatement process developers and also for fuel, engine and vehicle developers in Finland and internationally.

Even though new scientific questions often arise while others are resolved, the work needs to be finalized at a certain point. Here, at the end, I would like to raise a few perspectives concerning the future work. The next step in the development of the accelerated deactivation procedure would evidently be the use of a thermal deactivation step before the sulfur deactivation. It would also be interesting to refine this study by conducting Operando tests to monitor the catalyst surface during the oxidation of DMDS. The main objective of these tests would be to discover the effect of doping on the support material and to observe what kind of changes occur in the active phase and support (the formation and deposition of sulfur residues on the catalyst surface) during the reaction. The results of this study can also strengthen the know-how on the by-products' formation and reaction mechanisms. Last but not least, another perspective would be to extrapolate these laboratory-scale results to take them closer to the industrial application by developing new catalyst types (tube, monoliths, beads, foam etc.) which would smooth the use of the developed catalytic materials in industrial applications and improve the mass and heat transfer.

List of references

ADEL Administration de l'environnement, Grand-duché de Luxembourg (2013), EXP-321A-COV-220703.

ADEME (2013) Les composés organiques volatils – Réduction des émissions de COV dans l'industrie.

ADEME (2016) The French Environment and Energy Management Agency, Les composés organiques volatils (COV), http://www.ademe.fr/entreprises-monde-agricole/reduire-impacts/reduire-emissions-polluants/dossier/composes-organiques-volatils-cov/definition-sources-demission-impacts.

Ago H, Nakamura K, Immamura S, Tsuji M (2004) Growth of double-walled carbon nanotubes with diameter controlled iron oxide nanoparticles supported on MgO. Chem. Phys. Lett. 391: 308–313.

Akhtar F, Andersson L, Ogunwumi S, Hedin N, Bergström L (2014) structuring adsorbents and catalysts by processing of porous powders. J. Eur. Ceram. Soc. 34: 1643–1666.

Ali AM, Daous MA, Khamis AA, Driss H, Burch R, Petrov LA (2015) Strong synergism between gold and manganese in an Au – Mn/triple-oxide-support (TOS) oxidation catalyst. Appl. Catal. A Gen. 489: 24–31.

Anderson JR (1975) Structure of Metallic Catalysts. Academic Press: London, p. 478.

Andersson B, Lovblod R, Grennbelt P (1973) Diffuse emissions of odourous sulfur compounds from kraft pulp mills, 1 VLB145. Swedish Water and Air Pollution Research Laboratory, Gothenburg.

Aristizabal A, Contrerasa S, Barrabes N, Llorca J, Tichit D, Medina F (2011) Catalytic reduction of nitrates in water on Pt promoted Cu hydrotalcite-derived catalysts: Effect of the Pt–Cu alloy formation. Appl. Catal. B. 110: 58–70.

Arosio F, Colussi S, Groppi G, Trovarelli (2006) A Regeneration of S-poisoned Pd/Al_2O_3 catalysts for the combustion of methane. Catal. Today. 117: 569–576.

Avdeeva LB, Kochubey DI, Shaikhutdinov ShK (1999) Cobalt catalysts of methane decomposition: accumulation of the filamentous carbon. Appl. Catal. A. 177: 43–51.

Barakat T (2012) Oxydation des composés organiques volatils en présence de catalyseurs Au et/ou Pd déposé sur TiO nanostructuré dopé. Université du Littoral Côte d'Opale. France.

Barbero BP, Gamboa JA, Cadus LE (2006) Synthesis and characterisation of $La_{1x}Ca_xFeO_3$ perovskite-type oxide catalysts for total oxidation of volatile organic compounds. Appl. Catal. B Environ. 65: 21–30.

Barbier J (1985) Effect of poisons on the activity and selectivity of metallic catalysts. In Deactivation and Poisoning of Catalysts, Oudar J, Wise H, (Eds.), Marcel Dekker: New York, NY, USA, pp. 109–150.

Bartholomew CH (1987) Mechanisms of nickel catalyst poisoning. In Catalyst Deactivation (Studies in Surface Science and Catalysis), Delmon B, Froment GF (Eds.). Elsevier: Amsterdam, The Netherlands, 34: pp. 81–104.

Bartholomew CH (2001) Mechanisms of catalyst deactivation. Appl Catal A. 212: 17–60.

Bartholomew CH, Agrawal PK. Katzer JR (1982) Sulfur poisoning of metals. Adv. Catal. 31: 135–242.
Bartholomew CH, Farrauto RJ (2006) Fundamentals of Industrial Catalytic Processes, 2nd ed. Wiley-Interscience: Hoboken, NJ, USA.
Bartholomew CH, Fuentes GA (1997) Catalyst Deactivation, Studies in Surface Science and Catalysis, Vol. 111, ed. Elsivier: Amsterdam.
Bastos S, Carabineiro S, Orfao J, Pereira M, Delgado J, Figueiredo J (2012) Total oxidation of ethyl acetate, ethanol and toluene catalyzed by exotemplated manganese and cerium oxides loaded with gold. Catal. Today 180: 148–154.
Beck DD, Kruger MH, Monroe DR (1991) The Impact of Sulfur on Three-Way Catalyst: Storage and Removal. SAE Paper no. 910844.
Bentley LR, Chasteen TG (2004) Environmental VOSCs – formation and degradation of dimethyl sulfide, methanethiol and related materials. Chemosphere. 55: 291–317.
Bhatia S (1989) Zeolite Catalysis: Principles and Applications. CRC Press.
Bond GC (1962) Catalysis by Metals, Academic Press, London.
Bouwman R, Biloen P (1977) Valence state and interaction of platinum and germanium on γ-Al_2O_3 investigated by X-ray photoelectron spectroscopy. J. Catal. 48: 209–2016.
Briggs D, Seah MP (1990) (Eds.), Practical Surface Analysis by Auger and X-ray Photoelectron Spectroscopy, 2nd ed.. Wiley: Chichester, UK.
Burch R, Loader PK (1994) Investigation of Pt/Al_2O_3 and Pd/Al_2O_3 catalysts for the combustion of methane at low concentrations. Appl. Catal. B 5: 149–164.
Busca G, Lietti L, Ramis G, Berti F (1998) Chemical and mechanistic aspects of the selective catalytic reduction of NOx by ammonia over oxide catalysts: A review. Appl. Catal. B. 18: 1–36.
Butt JB (1982) Catalyst poisoning and chemical process dynamics. In Progress in Catalyst Deactivation (NATO Advanced Study Institute Series E, No. 54), Figueiredo JL (Ed.). Martinus Nijhoff Publishers: Boston, MA, USA, pp. 153–208.
Carter BC, Norton GM (2007) Sols, Gels, and Organic Chemistry, Ceramic Materials. Science and Engineering. Springer Science & Business Media New York.
Carvalho LS, Pieck CL, Rangel MC, Fígolib NS, Grau JM, Reyes P, Parera JM (2004) Trimetallic naphtha reforming catalysts. I. Properties of the metal function and influence of the order of addition of the metal precursors on Pt − Re − Sn/γ-Al_2O_3 − Cl.vAppl. Catal. A: Gen. 269: 91–103.
Cauqui MA, Rodriguez-Izquierdo JMJ (1992) Application of the Sol–Gel Methods to Catalyst Preparation. Non-Cryst. Solids 148: 724–738.
Cavataio G, Jen H-W, Girard JW, Dobson D, Warner JR (2009) Impact and Prevention of Ultra-Low Contamination of Platinum Group Metals on SCR Catalysts Due to DOC Design. Lambert CK SAE Paper -01-0627.
Cellier C, Gaigneaux EM, Grange P (2004) Sulfur resistance and high activity of hydrated manganese sulfate in the catalytic oxidation of methanethiol. J. Catal. 222: 255–259.
Chang JS (2006) Physics and chemistry of atmospheric plasmas (in Japanese) J. Plasma Fusion Res., 83: 682–692.

Chang JS (2009) Thermal plasma solid waste and water treatments: A critical review. Intern J. Plasma Environmental Science and Technology l3: 67–84.

Chen X, Carabineiro S, Bastos S, Tavares P, Orfao J, Pereira M, Figueiredo J (2013) Exotemplated copper, cobalt, iron, lanthanum and nickel oxides for catalytic oxidation of ethyl acetate. J. Environ. Chem. Eng. 1: 795–804.

Chu H, Hao GH, Tseng TK (2003) Laboratory study of poisoning of a MnO/Fe_2O_3 catalyst by dimethyl sulfide and dimethyl disulfide. J. Hazard. Mater. B. 100: 301–316.

Clark J (2013) Types of Catalysis. http://www.chemguide.co.uk/physical/catalysis/introduction.html.

Clark J (2013-b) The effect of catalysts on reaction rates. http://www.chemguide.co.uk/physical/basicrates/catalyst.html.

Colls J. (2002) Air Pollution. Spon Press: New York.

Corro G, Fierro JLG, Odilon VC (2003) An XPS evidence of Pt^{4+} present on sulfated Pt/Al_2O_3 and its effect on propane combustion. Catal. Commun. 4: 371–376.

Dalla Lana IG, Karge HG, George ZM (1993) Dissociative adsorption of sulfur dioxide on .gamma.-alumina investigated by TPD and mass spectrometry. J. Phys. Chem. 97: 8005–8011.

Darif B, Ojala S, Pirault-Roy L, Bensitel , Brahmi R, Keiski RL (2016) Study on the catalytic oxidation of DMDS over Pt-Cu catalysts supported on Al_2O_3, $AlSi_{20}$ and SiO_2. Appl. Catal B: Environ 181: 24–33.

De Guardia A, Bouzaza A, Martin G, Laplanche A (1996) Procédé d'épuration de gaz contenant des COV soufrés par lavage à l'huile et oxydation à l'ozone des polluants absorbés, Pollution atmosphérique, 152: 82–92.

de Rivas B, Lopez-Fonseca R, Jimenez-Gonzalez C, Gutierrez-Ortiz JI (2012) Highly active behaviour of nanocrystalline Co_3O_4 from oxalate nanorods in the oxidation of chlorinated short chain alkanes, Chem. Eng. J. 184: 184–192.

Deeba M, Lui YK, Dettling JC (2000) Four-way diesel exhaust catalyst and method of use. U.S. Patent 6,093,378, 25 July.

DEFRA Department for environment food and rural affairs (2011) About Air Pollution: UK and EU Air Quality Policy Context. https://uk-air.defra.gov.uk/air-pollution/uk-eu-policy-context.

Deng S, Sourirajan A, Matsuura T (1996) Study of volatile hydrocarbon emission control by an aromatic poly (etherimide) membrane, Indian Engineering and Chemical Research, 34: 4494.

Dry ME (1981) The Fischer-Tropsch synthesis. In Catalysis—Science and Technology; Anderson J, Boudart M (Eds.). Springer-Verlag: New York, NY, USA, pp. 159–218.

Dunleavy JK (2006) Sulfur as a Catalyst Poison. Platinum Metals Rev. 50: 110.

Duong LV, Wood BJ, Kloprogge JT (2005) XPS study of basic aluminum sulphate and basic aluminium nitrate. Mater. Lett. 59: 1932–1936.

EC (1999) Directive 1999/13/EC of 11 March 1999 on the limitation of emissions of volatile organic compounds due to the use of organic solvents in certain activities and installations.

EC (2001) Directive 2001/81/EC of the European Parliament and the Council of 23 October 2001 on national emission ceilings for certain atmospheric poluttants.

EC (2004) Directive 2004/42/CE of the European Parliament and of the Council of 21 April 2004 on the limitation of emissions of volatile organic compounds due to the use of organic solvents in certain paints and varnishes and vehicle refinishing products and amending Directive 1999/13/EC.

EC (2010) Directive 2010/75/EU of the European Parliament and of the Council of 24 November 2010 on industrial emissions (integrated pollution prevention and control), including provisions on certain installations and activities using organic solvents. http://eur-lex.europa.eu/LexUriServ/LexUriServ.
do?uri=CELEX:32010L0075:EN:NOT.

EEA (2013) Air Quality Report, p. 51. http://www.eea.europa.eu/publications/air-quality-in-europe-2013/at_download/file.

EEA (2015) Air quality in Europe report, EEA Report No 5/2015, European Environment Agency

El Assal Z, Pitkäaho S, Ojala S, Maache R, Bensitel M, Pirault-Roy L, Brahmi L, Keiski RL (2013) Total oxidation of dichloromethane over metal oxide catalysts. Top Catal. Volume 56: 679–687

Environmental Works (2008) In Encyclopedia Britannica. http://library.eb.co.uk/eb/article-214280.

EPA US (1997) Fact Sheet: EPA's Final Pulp, Paper, and Paperboard ''Cluster Rule'' – Overview, EPA-821-F-97-010.

EPA US (2005) Environmental Protection Agency. Toxic Release Inventory (TRI) Program.

EPD (2010) Environmental Protection Department Hong Kong Special Administrative Region Government: A Guide to the Air Pollution Control (Volatile Organic Compounds) Regulation**.**

Epron F, Gauthard F, Barbier J (2002) Influence of oxidizing and reducing treatments on the metal–metal interactions and on the activity for nitrate reduction of a Pt-Cu bimetallic catalyst. Appl. Catal. A: Gen. 237: 253–261.

Epron F, Gauthard F, Pin´eda C, Barbier J (2001) Catalytic eduction of nitrate and nitrite on Pt-Cu/Al_2O_3 catalysts in aqueous solution: Role of the interaction between copper and platinum in the reaction. J. Catal. 198: 309–318.

European Environment Agency (2010). European Union emission inventory report 1990–2008 under the UNECE Convention on Long-range Transboundary Air Pollution (LRTAP). EEA Technical report 7/2010, ISBN 978-92-9213-102-9, Copenhagen, Denmark.

Farrauto RJ, Bartholomew CH (1997) Fundamentals of Industrial Catalytic Processes, Blackie, Chapman & Hall: London, p. 640.

Fazle Kibria AKM, Mo YH, Nahm KS, Kim MJ (2002) Synthesis of narrow-diameter carbon nanotubes from acetylene decomposition over iron-nickel catalyst supported on alumina. Carbon 40: 1241–1247.

Forzatti P, Lietti, L (1999) Catalyst deactivation, Catal. Today 52: 165–181.

Galvita VV, Filez M, Poelman H, Bliznuk V, Marin GB (2014) The role of different types of CuO in CuO – CeO_2/Al_2O_3 for total oxidation. Catal. Lett. 144: 32–43.

Gangwal S, Mullins M, Spivey J, Caffrey P, Tichenor B (1988) Kinetics and selectivity of deep catalytic oxidation of n-hexane and benzene. Appl. Catal. 36: 231–247.

Garcia T, Agouram S, Sanchez-Royo JF, Murillo R, Mastral AM, Aranda A, Vazquez I, Dejoz A, Solsona B (2010) Deep oxidation of volatile organic compounds using ordered cobalt oxides prepared by a nanocasting route. Appl. Catal. A Gen. 386: 16–27.

Garcia T, Solsona B, Cazorla-Amoros D, Linares-Solano A, Taylor SH (2006) Total oxidation of volatile organic compounds by vanadium promoted palladiumtitania catalysts: comparison of aromatic and polyaromatic compounds. Appl. Catal. B Environ. 62: 66–76.

Golodets GI (1983) Heterogeneous catalytic reactions involving molecular oxygen, Studies in Surface Science and Catalysis, 1st ed. Elsivier, Amsterdam. 15: 365.

Gómez LE, B. Sollier MM, Mizrahi D, Ramallo López JM, Miró EE, Boix AV (2014) Preferential CO oxidation on Pt – Cu/Al_2O_3 catalysts with low Pt loadings. INT J. Hydrogen. Energ. 39: 3719–3729.

Gregg SJ, Sing KSW (1982) Adsorption, Surface and Porosity, 2nd ed. Academic Press: London, UK.

Grove DE (2003) Catalysts – Myths and reillties. Platinum Met. Rev. 47: 44.

Guillard C, Baldassare D, Duchamp C, Ghazzal MN, Daniele S (2007) Photocatalytic degradation and mineralization of a malodorous compound (dimethyldisulfide) using a continuous flow reactor. Catal. Today 122: 160–167.

Hagen J (2006) Industrial Catalysis: A Practical Approach, 2nd ed. Wiley-Vch.

Han W, Deng J, Xie S, Yang H, Dai H, Au CT (2014) Gold supported on iron oxide nanodisk as efficient catalyst for the removal of toluene. Ind. Eng. Chem. Res. 53: 3486–3494.

Hawkins GB (2016) Naphta Sulfur Guards, GBH Entreprises Ltd. http://fr.slideshare.net/GerardBHawkins/feedstock-purificatiion-in-hydrogen-plants

Hayes RE, Kolaczkowski ST (1997) Introduction to catalytic combustion. Gordon Breach: Amsterdam.

Heck R, Farrauto R (1995) Catalytic Air Pollution Control: Commercial Technology. Van Nostrand Reinhold: New York, NY, USA.

Hegedus LL, McCabe RW (1980) Catalyst poisoning. In Catalyst Deactivation (Studies in Surface Science and Catalysis), Delmon B, Froment GF (Eds.). Elsevier: Amsterdam, the Nethelands, 6: pp. 471–505.

Hegedus LL, McCabe RW (1984) Catalyst Poisoning; Marcel Dekker: New York, NY, USA.

HORIBA (1996–2016) Particle Size and Shape of Catalyst Supports. http://www.horiba.com/scientific/products/particlecharacterization/applications/catalyst-supports/.

Hoyos LJ, Praliaud H, Primet M (1993) Catalytic combustion of methane over palladium supported on alumina and silica in presence of hydrogen sulphide. Appl. Catal. A: Gen 98: 125–138.

Hu LR, Williams S (2007) Sulfur Poisoning and Regeneration of Pd Catalyst under Simulated Emission Conditions of Natural Gas Engine. 2007-01-4037.

Huang YC, Luo C.H, Yang S, Lin YC, Chuang CY (2010) Improved removal of indoor volatile organic compounds by activated carbon fiber filters calcined with copper oxide catalyst. Clean Soil Air Water 38: 993–997.

Huber GW, Guymon CG, Stephenson BC Bartholomew CH (2001) Hydrothermal stability of Co/SiO_2 Fischer-Tropsch synthesis catalysts. In Catalyst Deactivation (Studies in Surface Science and Catalysis), Spivey JJ, Roberts GW, Davis BH (Eds.). Elsevier: Amsterdam, the Nethelands. 139: 423–430.

Jennings MS, Krohn NE, Berry RS, Palazzolo MA, Parks RM, Fidler KK (1985) Catalytic incineration for control of VOC emissions. Noyes Publications, Park Rifge, NJ American Institute of Chemical Engineers: New York, NY.

Kamal MS, Razzak SA, Hossain MM (2016) Catalytic oxidation of volatile organic compounds (VOCs) – A review. Atmos. Environ. 140: 117–134.

Kang M, Park ED, Kim JM, Yie JE (2006) Cu-Mn mixed oxides for low temperature NO reduction with NH_3. Catal. Today 111: 236–241.

Karge HG, Dalla Lana IG (1984) IR studies of sulfur dioxide adsorption on a Claus catalyst by selective poisoning of sites. J. Phys. Chem. 88: 1538–1543.

Katona T, Guczi L, Somorjai GA (1991) Reduction of nitric oxide by ammonia at atmospheric pressures over platinum polycrystalline foils as model catalysts. J. Catal. 132: 440.

Kazachkin DV, Luebke DR, Kovalchuk VI, d'Itri JL (2008) Hydrogen-Assisted 1, 2-Dichloroethane Dechlorination Catalyzed by $Pt-Cu/SiO_2$: Insights into the Nature of Ethylene-Selective Active Sites. J. SibFU. 4: 303–325.

Khan FI, Ghoshal A Kr (2000) Removal of volatile organic compounds from polluted air. Journal of Loss Prevention in the Process Industries, 13: 527–545.

Kharas KCC (1992) Performance, selectivity, and mechanism in Cu-ZSM-5 lean-burn catalysts. Appl. Catal. B. 2: 207–224.

Kim MG, Kim HS, Ha YG, J. He, Kanatzidis MG, Facchetti A, Marks TJ (2010) High-performance solution-processed amorphous zinc-indium-tin oxide thin-film transistors. J. Am. Chem. Soc. 132: 10352–10364.

Kohler U, Wassmuth HW (1982) Surface reactions of sulfur with oxygen on Pt(111). Surf. Sci. 117: 668–675.

Kriston A, Xie T, Popov BN (2014) Impact of ultra-low platinum loading on mass activity and mass transport in H_2-oxygen and H_2-Air PEM fuel cells. Electrochimica Acta. 121: 116–127.

Kröcher O, Widmer M, Elsener M, Rothe D (2009) Adsorption and desorption of SO_x on diesel oxidation catalysts. Ind Eng Chem Res. 48: 9847-9857.

Krüger RL, Dallago RM, Di Luccio M (2009) Degradation of dimethyl disulfide using homogeneous Fenton's reaction. J. Hazard. Mater. 169: 443–447.

Ku RC, Wynblatt P (1981) SO_2 adsorption on Rh(110) and Pt(110) surfaces. Appl. Surf. Sci. 8:250-259.

Kucherov AV, Gerlock JL, Jen HW, Shelef M (1995) *In Situ* ESR Monitoring of CuH-ZSM-5 Up to 500 °C in Flowing Dry Mixtures of No(NO_2), C_3H_6(C_2H_5OH), and Excess O_2. J. Catal. 152: 63–69.

Kukovecz A, Konya Z, Nagaraju N, Willems I, Tamasi A, Fonseca A, Nagy JB, Kiricsi I (2000) Catalytic synthesis of carbon nanotubes over Co, Fe and Ni containing conventional and sol-gel silica-aluminas. Phys. Chem. Chem. Phys. 2: 3071–3076.

Lahousse C, Bernier A, Grange P, Delmon B, Papaefthimiou P, Ioannides T, Verykios X (1998) Evaluation of γ-MnO_2 as a VOC removal catalyst: Comparison with a noble metal catalyst. J. Catal. 178: 214–225.

Lamonier J, Labaki M, Wyrwalski F, Siffert S, Aboukais A (2008) Thermal behaviour and catalytic properties towards propene combustion of zirconia modified by different first row transition metals. J. Anal. Appl. Pyrol. 81: 20–26.

Lampert JK, Kazi MS, Farrauto RJ (1997) Palladium catalyst performance for methane emissions abatement from lean burn natural gas vehicles. Appl Catal. B: Environ. 14: 211–223.

Leprince T, Aleixo J, Williams S, Naseri M (2004) Regeneration of palladium based catalyst for methane abatement. CIMAC Congress, Paper No. 210.

Liao PC, Fleisch TH, Wolf EE (1982) Activity and XPS studies of sulfur poisoning effect on Pt-Cu/γ-Al_2O_3 oxidation catalysts. J. Catal. 75: 396.

Lin CX, Yuan P, Yu CZ, Qiao SZ, Lu GQ (2009) Cooperative self-assembly of silica-based mesostructures templated by cationic fluorocarbon/Hydrocarbon mixed surfactants. Microporous Mesoporous Mater. 126: 253–261.

Lin Y-H, Tseng T-K, Chu H (2014) Photocatalytic degradation of dimethyl disulfide on S and metal-ions co-doiped TiO_2 under visible-light irradiation. Appl. Catal. A. 469: 221–228

Lindfors V, Laurila T (2000) Biogenic volatile organic compound (VOC) emissions from forests in Finland. Boreal Env. Res. 5: 95–113.

Liotta L, (2010) Catalytic oxidation of volatile organic compounds on supported noble metals. Appl. Catal. B Environ. 100: 403–412.

Liotta L, Ousmane M, Di Carlo G, Pantaleo G, Deganello G, Marci G, Retailleau L, Giroir-Fendler A (2008) Total oxidation of propene at low temperature over Co_3O_4-CeO_2 mixed oxides: role of surface oxygen vacancies and bulk oxygen mobility in the catalytic activity. Appl. Catal. A General. 347: 81–88.

Lowry GV, Reinhard M (2000) Pd-catalyzed TCE dechlorination in groundwater: Solute effects, biological control, and oxidative catalyst regeneration. Environ. Sci. Technol. 34: 3217–3223.

Lucideon (2016) Testing & Characterization Techniques BET Surface Area Analysis & BJH Pore Size and Volume Analysis. http://www.lucideon.com/testing-characterization/techniques/brunauer-emmett-teller-surface-area-analysis-barrett-joyner-halenda-pore-size-and-volume-analysis.

Lylykangas R (2010) Formia Emissions Control, Thermal or Catalytic VOC Oxidation? http://formiasmartvoc.com/thermal-or-catalytic-voc-oxidation.

Manson I (2000) Self-regenerating diesel exhaust particulate filter and material. U.S. Patent 6,013,599, 11 January.

Mason G (1982) The effect of pore space connectivity on the hysteresis of capillary condensation in adsorption-desorption isotherms. J. Colloid Interface Sci. 88: 36–46.

Mason G (1983) Proceedings of the Royal Society of London. Series A, Electron. J. Math. Phys. Sci. 47: 390.

Matori KA, Wah LC, Hashim M, Ismail I, Mohd Zaid MH (2012) Phase Transformations of α-alumina made from waste aluminum via a precipitation technique. Int. J. Mol. Sci. 13: 16812–16821.

Maxted EB (1951) The poisoning of metallic catalysts. Adv. Catal. 3: 129–177.

Meier A, Kirillov VA, Kuvnishov GG, Mogilnykh YuI, Reller A, Steinfeld A, Weidenkaff A (1999) Solar thermal decomposition of hydrocarbons and carbon monoxide for the production of catalytic filamentous carbon. Chem. Eng. Sci. 54: 3341–3348.

Mishra P (2002) Low-temperature synthesis of α-alumina from aluminium salt and urea. Mater. Lett. 55: 425–429.

Morales MR, Aguero FN, Cadus LE (2013) Catalytic combustion of n-hexane over alumina supported Mn–Cu–Ce catalysts. Catal. Lett. 143: 1003–1011.

Morales. MR, Barbero BP, Cadus LE (2006) Total oxidation of ethanol and propane over Mn-Cu mixed oxide catalysts. Appl. Catal. B Environ. 67: 229–236.

Morris D. Argyle and Calvin H. Bartholomew (2015) Heterogeneous catalyst deactivation and regeneration: A Review. Catalysts 5: 145–269.

Mouammine A, Ojala S, Pirault-Roy L, Bensitel M, Keiski R, Brahmi R (2013) Catalytic partial oxidation of methanol and methyl mercaptan: Studies on the selectivity of TiO_2 and CeO_2 supported V_2O_5 catalysts. Top. Catal. 56: 650–657.

Moulijn JA, van Diepen AE, Kapteijn F (2001) Catalyst deactivation: is it predictable?: What to do? Appl. Catal. A. 212: 3–16.

Müller J-F (1992) Geographical distribution and seasonal variation of surface emissions and deposition velocities of atmospheric trace gases. J. Geophys. Res. 97: 3787–3804.

Muzenda E, Belaid M (2013) Volatile Organic Compounds Abatement: A Critical Discussion of Destruction Techniques, 2nd International Conference on Chemical, Ecology and Environmental Sciences (ICEES'2013) June 17–18, London (UK).

Nagaraju N, Fonseca A, Konya Z, Nagy (2002) Alumina and silica supported metal catalysts for the production of carbon nanotubes JB, J. Mol. Catal. A. 181: 57.

NanoComposix (2012) Transmission electron microscopy analysis of nanoparticles. http://50.87.149.212/sites/default/files/nanoComposix%20Guidelines%20for%20TEM%20Analysis.pdf.

Nevanperä TK, Ojala S, Bion N, Epron F, Keiski RL (2016) Catalytic oxidation of dimethyl disulfide (CH_3SSCH_3) over monometallic Au, Pt and Cu catalysts supported on γ-Al_2O_3, CeO_2 and CeO_2-Al_2O_3. Applied. Catal. B: Environmental 182: 611–625.

Neyestanaki AK, Klingstedt F, Salmi T, Murzin DY (2004) Deactivation of postcombustion catalysts: a review. Fuel. 83: 395–408.

Neyestanaki AK, Kumar N, Lindfors L-E (1995) Catalytic combustion of propane and natural gas over Cu and Pd modified ZSM zeolite catalyst. Appl. Catal. B. 7: 95–111.

Ojala S, Lassi U, Härkönen M, Maunula T, Silvonen R, Keiski RL (2006) Durability of VOC catalysts in solvent emission oxidation. Chem. Eng. J. 120: 11–16.

Ojala S, Lassi U, Ylönen U. Keiski RL (2005) Abatement of malodorous pulp mill emissions by catalytic oxidation-pilot experiments in Stora Enso Pulp Mill, Oulu, Finland. Tappi J. 4: 9–14.

Ojala S, Pitkaaho S, Laitinen T, Koivikko NN, Brahmi R, Gaalova J, Matejova L, Kucherov A, Paivarinta S, Hirschmann C (2011) Catalysis in VOC abatement. Top. Catal. 54: 1224–1256.

Onfroy T, Clet G, Houalla M (2005) Quantitative IR characterization of the acidity of various oxide catalysts. Microporous Mesoporous Mater. 82: 99–104.

Oudar J, Wise H (1985) Deactivation and Poisoning of Catalysts. Marcel Dekker: New York, NY, USA.

Pacchioni G, Clotet A, Ricart JM (1994) A theoretical study of the adsorption and reaction of SO_2 at surface and step sites of MgO(100) surface. Surf. Sci. 315: 337–350.

Papaefthimiou P, Ioannides T, Verykios XE (1997) Combustion of non-halogenated volatile organic compounds over group VIII metal catalysts. Appl. Catal. B Environ. 13: 175–184.

Papaefthimiou P, Ioannides T, Verykios XE (1998c). Performance of doped Pt/TiO_2 (W^{6+}) catalysts for combustion of volatile organic compounds (VOCs). Appl. Catal. B Environ. 15: 75–92.

Park JW, Jeong JH, Yoon WL, Jung H, Lee HT, Lee DK, Park YK, Rhee YW (2004) Activity and Characterization of the Co-Promoted $CuO–CeO_2/\gamma$-Al_2O_3 Catalyst for the Selective Oxidation of CO in excess Hydrogen. Appl Catal A. Gen 274: 25–32.

PE (2016) XPS/ESCA. PHYSICAL ELECTRONICS, a division of ULVAC-PHI. https://www.phi.com/surface-analysis-techniques/xps-esca.html.

Peigney A, Laurent C, Rousset A (1999) Influence of the composition of a H_2-CH_4 gas mixture on the catalytic synthesis of carbon nanotubes-Fe/Fe_3C-Al_2O_3 nanocomposite powders. J. Mater. Chem. 9: 1167–1177.

Perego C, Villa P (1997) Catalyst preparation methods. Catal. Today 34: 281–305.

Peter-Hoblyn JD, Valentine JM, Sprague BN, Epperly WR (1999) Methods for reducing harmful emissions from a diesel engine. U.S. Patent 6,003,303, 21 December.

Peuckert M, Bonzel HP (1984) Characterization of oxidized platinum surfaces by X-ray photoelectron spectroscopy. Surf. Sci. 145: 239–259.

PIS Philips Innovation Services (2013) Inductively Coupled Plasma-Atomic Emission Spectrometry (ICP-OES). http://www.innovationservices.philips.com/sites/default/files/materials-analysis-icp-oes.pdf.

Pitkäaho S, Ojala S, Kinnunen T, Silvonen R, Keiski RL (2011) Catalytic oxidation of dichloromethane and perchloroethylene: Laboratory and industrial scale studies. Top Catal. 54: 1257–1265.

Popat A, Liu J, Lu GQ, Qiao SZ (2012) A pH-responsive drug delivery system based on chitosan coated mesoporoussilica nanoparticles. J. Mater. Chem. 22: 11173–11178.

Rajesh H, Ozkan US (1993) Complete oxidation of ethanol, acetaldehyde and ethanol/methanol mixtures over copper oxide and copper-chromium oxide catalysts Ind. Eng. Chem. Res. 32: 1622–1630.

Reyes P, Oportus M, Pecchi G, Fréty R, Moraweck B (1996) Influence of the nature of the platinum precursor on the surface properties and catalytic activity of alumina-supported catalysts. Catal. Lett. 37: 193–197.

Robinson WRAM, Van Veen JAR, de Beer VHJ, van Santen RA (1999) Development of deep hydrodesulfurization catalysts: II. NiW, Pt and Pd catalysts tested with (substituted) dibenzothiophene. Fuel Process. Technol. 61: 103–116.

Rojas S (2013) Preparation of catalysts, Heterogeneous catalysts ICP-CSIC. https://www.carenafp7.eu/index.php?option=com.

Rooke JC, Barakat T, Brunet J, Li Y, Finol MF, Lamonier JF, Giraudon JM, Cousin R, Siffert S, Su BL (2015) Hierarchically nanostructured porous group V b metal oxides from alkoxide precursors and their role in the catalytic remediation of VOCs. Appl. Catal. B Environ. 162: 300–309.

Rossiin JA (1989) Complete catalytic oxidation of diethyl sulfide over a 1% platinum/alumina catalyst. Ind. Eng. Chem. Res. 28: 1562–1564.

Rostrup-Nielsen J, Trimm DL (1977) Mechanisms of carbon formation on nickel-containing catalysts. J. Catal. 48: 155–165.

Rostrup-Nielsen JR (1971) Some principles relating to the regeneration of sulfur-poisoned nickel catalyst. J. Catal. 21: 171–178.

Rostrup-Nielsen JR (1991) Promotion by poisoning In Catalyst Deactivation (Studies in Surface Science and Catalysis), Bartholomew CH, Butt JB (Eds.). Elsevier: Amsterdam, the Nethelands. 68: pp. 85–101

Rouessac F, Rouessac A (2007) Chemical Analysis, Modern Instrumentation Methods and Techniques, 2nd ed. John Wiley: West Sussex, England.

Russell A, Epling WS (2011) Diesel oxidation catalysts. Catal Rev Sci Eng. 53: 337.

Ruthven, DM (1984) Principles of Adsorption Processes. John Wiley: New York.

Sales EA, de Souza TRO, Santos RC, Andrade HMC (2005) N_2O decomposition coupled with ethanol oxidative dehydrogenation reaction on carbon-supported copper catalysts promoted by palladium and cobalt. Catal. Today. 107–08: 114–119.

Sangwichien C, Aranovich GL, Donohue MD (2002) Density functional theory predictions of adsorption isotherms with hysteresis loops. Colloids Surfaces A: Physicochem. Eng. Asp. 206: 313–320.

Schwarz JA, Contescu C, Contescu A (1995) Methods for preparation of catalytic materials. Chem. Rev. 95: 477–510

Schwarz JA, Contescu C, Contescu A (1995) Methods for preparation of catalytic materials. Chemical Reviews 95: 3.

Scokart PO, Rouxhet PG (1982) Comparison of the acid-base properties of various oxides and chemically treated oxides. J. Colloid and Interface Sci. 86: 96–104.

Sedjame HJ, Fontaine C, Lafaye G, Barbier Jr, J (2014) On the promoting effect of the addition of ceria to platinum based alumina catalysts for VOCs oxidation. Appl. Catal. B Environ. 144: 233–242.

Severino F, Brito J, Carias O, Laine J (1986) Comparative study of alumina-supported CuO and $CuCr_2O_4$ as catalysts for CO oxidation. J. Catal. 102: 172–179.

Shen L, Zhang X, Li Y, Yang X, Luo J, Xu G (2004) Effect of organic additives in catalyst preparation on the growth of single-wall carbon nanotubes prepared by catalyst-assisted chemical vapour deposition. Nanotechnology. 15: 337–340.

Sing KSW, Everett DH, Haul RAW, Moscou L, Pierotti RA, Rouquerol J, Siemieniewska T (1985) reporting physisorption data for gas/solid systems with special reference to the determination of surface area and porosity. Pure and Appl. Chem. 57: 603–619.

Solsona B, Garcia T, Aylon E, Dejoz AM, Vazquez I, Agouram S, Davies TE, Taylor SH (2011) Promoting the activity and selectivity of high surface area Ni-Ce-O mixed oxides by gold deposition for VOC catalytic combustion. Chem. Eng. J. 175: 271–278.

Solsona, B, Davies TE, Garcia T, Vazquez I, Dejoz A, Taylor SH (2008) Total oxidation of propane using nanocrystalline cobalt oxide and supported cobalt oxide catalysts. Appl. Catal. B Environ. 84: 176–184.

Spivey JJ (1987) Complete catalytic oxidation of volatile organics. Ind. Eng. Chem. Res. 26: 2165–2180.

TFS Thermo Fisher Scientific (2013–2016) XPS-Carbon. http://xpssimplified.com/elements/carbon.php.

Trimm D (1983) Catalyst design for reduced coking review. Appl. Catal. 5: 263–290.

Trimm DL (2001) The regeneration or disposal of deactivated heterogeneous catalysts. Appl. Catal. A. 212:153-160.

Tseng H-H, Lin H-Y, Kuo Y-F, Su Y-T (2010) Synthesis, characterization and promoter effect of Cu-Zn/γ-Al_2O_3 catalysts on NO reduction with CO. Chem. Eng. J. 160: 13–19.

Tsou J, Magnoux P, Guisnet M., Orfao J, Figueiredo JL (2005) Catalytic oxidation of volatile organic compounds: oxidation of methyl-isobutyl-ketone over Pt/zeolite catalysts. Appl. Catal. B Environ. 57: 117–123.

U.S. EPA (2014). Data from the 2011 National Emissions Inventory, Version 1. Accessed 2014. https://www.epa.gov/air-emissions-inventories/2011-national-emissions-inventory-nei-data.

Urban MW (1993) Vibrational Spectroscopy of Molecules and Macromolecules on Surfaces. Wiley: Chichester, pp. 171–185.

US EPA (1973) Atmospheric emissions from the pulp and paper manufacturing industry. EPA- 450/1-73-002. USEPA, Research Triangle Park.

Valiente AM, Lopez PN, Ramos IR, Ruiz AG, Li C, Xin Q (2000) In situ study of carbon nanotube formation by C_2H_2 decomposition on an iron-based catalyst. Carbon 38: 2003–2006.

Van Veen JAR, Sie ST (1999) Fuel processing technology special issue: Deep hydrodesulfurization of diesel fuel. Fuel. Proc. T 61: 1–4.

Vander Wal RL, Ticich TM, Curtis VE (2001) Substrate-support interactions in metalcatalyzed carbon nanofiber growth. Carbon. 39: 2277.

Vasile A, Bratan V, Hornoiu C, Caldararu M, Ionescu NI, Yuzhakova T, Redey A (2013) Electrical and catalytic properties of cerium-tin mixed oxides in CO depollution reaction. Appl. Catal. B Environ. 140: 25–31.

Wagner CD, Riggs WM, Davis LE, Moulder JF (Eds.) (1990) Handbook of X-ray Photoelectron Spectroscopy, Perkin-Elmer Corporation, USA.

Wang C-H, Lee C-N, Weng H-S (1998) Effect of acid treatment on the performance of the CuO–MoO_3/Al_2O_3 catalyst for destructive oxidation of $(CH_3)_2S_2$. Ind. Eng. Res. 37: 1774–1780.

Wang C-H, Lin S-S, Liou S-B, Weng H-S (2002) The promoter effect and a rate expression of the catalytic incineration of $(CH_3)_2S_2$ over an improved CuO–MoO_3/γ-Al_2O_3 catalyst. Chemosphere. 49: 389–394.

Wang C-H, Weng H-S (1997) Al_2O_3-supported mixed-metal oxides for destructive oxidation of $(CH_3)_2S_2$. Ind. Eng. Chem. Res. 36: 2537–2542.

Wang C-H, Weng H-S (1998) Promoting effect of molybdenum on CuO/gamma-Al_2O_3 catalyst for the oxidative decomposition of $(CH_3)_2S_2$. Appl Catal A-Gen. 170: 73–80.

Wang JA, Bokhimi X, Morales A, Novaro O, López T, and Gómez R (1999) Aluminum local environment and defects in the crystalline structure of sol-gel alumina Catalyst. J. Phys. Chem. B, 103: 299–303.

Wang Y, Zhang C, Liu F, He H (2013b) Well-dispersed palladium supported on ordered mesoporous Co_3O_4 for catalytic oxidation of o-xylene. Appl. Catal. B Environ. 142: 72–79.

Wang Y, Zhang C, Yu Y, Yue R, He H (2015) Ordered mesoporous and bulk Co_3O_4 supported Pd catalysts for catalytic oxidation of o-xylene. Catal. Today. 242: 294–299.

Wanke SE and Flynn PC (1975) The Sintering of Supported Metal Catalysts. Catal.Rev. Sci. Eng. 12: 93–135.

William JC, Lead PE (1997) VOC Control strategies in plant design. In Chemical Processing: Project Engineering Annual (p. 44).

Winkler A, Ferri D, Aguirre M (2009) The influence of chemical and thermal aging on the catalytic activity of a monolithic diesel oxidation catalyst. Appl Catal B. 93: 177–184.

Xia Y, Dai H, Jiang H, Deng J, He H, Au CT (2009) Mesoporous chromia with ordered three-dimensional structures for the complete oxidation of toluene and ethyl acetate. Environ. Sci. Technol. 43: 8355–8360.

Xu Z, Inumaru K, Yamanaka S (2001) Catalytic properties of metal loaded silicapillared manganese titanate for CO oxidation. Appl. Catal A. 210: 217–224.

Yoldas BE (1975) Alumina Sol Preparation from Alkoxide. Am. Ceram. Soc. Bull. 54: 289–90.

Yu D, Liu Y, Wu Z (2010) Low-temperature catalytic oxidation of toluene over mesoporous MnOx – CeO_2/TiO_2 prepared by sol-gel method. Catal. Commun. 11: 788–791.

Yu QC, Zhang SC, Yang B (2011) Dispersion of Copper Oxide Supported on γ-Alumina and its Sulfation Properties. Trans. Nonferrous Met. Soc. China 21: 2644–2648.

Yu YAO YF (1984) The oxidation of CO and hydrocarbons over noble metal catalysts, J. Catal. 87:152–162.

Yuan Z, Ren T, Azioune A, Pireaux J (2006) Self-assembly of hierarchically mesopous-macroporous phosphate nanocrystalline aluminum (oxyhydr)oxide materials. Chem. Mater. 18: 1753–1767.

Zaki MI, Hasan MA, Al-Sagheer FA, Pasupulety L (2001) In situ FTIR spectra of pyridine adsorbed on SiO_2-Al_2O_3, TiO_2, ZrO_2 and CeO_2: general considerations for the identification of acid sites on surfaces of finely divided metal oxides. Physicochem. Eng. Aspects 190: 261–274.

579. Kinnunen, Tuomo (2016) Product management perspectives on stakeholder and business opportunity analyses in the front-end of product creation

580. Heiderscheidt, Elisangela (2016) Evaluation and optimisation of chemical treatment for non-point source pollution control : purification of peat extraction runoff water

581. Su, Xiang (2016) Lightweight data and knowledge exchange for pervasive environments

582. Kaijalainen, Antti (2016) Effect of microstructure on the mechanical properties and bendability of direct-quenched ultrahigh-strength steels

583. Lanz, Brigitte (2016) Compact current pulse-pumped GaAs–AlGaAs laser diode structures for generating high peak-power (1–50 watt) picosecond-range single optical pulses

584. Kähäri, Hanna (2016) A room-temperature fabrication method for microwave dielectric Li_2MoO_4 ceramics and their applicability for antennas

585. Chowdhury, Helal (2016) Data download on the move in visible light communications: design and analysis

586. Kekäläinen, Kaarina (2016) Microfibrillation of pulp fibres : the effects of compression-shearing, oxidation and thermal drying

587. Raatikainen, Mika (2016) Intelligent knowledge discovery on building energy and indoor climate data

588. Varjo, Sami (2016) A direct microlens array imaging system for microscopy

589. Haapakangas, Juho (2016) Coke properties in simulated blast furnace conditions : investigation on hot strength, chemical reactivity and reaction mechanism

590. Erkkilä-Häkkinen, Sirpa (2016) Rakentamisen työturvallisuuteen suhtautuminen toimijoiden kokemuksina

591. Hassani Nezhad Gashti, Ehsan (2016) Thermo-mechanical behaviour of ground-source thermo-active structures

592. Sulasalmi, Petri (2016) Modelling of slag emulsification and slag reduction in CAS-OB process

593. Liyanage, Madhusanka (2016) Enhancing security and scalability of Virtual Private LAN Services

Book orders:
Granum: Virtual book store
http://granum.uta.fi/granum/

UNIVERSITY OF OULU P.O. Box 8000 FI-90014 UNIVERSITY OF OULU FINLAND

ACTA UNIVERSITATIS OULUENSIS

UNIVERSITY of OULU
OULUN YLIOPISTO

ISBN 978-952-62-1421-4 (Paperback)
ISBN 978-952-62-1422-1 (PDF)
ISSN 0355-3213 (Print)
ISSN 1796-2226 (Online)